



NAM

Out-of-Plane Two-Way Bending Shake- Table tests on both Single Leaf and Cavity Walls

**Satyadhrik Sharma, Umberto Tomassetti, Luca Grottoli, Francesco
Graziotti**

Eucentre

(European Centre for Training and Research in Earthquake Engineering)

Date July 2018

Editors Jan van Elk & Jeroen Uilenreef

General Introduction

For the modeling of the seismic response of unreinforced masonry buildings, knowledge of the properties of building material used in the Groningen area, and the behavior of wall systems is essential. An experimental program to test the properties of the building materials (in-situ (Ref. 1) and in the laboratory (Ref. 2 and 3), the behavior of wall systems (Ref. 4 and 5) and full-scale masonry buildings (Ref. 6, 7, 8 and 9) was therefore executed.

This report describes experiments carried out during 2017 and 2018 in Eucentre, Pavia, on both single-leaf and cavity walls of calcium-silicate and masonry brick. Testing of walls was done to investigate the two-way bending out-of-plane (OOP) failure mechanism of these walls, involving at least one restrained vertical edge. This is one of the most commonly reported and surveyed cause of structural damage.

In total eleven tests have been described in this report. Seven of these have been performed on the uniaxial shake-table also used for testing of full scale buildings. However, four of the tests have been performed on the new multiaxial shake table at Eucentre.

References

1. In-situ testing of URM houses (building unit: Loppersum, Zijlvest 25), Eucentre (F. Graziotti, A. Rossi, I. Senaldi, S. Peloso), 5th December 2014.
2. Material Characterisation – Version 1.3, Eucentre, P&P, TU-Delft, TU-Eindhoven, October 2015.
3. Summary report for the characterisation of original Groningen masonry, TU Delft (S. Safari, J. Rots), 18th December 2015.
4. Experimental campaign on cavity walls systems representative of the Groningen building stock (incl. EUC-BUILD1), Eucentre (F. Graziotti, U. Tomassetti, A. Rossi, S. Kallioras, M. Mandirola, E. Cenja, A. Penna, G. Magenes), 16th June 2016.
5. In-plane tests of replicated masonry walls, TU Delft (G. Ravenshorst, F. Messali), 18th April 2016
6. URM Modelling and Analysis Cross Validation – Arup, Eucentre, TU Delft, Reference 229746_032.0_REP127_Rev.0.03 April 2015.
7. Eucentre Shake-table Test of Terraced House Modelling Predictions and Analysis Cross Validation, staff from ARUP, Eucentre (Pavia) and TU Delft, November 2015 [this document also includes; (1) Instruments full-scale test-house Eucentre Laboratory, (2) Protocol for Shaking Table Test on Full Scale Building (Eucentre) V_1, and (3) Selection of Acceleration Time-Series for Shake Table Testing of Groningen Masonry Building at the EUCENTRE, Pavia, all three by staff from Eucentre (Pavia)].
8. Experimental campaign on a clay URM full-scale specimen representative of the Groningen building stock (EUC-BUILD2), Eucentre (F. Graziotti, U. Tomassetti, A. Rossi, B. Marchesi, S. Kallioras, M. Mandirola, A. Fragomeli, E. Mellia, S. Peloso, F. Cuppari, G. Guerrini, A. Penna, G. Magenes, G), 20th July 2016.
9. Collapse shake-table testing of terraced house (LNEC-BUILD1), Eucentre and LNEC (U. Tomassetti, A. A. Correia, F. Graziotti, A.I. Marques, M. Mandirola, P.X. Candeias), 1st September 2017.



NAM

Title	Out-of-Plane Two-Way Bending Shake-Table tests on both Single Leaf and Cavity Walls		Date	July 2018
			Initiator	NAM
Autor(s)	Satyadhrik Sharma, Umberto Tomassetti, Luca Grottoli, Francesco Graziotti	Editors	Jan van Elk and Jeroen Uilenreef	
Organisation	Eucentre in Pavia (European Centre for Training and Research in Earthquake Engineering)	Organisation	NAM	
Place in the Study and Data Acquisition Plan	<p><u>Study Theme:</u> Seismic Response of Buildings (URM)</p> <p><u>Comment:</u> For the modeling of the seismic response of unreinforced masonry buildings, knowledge of the properties of building material used in the Groningen area, and the behavior of wall systems is essential. An experimental program to test the properties of the building materials (in-situ (Ref. 1) and in the laboratory (Ref. 2 and 3), the behavior of wall systems (Ref. 4 and 5) and full-scale masonry buildings (Ref. 6, 7, 8 and 9) was therefore executed. This report describes experiments carried out during 2017 and 2018 in Eucentre, Pavia, on both single-leaf and cavity walls of calcium-silicate and masonry brick. Testing of walls was done to investigate the two-way bending out-of-plane (OOP) failure mechanism of these walls, involving at least one restrained vertical edge. This is one of the most commonly reported and surveyed cause of structural damage. In total eleven tests have been described in this report. Seven of these have been performed on the uniaxial shake-table also used for testing of full scale buildings. However, four of the tests have been performed on the new multiaxial shake table at Eucentre.</p>			
Directly linked research	(1) Building Material properties (2) Shake table tests (3) Fragility curves for building typologies (URM) (4) Risk Assessment			
Used data	Experiments			
Associated organisation	NAM			
Assurance	Eucentre			



EUCENTRE
FOR YOUR SAFETY.

OUT-OF-PLANE TWO-WAY BENDING SHAKING TABLE TESTS ON SINGLE LEAF AND CAVITY WALLS

Document authors

Satyadhrik Sharma^{1,3}, Umberto Tomassetti^{1,2}, Luca Grottoli¹, Francesco Graziotti^{1,2}

¹*EUCENTRE*

²*Univerity of Pavia*

³*IUSS Pavia*

Research Report

Protocol EUC137/2018U



OUT-OF-PLANE TWO-WAY BENDING SHAKING TABLE TESTS ON SINGLE LEAF AND CAVITY WALLS

Document authors

Satyadhrik Sharma^{1,3}, Umberto Tomassetti^{1,2}, Luca Grottoli¹, Francesco Graziotti^{1,2}

¹*EUCENTRE*

²*Univerity of Pavia*

³*IUSS Pavia*

Protocol EUC137/2018U

According to law, EUCENTRE Foundation trademark cannot be reproduced, copied or utilized, without the written permission of the EUCENTRE Foundation, which is the owner, except in accordance with established contract conditions pertaining to the production of this document.

July 6th, 2018, Pavia

This report can be cited as:

Sharma S, Tomassetti U, Grottoli L, Graziotti F. Out-of-Plane Two-Way Bending Shaking Table Tests on Single Leaf and Cavity Walls. Technical Report EUC137/2018U, Eucentre, Pavia, Italy.2018; <http://www.eucentre.it/project-nam/>

The research article containing the same results can be cited as:

Graziotti F, Tomassetti U, Sharma S, Grottoli L, Magenes G. Experimental response of URM single leaf and cavity walls in out-of-plane two-way bending generated by seismic excitation. *Construction and Building Materials*. 2018; In Review

ACKNOWLEDGEMENTS

This report describes an activity that is part of the “Study of the vulnerability of masonry buildings in Groningen” project at the EUCENTRE, undertaken within the framework of the research program for hazard and risk of induced seismicity in Groningen sponsored by the Nederlandse Aardolie Maatschappij BV. The authors would like to thank all the parties involved in this project, namely EUCENTRE and University of Pavia (DICAr) laboratories that performed the tests, NAM, Arup and TU Delft. Special thanks go to J. Uilenreef, R. Pinho, A. Fragomeli, S. Scherini, S. Dainotti, L. Moriconi, M. Mandirola, B. Marchesi, F. Dacarro, S. Peloso, and S. Girello for the practical support.

ABSTRACT

Insight into damage observations from recent seismic events has confirmed that the activation of out-of-plane (OOP) local mechanisms is one of the major causes of structural collapse in unreinforced masonry (URM) buildings. Such failures are mostly due to the attainment of displacement levels incompatible with equilibrium configurations for the kinematic chain of the considered mechanism rather than the exceedance of stress capacity in structural elements.

However, very little research can be found currently in literature regarding the two-way bending OOP failure mechanism of walls involving at least one restrained vertical edge despite it being one of the most commonly reported and surveyed cause of structural damage. Consequently, a research project was conceptualized in EUCENTRE Pavia aimed at achieving a better understanding of this. This experimental campaign takes a step towards addressing this lack of knowledge in the form of dynamic testing of seven full-scale calcium silicate (CS) masonry, one clay masonry and one cavity wall. Each full scale specimen composed of an OOP panel and one or two return walls varying in terms of boundary conditions, applied overburden or the presence/absence of an opening was subjected to sequences of incremental input motion till collapse. Experimental results are studied and presented in terms of deformed shapes, failure mechanisms, force-displacement hysteretic curves and in an attempt to understand the dynamic behaviour of such substructures. Detailed mechanical characterisation of all materials used in these specimens is also reported.

TABLE OF CONTENTS

ACKNOWLEDGEMENTS	V
ABSTRACT	VI
TABLE OF CONTENTS	VII
LIST OF TABLES.....	IX
LIST OF FIGURES.....	X
1 INTRODUCTION	14
2 MATERIAL CHARACTERIZATION	16
2.1 CAMPAIGN A.....	19
2.1.1 MORTAR CHARACTERISATION TESTS.....	19
2.1.2 UNIT CHARACTERISATION TESTS	22
2.1.2.1 Determination of Compressive Strength	22
2.1.2.2 Determination of Flexural Strength	23
2.1.3 MASONRY CHARACTERISATION TESTS	26
2.1.3.1 Determination of Compressive Strength	26
2.1.3.2 Determination of Shear Strength (Translational)	30
2.1.3.3 Determination of Shear Strength (Torsional)	35
2.1.3.4 Determination of Bond Strength.....	38
2.1.3.5 Out-of-Plane Flexural Strength of Masonry	41
2.2 CAMPAIGN B.....	45
2.2.1 MORTAR CHARACTERISATION TESTS.....	45
2.2.2 UNIT CHARACTERISATION TESTS	45
2.2.3 MASONRY CHARACTERISATION TESTS	46
2.2.3.1 Determination of Compressive Strength	46
2.2.3.2 Determination of Shear Strength (Translational)	46
2.2.3.3 Determination of Shear Strength (Torsional)	47
2.2.3.4 Determination of Bond Strength.....	48
2.2.3.5 Out-of-Plane Flexural Strength of Masonry	50
3 SHAKE TABLE TESTING OF FULL SCALE SPECIMENS	52
3.1 CAMPAIGN A.....	52
3.1.1 SPECIMENS GEOMETRY AND BOUNDARY CONDITIONS	52
3.1.2 TESTING SETUP AND INPUT MOTION SEQUENCES	53
3.1.2.1 Testing setup	53
3.1.2.2 Instrumentation and data acquisition.....	54
3.1.2.3 Input signals and testing sequence.....	55
3.1.3 TEST RESULTS	58
3.1.3.1 Dynamic Identification.....	58

3.1.3.2	Damage Patterns and Failure Mechanisms.....	59
3.1.3.3	Hysteretic Behaviour.....	64
3.1.3.4	Specimen Strength Capacity.....	66
3.2	CAMPAIGN B.....	68
3.2.1	SPECIMENS GEOMETRY AND BOUNDARY CONDITIONS	68
3.2.2	TESTING SETUP AND INPUT MOTION SEQUENCES	68
3.2.2.1	Testing setup	68
3.2.2.2	Instrumentation and data acquisition.....	69
3.2.2.3	Input signals and testing sequence.....	69
3.2.3	TEST RESULTS	73
3.2.3.1	Dynamic Identification.....	73
3.2.3.2	Damage pattern and failure mechanisms.....	73
3.2.3.3	Hysteretic Behaviour.....	76
3.2.3.4	Specimen Strength Capacity.....	77

LIST OF TABLES

Table 1.1: Summary of main features of full scale specimens tested in Campaign A.	14
Table 1.2: Summary of main features of full scale specimens tested in Campaign B.	15
Table 2.1 Summary of masonry mechanical properties (Campaign A)	17
Table 2.2 Summary of masonry mechanical properties (Campaign B)	18
Table 2.3: Mix proportion of mortars used for CS and Clay bricks.....	19
Table 2.4: Mean compressive and flexural strengths of mortars used for CS and clay brick masonry.	21
Table 2.5: Compressive strength of CS and clay units.	23
Table 2.6: Flexural strength of CS units.	25
Table 2.7: Flexural strength of clay units.	25
Table 2.8: Compressive strengths and elastic modulus of CS and clay masonry wallettes.	29
Table 2.9: Summary of results of direct shear testing of CS and clay masonry triplets.....	34
Table 2.10: Summary of results of torsional shear testing of CS and clay masonry doublets.	37
Table 2.11: Summary of results from bond wrench testing of CS and clay brick masonry.....	41
Table 2.12: Flexural strength of CS and clay masonry.	44
Table 2.13: Mean compressive and flexural strengths of mortars used for CS brick masonry.....	45
Table 2.14: Compressive strengths and elastic modulus of CS masonry wallettes.....	46
Table 2.15: Summary of results of direct shear testing of CS masonry triplets.....	47
Table 2.16: Summary of results of torsional shear testing of CS masonry doublets.....	48
Table 2.17: Summary of results from bond wrench testing of CS brick masonry.	49
Table 2.18: Flexural strength of CS masonry.	50
Table 3.1: Test specimens: boundary conditions and applied overburden pressure.	52
Table 3.2: Characteristics of employed input motions at scaling factor equal to 1.....	55
Table 3.3: Testing sequence of the specimens.	57
Table 3.4: Dynamic identification of the specimens.....	59
Table 3.5: Test specimens: boundary conditions and applied overburden pressure.	68
Table 3.6: Characteristics of employed horizontal input motions at scaling factor equal to 1.	70
Table 3.7: Characteristics of employed vertical input motions at scaling factor equal to 1.....	70
Table 3.8: Testing sequence of the specimens.	72
Table 3.9: Dynamic identification of the specimens.....	73

LIST OF FIGURES

Figure 2:1: Mould used for casting the specimens and resulting mortar specimens.....	19
Figure 2:2: Set-up of flexural test on the mortar sample corresponding to CS (left) and for clay (right) masonry.	20
Figure 2:3: Test setup in the laboratory for determination of flexural strength of mortar.	20
Figure 2:4: Test setup for determination of compressive strength of mortar.	21
Figure 2:5 Dimensions of units used in construction (expressed in mm).	22
Figure 2:6: Test setup in the laboratory (right) and failure of CS units (left) during determination of compressive strength of units.	22
Figure 2:7: Distribution of compressive strength of CS (right) and clay units (left).	23
Figure 2:8 : Schematic of test set-up when brick is in loaded in laying plane (left) and rotated by 90° to the loading plane(right).....	24
Figure 2:9: Test setup in the laboratory (right) and failure of CS units (left) during determination of flexural strength of units.....	24
Figure 2:10: Distribution of flexural strength of CS units along the weak (right) and strong (left) axes.	25
Figure 2:11: Distribution of flexural strength of clay units along the weak (right) and strong (left) axes.....	26
Figure 2:12: Schematic of tested CS (left) and clay (right) masonry compression wallettes.	26
Figure 2:13: Schematic of adopted instrumentation for CS wallettes tested in compression. (left-front, middle- back and right- side views respectively).	27
Figure 2:14: Schematic of adopted instrumentation for clay wallettes tested in compression. (left-front, middle- back and right- side views respectively).	27
Figure 2:15: An instrumented CS compression wallette in the laboratory.	27
Figure 2:16: Loading history (vertical stress vs time) adopted for compression testing of the wallettes.	28
Figure 2:17: Failure of CS (left) and clay (right) wallette under compression perpendicular to bed joints.....	28
Figure 2:18: Distribution of compressive strength for CS (left) and clay (right) masonry wallettes.	29
Figure 2:19: Distribution of secant elastic modulus for CS (left) and clay (right) masonry wallettes.....	29
Figure 2:20: Variation of vertical and horizontal strain with vertical stress for a CS masonry wallette.....	30
Figure 2:21: Schematic of masonry triplets tested under translational shear (left) and CS masonry specimens in the laboratory (right).	30
Figure 2:22: Instrumentation adopted for shear testing of triplets.	31
Figure 2:23: Applied loads during shear tests carried out on masonry triplets.	31
Figure 2:24:Part of test apparatus used to apply vertical pre-compression and accommodate dilatancy.	32
Figure 2:25: Actuator used to apply shear load to the specimen.	32
Figure 2:26: Test set-up in laboratory for evaluating the shear strength of masonry joints.....	33
Figure 2:27: Failure modes observed for CS masonry triplets in the laboratory.	33
Figure 2:28: Acceptable failure modes while evaluating the initial shear strength of masonry.	33
Figure 2:29 Graphical representation of Coulomb’s friction law.	34
Figure 2:30:Coulomb’s friction law representation of results of CS and clay triplets in direct shear.	35
Figure 2:31: Schematic of masonry doublets tested under torsional shear (left) and CS masonry doublets in the laboratory (right).	35
Figure 2:32: Schematic of torsional shear testing setup (left) and the testing setup in the laboratory (right).	36

Figure 2:33: Failure modes observed for CS (left) and clay (right) masonry doublets in the laboratory. 36

Figure 2:34:Coulomb’s friction law representation of results of CS and clay doublets in torsional shear. 38

Figure 2:35: Schematic of CS (left) and clay (right) masonry triplets tested for bond strength. 38

Figure 2:36: Schematic of the test setup adopted for the bond wrench test. 39

Figure 2:37: Setup for performing bond wrench tests on CS (left) and clay (right) brick masonry. 39

Figure 2:38: Example of failure modes from bond wrench tests in the laboratory. 39

Figure 2:39: Acceptable modes of failure for measuring strength of a bond in accordance with EN 1052-5. 40

Figure 2:40: Distribution of bond strengths along with associated failure mode for CS (left) and clay (right) masonry. 41

Figure 2:41: Schematic of specimens tested for evaluating flexural strength of CS masonry 42

Figure 2:42: CS masonry specimens tested for flexural strength in the laboratory. 42

Figure 2:43: Load supports and instrumentation. 42

Figure 2:44: Instrumentation used for each specimen. 43

Figure 2:45: Test setup adopted in the laboratory for determining the flexural strength of masonry. 43

Figure 2:46: Line failure observed for CS masonry wallettes tested for flexural strength in the laboratory. 44

Figure 2:47: Force vs. mid-span displacement for CS masonry Wallette. 45

Figure 2:48: Distribution of compressive strength for CS masonry wallettes. 46

Figure 2:49: Distribution of secant elastic modulus for CS masonry wallettes. 46

Figure 2:50:Coulomb’s friction law representation of results of CS and clay triplets in direct shear. 47

Figure 2:51:Coulomb’s friction law representation of results of CS and clay doublets in torsional shear. 48

Figure 2:52: Distribution of bond strengths along with associated failure mode for CS masonry. 49

Figure 2:53: Schematic of CS masonry wallets tested in Campaign B. 50

Figure 2:54: Force vs. mid-span displacement for a CS wallette. 51

Figure 3:1: Overall geometry of the test set-up (a), connection between top beam and rigid frame in case of CS-010/005-RR (b) and all other specimens, (c); fixity of the return wall top for single leaf (d) and cavity (e) specimens. 53

Figure 3:2: Testing layout: general view of CSW-000-RF (a) and CS-005-RR (b) testing setup, spring system for the application of the top overburden pressure (c), support for the uplift of the top beam in case of CS-000-RF (d); fixity of the top of return walls (e), elongation of connection between rigid frame and top beam (f), connection between the top beam and beam above the return walls (g). 54

Figure 3:3. Acceleration time histories of the employed table motions (a) 5% damped acceleration (b) and displacement (c) response spectra. 56

Figure 3:4. Example scheme of crack pattern associated with different damage states. 58

Figure 3:5: CS-005-RR: evolution of the crack pattern (a-c). 3D deformed shapes in positive (top) and negative (bottom) directions: first cracking (Test #22, PTA=1.93 g, Peak MHD=+8.0 mm/-2.4 mm) (d) and failure mechanism (Test #28, PTA=0.92 g, Peak MHD=+7.2 mm/-2.9 mm) (e); pictures of specimen collapse (f-g). 60

Figure 3:6. CS-000-RF: evolution of the crack pattern (a-b). 3D deformed shapes in positive (top) and negative (bottom) directions: first cracking (Test #18, PTA=1.28 g, Peak TD=+12.8 mm/-8.4 mm) (c) and failure mechanism (reproduced from video); pictures of OOP panel overturning (e-f). 61

Figure 3:7. CSW-000-RF: evolution of the crack pattern (a-b). 3D deformed shapes in positive (top) and negative (bottom) directions: first cracking (Test #20, PTA=1.28 g, Peak MHD=+8.9 mm/-7.3 mm) (c) and failure mechanism (Test #27, PTA=0.91 g, Peak TD=+68.3 mm/-55.3 mm) (d); pictures of the residual deformation at the end of the test (e-f). 62

Figure 3:8. CL-000-RF: evolution of the crack pattern (a-b-c). 3D deformed shapes in positive (top) and negative (bottom) directions: first cracking (Test #21, PTA=1.33 g, Peak TD=+8.5 mm/-5.4 mm) (d) and failure mechanism (Test #23, PTA=0.91 g, Peak TD=+113.9 mm/-172.0 mm) (e); pictures of the residual deformation at the end of the test (f-g). 63

Figure 3:9. CAV-000-RF: crack pattern (a-b). 3D deformed shapes in positive (top) and negative (bottom) directions: CS inner leaf (Test #21, PTA=1.37 g, Peak TD=+40.4 mm/-25.0 mm) (c) and clay outer leaf (Peak TD=+35.8 mm/-25.4 mm) (d); pictures of residual deformation on CS inner leaf (e), failure of CS left return wall connection (f, top), clay leaf damage (f, bottom). 64

Figure 3:10: Hysteretic response of every specimen (Location of displacement indicated by red dot)..... 66

Figure 3:11. Specimen capacities in terms of PTA vs. Wall Displacement..... 67

Figure 3:12: Testing layout: general view of the shaking table and the testing setup (a), general view of CS-000-RF2 (b) and CS-000-L1&L2 (c), return wall restrain system fixed with diagonal to the rigid frame (d), spring system for the application of the top overburden pressure and support for the uplift of the top beam (e). 69

Figure 3:13. Acceleration time histories of the employed horizontal input motions (a) 5% damped acceleration (b) and displacement (c) response spectra. 70

Figure 3:14. Acceleration time histories of the employed vertical input motions (a) 5% damped acceleration (b) and displacement (c) response spectra. 71

Figure 3:15. CS-000-RFV: crack pattern Test #20 (a), crack pattern Test #24 (b), crack pattern Test #26 (c), crack pattern Test #28 (d). 3D deformed shapes in positive (top) and negative (bottom) directions: (Test #20, PTA X=-1.07 g, PTA Z=0.52 g, Peak TD=+6.2 mm/-6.6 mm) (e), (Test #20, PTA X=0.74 g, PTA Z=-0.49 g, Peak TD=+6.2 mm/-10.7 mm) (f); pictures of specimen collapse (g-h). 74

Figure 3:16. CS-000-L1&L2: crack pattern Test #17 (a), crack pattern Test #19 (b). 3D deformed shapes in positive (top) and negative (bottom) directions: L1 portion (Test #17, PTA=0.76 g, Peak TD=+2.1 mm/-4.9 mm) (c), L2 portion (Test #17, PTA=0.76 g, Peak TD=+4.9 mm/-10.5 mm) (d); pictures of specimen collapse (e-f)..... 75

Figure 3:17. CS-000-RF2: crack pattern Test #19 (a).3D deformed shapes in positive (top) and negative (bottom) directions: (Test #18, PTA=0.91 g, Peak TD=+2.8 mm/-8.2 mm) (b); pictures of specimen collapse (c-e). 76

Figure 3:18: Hysteretic response of every specimen. 77




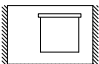

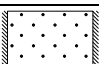
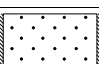
Figure 3:19. Specimen capacities in terms of PTA vs. Wall Top Displacement (TD). 78

1 INTRODUCTION

This report presents the experimental results of nine full scale unreinforced masonry walls that were tested dynamically in the out of plane direction while being subjected to two way bending. The testing of these nine walls can be organized into two separate sub-campaigns:

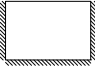
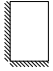


- **Campaign A:** Five full scale specimens were tested as a part of this phase of the campaign in 2017. All dynamic tests in this phase were carried out at the uniaxial shake table of EUCENTRE Pavia. The main input motions used in this part of the campaign corresponded to second floor accelerograms recorded either from a building prototype tested by Graziotti *et al.* (Graziotti, Tomassetti, Kallioras, Penna, & Magenes, 2017) or from a calibrated numerical model of the same (Kallioras, 2017). More details about these accelerograms can be found in 3.1.2.3. Specimens tested in this part of the campaign were constructed in both CS and clay brick masonry. Mortar used for the construction of the CS specimens in this campaign also generally corresponded to a higher strength than compared to Campaign B. A summary of the main features of the specimens tested in this part of the campaign can be observed in Table 1.1. Detailed results of this part of the campaign are provided in section 3.1.

Table 1.1: Summary of main features of full scale specimens tested in Campaign A.

Specimen	l_{oop} [m]	m [kg]	σ_v OOP wall [MPa]	σ_v RET wall [MPa]	Horizontal restrain condition	Scheme
	h_{oop} [m]					
CS-010-RR	3.98	2056	0.10	0.10	Fixed (R) Fixed (R)	
	2.75					
CS-005-RR	3.98	2056	0.05	0.05	Fixed (R) Free (F)	
	2.75					
CS-000-RF	3.98	2056	0	0.05	Fixed (R) Free (F)	
	2.75					
CSW-000-RF	3.98	1530	0	0.05	Fixed (R) Free (F)	
	2.75					
CL-000-RF	4.02	2178	0	0.05	Fixed (R) Free (F)	
	2.76					
CAV-000-RF	CS	2056	0	0.05	Fixed (R) Free (F)	
	3.98					
	Clay	2375	0	0.05	Fixed (R) Free (F)	
	2.76					

- **Campaign B:** Four full scale specimens were tested as a part of this phase of the campaign in 2018. All dynamic tests in this phase were carried out at the multiaxial shake table of EUCENTRE Pavia. The main input motions used in this part of the campaign corresponded to first floor accelerograms recorded either from a building prototype tested by Graziotti *et al.* (Graziotti, Tomassetti, Kallioras, Penna, & Magenes, 2017). A specimen in this campaign was also subjected to simultaneous OOP and vertical input dynamic motions. More details about these accelerograms can be found in 3.2.2.3. Specimens tested in this part of the campaign were constructed in only CS brick masonry. Mortar used for the construction of the CS specimens in this campaign also generally corresponded to a lower strength than compared to Campaign A. A summary of the main features of the specimens tested in this part of the campaign can be observed in Table 1.2. Detailed results of this part of the campaign are provided in section 0.

Table 1.2: Summary of main features of full scale specimens tested in Campaign B.

Specimen	l_{OOP} [m] h_{OOP} [m]	m [kg]	σ_v OOP wall [MPa]	σ_v RET wall [MPa]	Horizontal restrain condition	Scheme
CS-000-RFV	3.98 2.75	2056	0	0.05	Fixed (R) Free (F)	
CS-000-L1&L2	L1 1.76 2.75	910	0	0.05	Fixed (R) Free (F)	
	L2 2.21 2.75	1140	0	0.05	Fixed (R) Free (F)	
CS-000-RF2	3.98 2.75	2056	0	0.05	Fixed (R) Free (F)	

Both sub-campaigns also involved detailed material characterization tests of units, mortar as well as masonry as assemblage. These tests were performed complying with recommendations of the latest European norms wherever applicable but non standardized charecterization tests were also developed as well as performed. Results as well as procedures followed in these tests for both sub-campaigns are provided in section 2. All material characterization tests reported here were performed in the DICAR Laboratory of the University of Pavia.

2 MATERIAL CHARACTERIZATION

The specimens tested on shake table were accompanied by complementary detailed material characterisation on both constituents (units and mortar) as well as masonry as a composite. In particular the following tests were performed:

- The flexural (f_t) and compressive strength (f_c) of the mortar were determined according to the prescriptions of EN 1015-11 (1999).
- The compressive (f_b) and flexural tensile strength (f_{bt}) of units in two laying planes were determined as per the guidelines of EN 772-1(2011) and NEN 6790 (2005) respectively. Since CS units from the same batch were used in both Campaign A and Campaign B, this part of material characterisation has not been repeated for Campaign B.
- Masonry wallets were tested in compression in the direction perpendicular to the horizontal bed-joints, according to EN 1052-1 (1998). These tests allowed the determination of the compressive strength of masonry (f_m), as well as the secant elastic modulus of masonry at 33% of the compressive strength (E).
- Masonry triplets were also subjected to translational shear tests for the determination of the initial shear strength (f_{v0}) and friction coefficient (μ), according to the guidelines given in EN 1052-3 (1998).
- In addition to traditional shear tests, torsional shear tests were also performed on masonry doublets with reduced bedded area representative of the overlap between adjacent bricks in two successive courses in a wall. This allowed the determination of the initial torsional shear strength ($f_{v0,tor}$) and friction coefficient (μ_{tor}). No guidelines currently exist for such tests to the knowledge of the authors.
- Bond wrench tests on masonry triplets and doublets were performed in order to determine the bond strength of masonry (f_w), according to EN 1052-5 (1998).
- The out-of-plane flexural strength (f_{s2}) of calcium silicate masonry was evaluated in accordance with EN 1052-2 (1999).

A detailed description of each individual characterization test is provided in the following subsections. Summary of these material properties corresponding to both parts of the experimental campaign are provided in Table 2.1 and Table 2.2 respectively.

Table 2.1 Summary of masonry mechanical properties (Campaign A) .

Material properties	Symbol	UM	CS		Clay	
			Mean	C.o.V.(%)	Mean	C.o.V.(%)
Density of masonry	ρ	$[kg/m^3]$	1833	-	2000	-
Compressive strength of mortar	f_c	$[MPa]$	8.79	17.86	4.48	11.38
Flexural strength of mortar	f_t	$[MPa]$	2.76	21.01	1.14	13.75
Compressive strength of masonry unit	f_b	$[MPa]$	15.38	6.06	46.80	11.08
Flexural strength of masonry units (weak axis)	f_{bt}	$[MPa]$	2.61	14.59	7.83	4.60
Flexural strength of masonry units (strong axis)	f_{bt}	$[MPa]$	3.16	13.61	8.50	5.29
Compressive strength of masonry in the direction perpendicular to bed joints	f_m	$[MPa]$	9.74	7.80	17.41	8.47
Elastic modulus of masonry in the direction perpendicular to bed joints (0-33% f_m)	E_m	$[MPa]$	5005	21.43	7229	24.19
Masonry (bed joint) initial shear strength (direct)	f_{v0}	$[MPa]$	0.81	-	0.17	-
Masonry (bed joint) shear friction coefficient (direct)	μ	$[-]$	0.46	-	0.67	-
Masonry (bed joint) initial shear strength (torsional)	$f_{v0,tor}$	$[MPa]$	1.81	-	1.14	-
Masonry (bed joint) shear friction coefficient (torsional)	μ_{tor}	$[-]$	1.14	-	1.55	-
Bond strength	f_w	$[MPa]$	0.95	18.15	0.41	55.25
Out-of-plane flexural strength of masonry	f_{x2}	$[MPa]$	1.29	8.52	-	-

Table 2.2 Summary of masonry mechanical properties (Campaign B) .

Material properties	Symbol	UM	CS	
			Mean	C.o.V.(%)
Density of masonry	ρ	$[kg/m^3]$	1833	-
Compressive strength of mortar	f_c	$[MPa]$	1.39	31.87
Flexural strength of mortar	f_t	$[MPa]$	0.31	50.30
Compressive strength of masonry unit	f_b	$[MPa]$	15.38	6.06
Flexural strength of masonry units (weak axis)	f_{bt}	$[MPa]$	2.61	14.59
Flexural strength of masonry units (strong axis)	f_{bt}	$[MPa]$	3.16	13.61
Compressive strength of masonry in the direction perpendicular to bed joints	f_m	$[MPa]$	7.29	11.75
Elastic modulus of masonry in the direction perpendicular to bed joints (0-33% f_m)	E_m	$[MPa]$	5943	9.61
Masonry (bed joint) initial shear strength (direct)	f_{v0}	$[MPa]$	0.55	-
Masonry (bed joint) shear friction coefficient (direct)	μ	$[-]$	0.13	-
Masonry (bed joint) initial shear strength (torsional)	$f_{v0,tor}$	$[MPa]$	0.84	-
Masonry (bed joint) shear friction coefficient (torsional)	μ_{tor}	$[-]$	1.37	-
Bond strength	f_w	$[MPa]$	0.22	51.05
Out-of-plane flexural strength of masonry	f_{s2}	$[MPa]$	0.74	8.93

2.1 CAMPAIGN A

2.1.1 MORTAR CHARACTERISATION TESTS

Characterisation tests were also performed on mortar used for both CS and clay masonry to obtain their compressive and flexural tensile strength. All tests were carried out in accordance with the European norm EN 1015-11.

SPECIMENS

Each mortar specimen tested had dimensions of 160x40x40 mm corresponding to the dimension of the mould used to cast the samples (Figure 2:1). Each specimen was kept in the mould for a period of 2-3 days. After being taken out of the mould they were kept in a moist environment for 5 days following which they were left uncovered till the test. All tests were conducted only after a 28 days of being taken out from the moist environment.

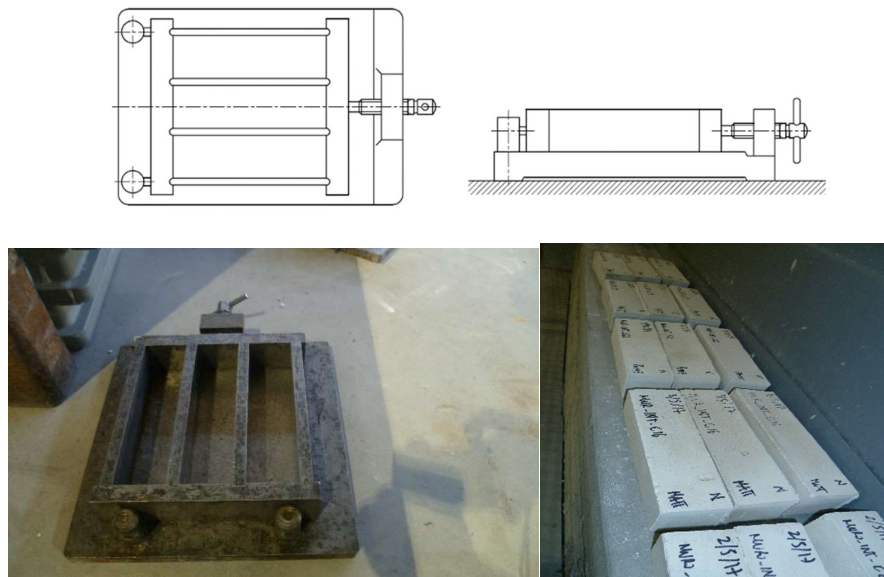


Figure 2:1: Mould used for casting the specimens and resulting mortar specimens.

It is important to note that the mortar mix used for CS and clay masonry differed in terms of water content.

Table 2.3: Mix proportion of mortars used for CS and Clay bricks.

	WATER (W)	MORTAR (M)	W/M
	[kg]	[kg]	[kg]
Mortar for CS bricks	3.5	25	14%
Mortar for Clay bricks	3.7	25	15%

All mortar specimens tested were cast during the construction of a masonry specimen. This was done to ensure characterization of mortar present in the tested masonry. Additionally, samples of mortar were cast twice per day during the construction of specimens and walls. In particular, three parallelepipeds of mortar were cast in the morning and afternoon respectively to obtain samples also representative of different phases of construction of a given masonry specimen.

TESTING PROCEDURE

Each specimen of mortar was initially tested in three point bending for obtaining the flexural tensile strength. Each specimen of mortar was supported by two rollers connected with the machine at a distance of 30 mm and 20 mm respectively from the nearer edge of mortar specimen corresponding to CS and clay brick masonry, while a third

cylinder located in the mid-span was the loading point. A schematic of the test setup used for both types of mortar specimens can be seen in Figure 2:2.

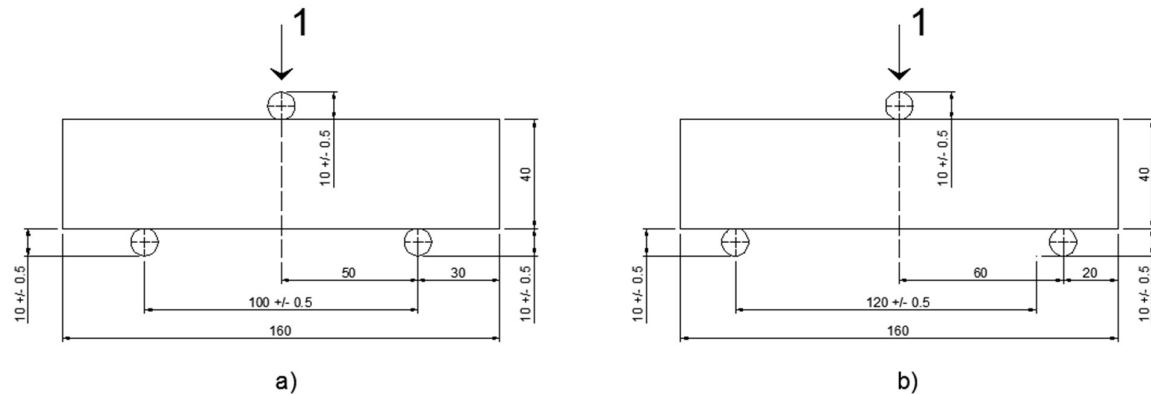


Figure 2:2: Set-up of flexural test on the mortar sample corresponding to CS (left) and for clay (right) masonry.

The difference in distances from the edges of the mortar specimens was due to the fact that two different machines with different spacing between the supporting rollers were used for mortar corresponding to CS and clay brick masonry. The machine used for mortar corresponding to CS masonry applied load at a constant rate between 50-100 N/s such that failure occurred in between 30 to 90 seconds (Figure 2:3). The machine used for mortar samples corresponding to all clay brick masonry specimens and both leaves of the cavity wall was operated in displacement control and applied displacements at a rate of 0.15 mm/min.

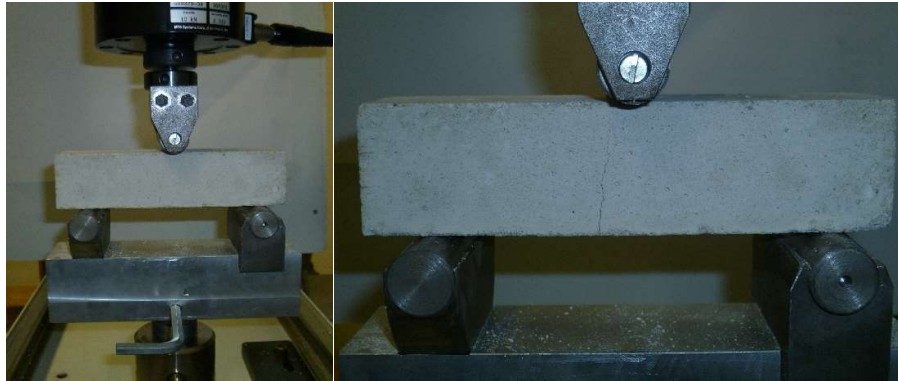


Figure 2:3: Test setup in the laboratory for determination of flexural strength of mortar.

The flexural test resulted in two broken parts of the parallelepiped of mortar which were almost identical in all cases. The test to evaluate the compressive strength is performed immediately after the flexural test, and on the prisms resulting therefrom, by applying a load until failure. The specimen is placed centered on the lower plate of the machine test with the flat face in contact to the lower plate. The upper plate of the machine is lowered until it contacts the upper face of the specimen (Figure 2:4). An increasing force is then applied gradually and without shock, in order to obtain the failure of the specimen between 30 and 90 seconds. Consequently, each mould used to cast specimens of mortar produced three specimens of mortar to be tested in flexural tension and each of these yielded two specimens to be tested in compression.

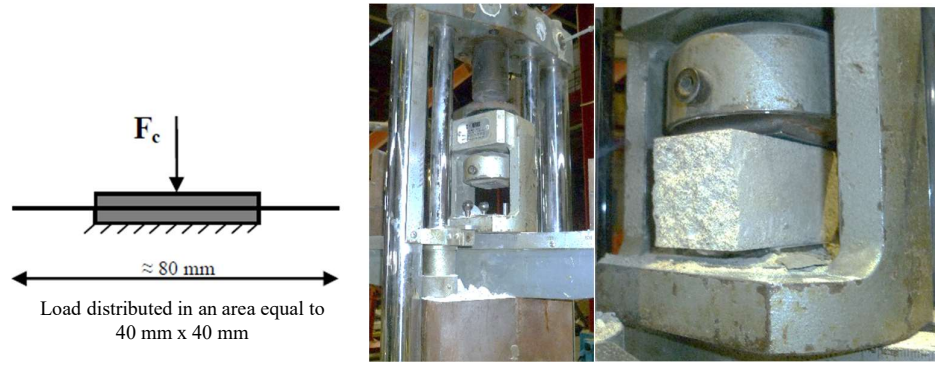


Figure 2.4: Test setup for determination of compressive strength of mortar.

RESULTS

The flexural tensile strength of the mortar specimens were evaluated according to the formula:

$$f_t = 1.5 \frac{F \cdot l}{b \cdot d^2}$$

where

F is the maximum load applied to the specimen;

l is the distance between the rollers i.e. 100 mm for CS specimen;

b is the width of the specimen = 40 mm;

d is the thickness of the specimen = 40 mm.

The compressive strength of mortar is then evaluated as:

$$f_c = \frac{F_c}{A_c}$$

where:

f_c is the compressive strength ;

F_c is the maximum compressive force applied to the specimen at the moment of failure;

A_c is the area of the specimen in contact with the plates of the machine test .

Mean flexural as well as compressive strengths of mortar used for both CS and clay brick masonry are summarised in Table 2.4.

Table 2.4: Mean compressive and flexural strengths of mortars used for CS and clay brick masonry.

	CS		Clay	
	f_c	f_t	f_c	f_t
	[MPa]	[MPa]	[MPa]	[MPa]
Mean	8.79	2.76	4.48	1.14
St.dev.	1.57	0.58	0.51	0.15
C.o.V.	17.86%	21.01%	11.38%	13.15%

2.1.2 UNIT CHARACTERISATION TESTS

Full scale specimens tested in Campaign A were constructed using CS as well as clay units. Characterisation of these units to evaluate their compressive strength as well as flexural tensile strength (along both strong and weak axis) were performed in the DICar Laboratory of University of Pavia . These tests were not repeated for the CS units used in Campaign B as units used in this campaign came from same batch. The dimensions of the used CS and clay units can be seen in Figure 2:5.

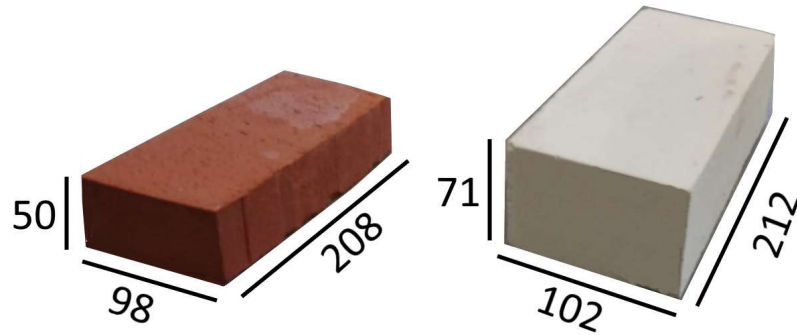


Figure 2:5 Dimensions of units used in construction (expressed in mm).

2.1.2.1 Determination of Compressive Strength

The compressive strength (f_b) of the used bricks were evaluated in accordance with the guidelines of EN 772-1(2011). The bricks were laid such that the 212x102mm and 208x98mm lay flat on plate of the compression machine i.e. the bricks were in the normal laying plane. The applied load was constantly increased from zero until the failure of the unit (Figure 2:6). Normalized compressive strengths were obtained for the bricks by multiplying experimentally obtained strengths with a shape factor depending on the width and height of the masonry units. This data for the CS and clay units are summarised in Table 2.5. The distribution of compressive strengths for both type of units can be observed in Figure 2:7.



Figure 2:6: Test setup in the laboratory (right) and failure of CS units (left) during determination of compressive strength of units.

Table 2.5: Compressive strength of CS and clay units.

No.	CS	Clay
	f_b	f_b
	[MPa]	[MPa]
1	15.39	49.69
2	15.27	40.38
3	13.83	43.52
4	14.80	40.92
5	15.16	53.63
6	16.11	49.65
7	16.97	49.72
8	14.93	-
Mean	15.31	46.80
St. Dev.	0.93	5.10
C.o.V.	6.06%	11.00%

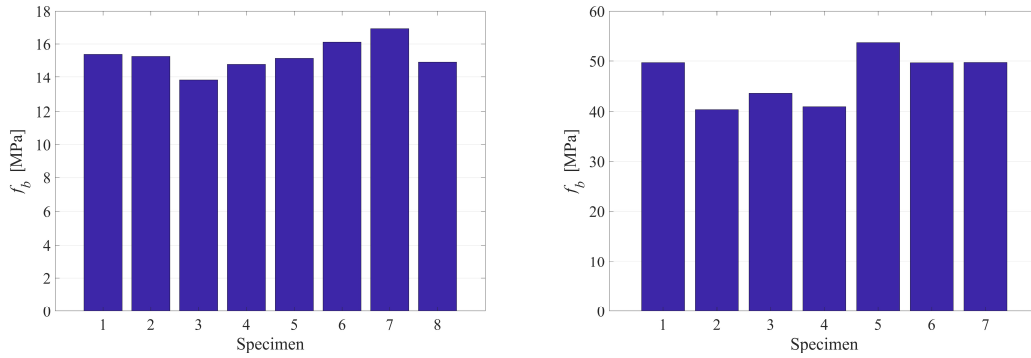


Figure 2.7: Distribution of compressive strength of CS (right) and clay units (left).

2.1.2.2 Determination of Flexural Strength

The flexural strength (f_{bt}) of the units were evaluated in accordance with the guidelines of NEN-6790 (2005). Flexural strength of units was evaluated along both their weak and strong axes i.e. brick in its normal laying plane and brick rotated by 90 degrees to its normal laying plane respectively. All units were loaded in three-point bending. Under this scheme, the specimen was supported by two rollers connected with the machine at a distance of 10 mm from the nearer edge of the brick, while a third cylinder located in the mid-span was the loading point. A schematic of how the test setup looked like in both testing directions is illustrated in Figure 2.8. The specimens were loaded monotonically till splitting of the unit was observed.

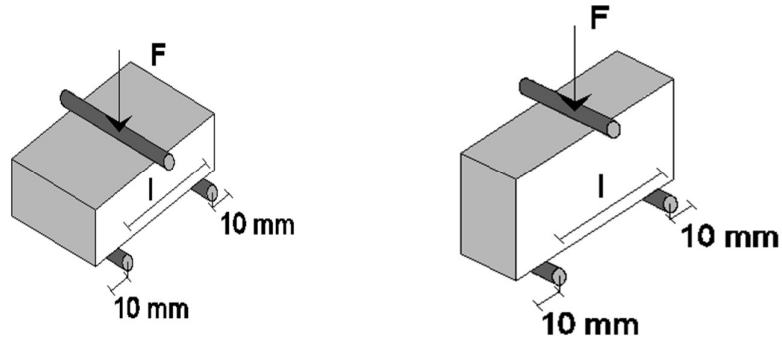


Figure 2:8 : Schematic of test set-up when brick is in loaded in laying plane (left) and rotated by 90° to the loading plane(right).



Figure 2:9: Test setup in the laboratory (right) and failure of CS units (left) during determination of flexural strength of units.

The flexural strength of the unit (f_{bt}) is then calculated as:

$$f_{bt} = 1.5 \frac{F \cdot l}{L_1 \cdot L_2^2}$$

where:

F is the ultimate load applied to the specimen;

l is the distance between the two supports/rollers;

L_1 is the dimension of the unit cross section perpendicular to the direction of loading;

L_2 is the dimension of the unit cross section parallel to the direction of loading.

Flexural strengths of CS and clay units along both axes are summarized in Table 2.6 and Table 2.7. The distribution in the flexural strength of CS and clay units can be observed in Figure 2:10 and Figure 2:11.

Table 2.6: Flexural strength of CS units.

No.	CS (Weak Axis)	CS (Strong Axis)
	f_{bt}	f_{bt}
	[MPa]	[MPa]
1	2.77	3.98
2	1.68	3.53
3	2.73	2.77
4	2.76	3.2
5	2.82	3.25
6	2.77	2.72
7	2.71	2.85
8	2.65	2.94
Mean	2.61	3.16
St. dev.	0.38	0.43
C.o.V.	14.55%	13.61%

Table 2.7: Flexural strength of clay units.

No.	Clay (Weak Axis)	Clay (Strong Axis)
	f_{bt}	f_{bt}
	[MPa]	[MPa]
1	7.71	8.30
2	7.85	8.50
3	8.09	8.80
4	7.19	7.90
5	7.97	8.40
6	8.00	9.30
7	8.35	8.10
8	7.49	-
Mean	7.83	8.50
St. dev.	0.36	0.45
C.o.V.	4.60%	5.29%

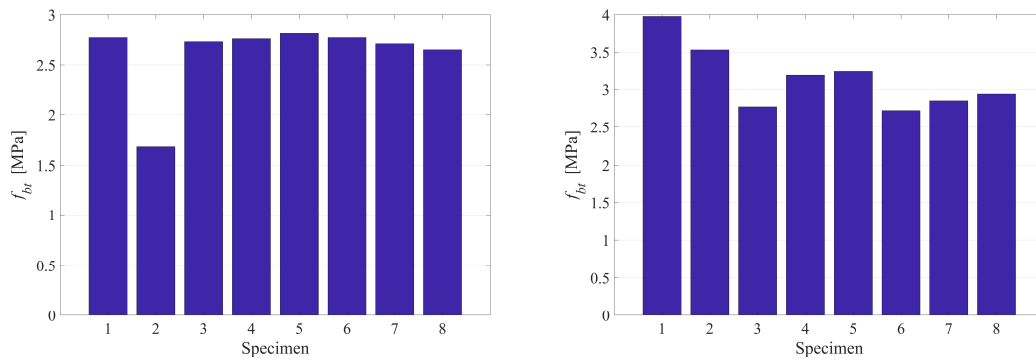


Figure 2.10: Distribution of flexural strength of CS units along the weak (right) and strong (left) axes.

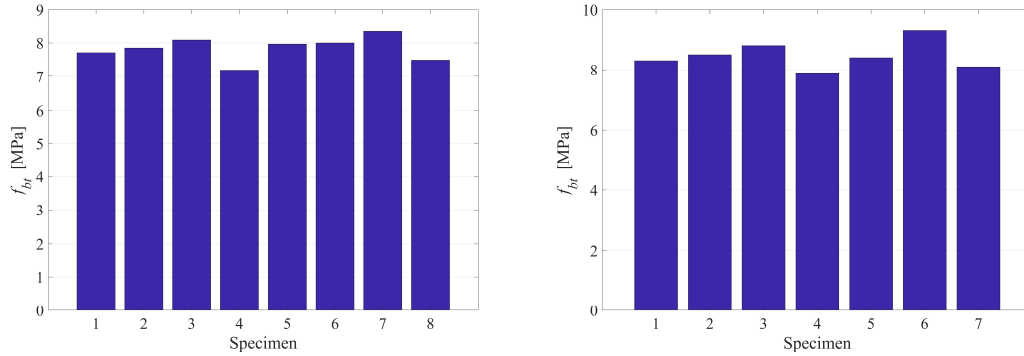


Figure 2:11: Distribution of flexural strength of clay units along the weak (right) and strong (left) axes.

2.1.3 MASONRY CHARACTERISATION TESTS

2.1.3.1 Determination of Compressive Strength

The behaviour of CS and clay masonry in compression in a direction perpendicular to bed joints was evaluated in accordance to the recommendations of EN 1052-1:1998. This test allowed the determination of the compressive strength of masonry (f_m), as well as the secant elastic modulus of masonry at 33% of the compressive strength (E_t).

SPECIMENS

EN 1052-1:1998 requires at least three wallettes conforming to certain geometrical configurations to be tested under compression perpendicular to the bed joints. Correspondingly, six wallettes of CS masonry and 7 wallettes of clay masonry were tested in compression. The mortar used for these specimens were tested to possess mean compressive strengths and flexural tensile strengths of 7.71 MPa, and 2.51 MPa respectively for CS masonry and 4.60 MPa and 1.17 MPa respectively for clay masonry. Schematic diagrams of these wallettes can be seen in Figure 2:12

Each of the specimen was instrumented with three potentiometers (two vertical and one horizontal) on each face of the wallette, resulting in a total of six potentiometers. The horizontal potentiometer was positioned at mid-height of the fourth layer of bricks. The same layout was adopted on the back side except for the difference that the horizontal potentiometer was placed at the mid-height of the third layer of bricks instead the fourth. In case of the clay wallettes, in the front side the horizontal potentiometer was placed at the fifth layer in the front and fourth layer in the back. A schematic of the adopted instrumentation for CS and clay masonry can be observed in Figure 2:13. An instrumented CS wallette in the laboratory can be observed in Figure 2:15.



Figure 2:12: Schematic of tested CS (left) and clay (right) masonry compression wallettes.

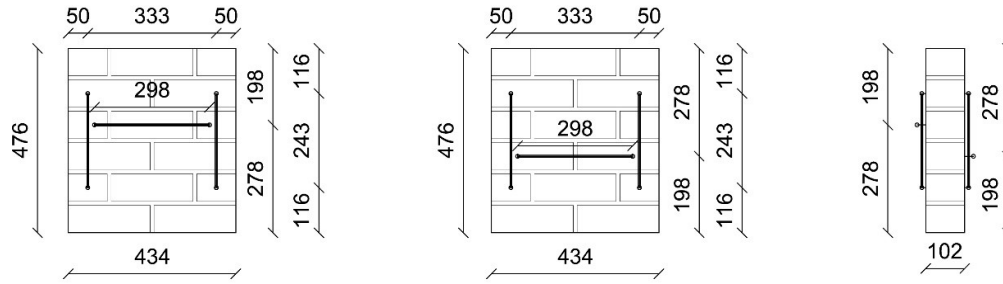


Figure 2:13: Schematic of adopted instrumentation for CS wallettes tested in compression. (left-front, middle-back and right- side views respectively).

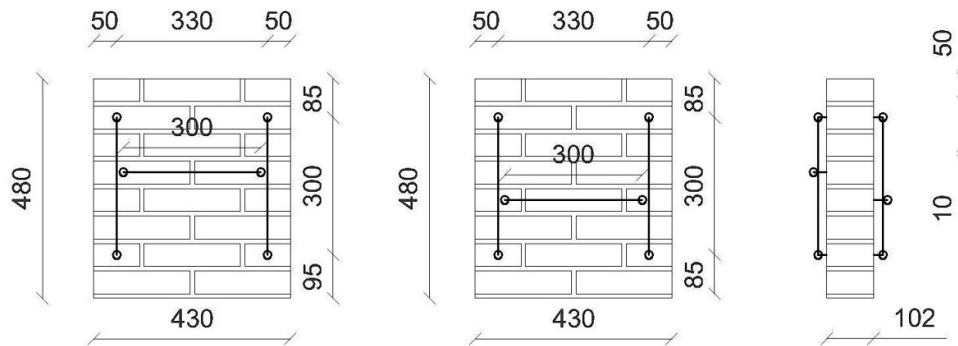


Figure 2:14: Schematic of adopted instrumentation for clay wallettes tested in compression. (left-front, middle-back and right- side views respectively).



Figure 2:15: An instrumented CS compression wallette in the laboratory.

TESTING PROCEDURE

The test envisaged the failure of the specimens by means of vertical compression load, evenly distributed and applied at their top. This vertical compressive load applied was perpendicular to the bed-joints of the masonry specimens. The loading protocol consisted of three loading steps each consisting of a series of three similar cycles of loading and unloading at constant force amplitude. Force amplitude was increased between each loading step

by approximately 100 kN. After the third cycle of the third loading step, the vertical load was increased until the failure of the specimen (Figure 2:17). The loading history adopted for compressive testing of the masonry wallettes can be observed in Figure 2:16. The loading velocity adopted was consistent with the prescriptions of EN 1052-1:1998 which allowed calculating the elastic modulus of masonry along with the compressive strength.

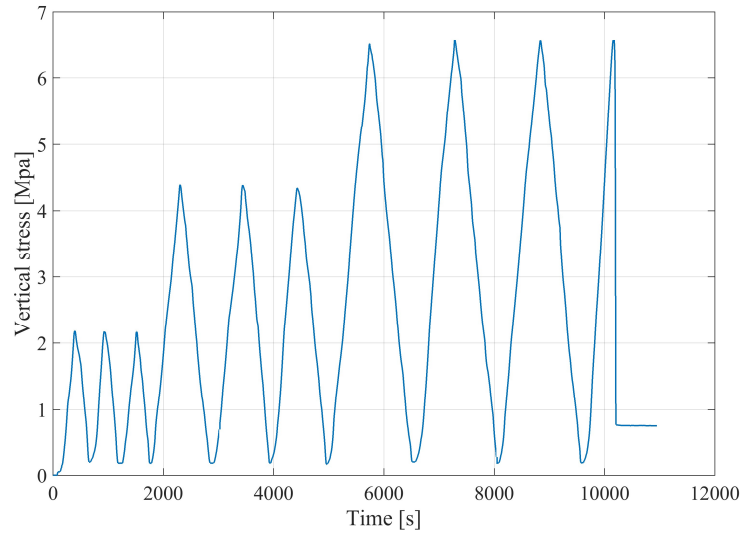


Figure 2:16: Loading history (vertical stress vs time) adopted for compression testing of the wallettes.



Figure 2:17: Failure of CS (left) and clay (right) walette under compression perpendicular to bed joints..

It is to be noted that layers of gypsum was applied on the top and bottom surface of each walette. This was done particularly to ensure an even distribution of stress and consequently remove any eccentricities in loading that may arise due to imperfections in the specimen geometry.

RESULTS

The compressive strength of masonry wallettes in compression was calculated with the following formula:

$$f_m = \frac{F_{max}}{A}$$

where:

F_{max} is the maximum force resisted by the walette ;

A is the transverse sectional area of the compression walette ;

The results of compressive strength (f_m) for all the wallettes tested are summarised in Table 2.8. Vertical and horizontal deformations/strains were calculated by averaging the deformation/strains recorded by each vertical and horizontal potentiometer in the same directions (Figure 2:20). It is to be noted that E_I is computed as the secant elastic modulus between 33% of f_m and the origin (0, 0) from a graph between vertical stress and vertical strain. The distribution of compressive strengths and secant modulus can be viewed in Figure 2:18 and Figure 2:19 respectively.

Table 2.8: Compressive strengths and elastic modulus of CS and clay masonry wallettes.

No.	CS		Clay	
	f_m	$E_I (0-33\% f_m)$	f_m	$E_I (0-33\% f_m)$
	[MPa]	[MPa]	[MPa]	[MPa]
1	10.48	6464	15.02	5919
2	9.26	4261	19.52	6615
3	9.11	5257	16.86	5333
4	10.43	5183	18.68	6855
5	10.33	3356	16.45	8016
6	8.80	5509	17.41	10322
7	-	-	15.52	6231
Mean	9.74	5005	17.41	7229
St. Dev.	0.76	1072.64	1.47	1748.89
C.o.V.	7.80%	21.43%	8.47%	24.19%

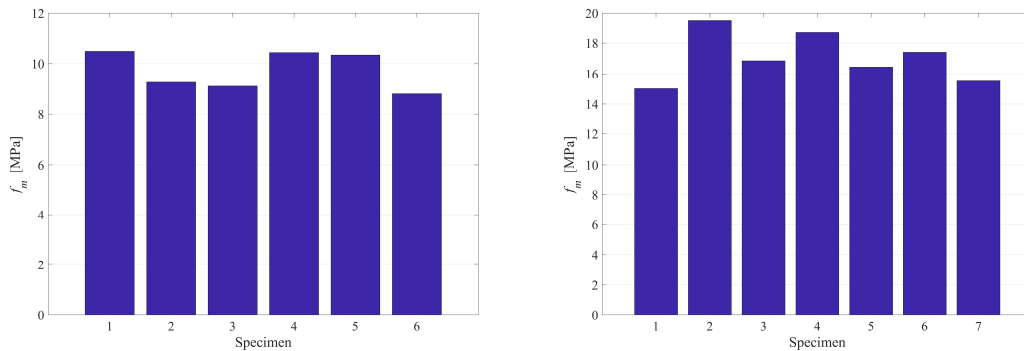


Figure 2:18: Distribution of compressive strength for CS (left) and clay (right) masonry wallettes.

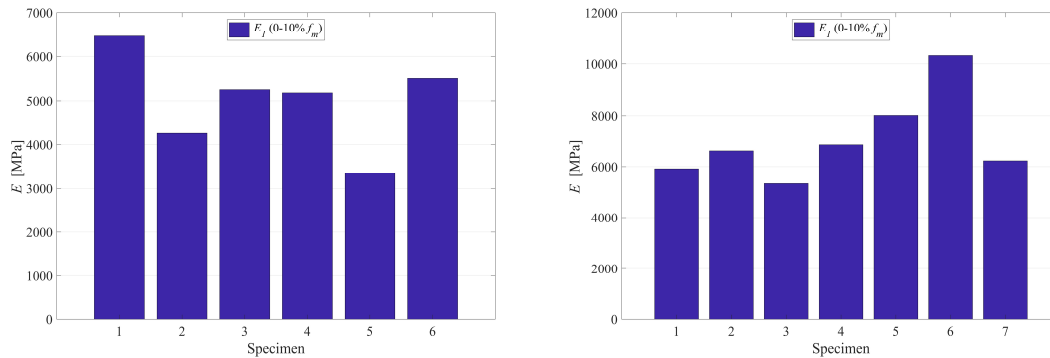


Figure 2:19: Distribution of secant elastic modulus for CS (left) and clay (right) masonry wallettes

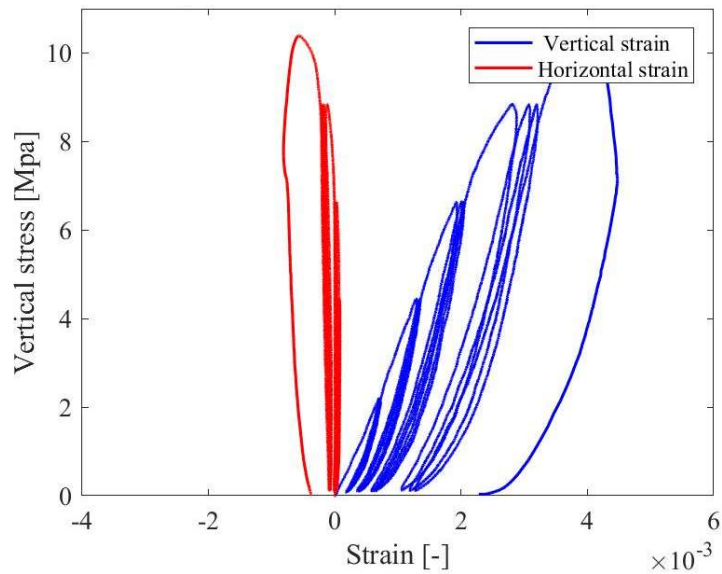


Figure 2:20: Variation of vertical and horizontal strain with vertical stress for a CS masonry wallette.

2.1.3.2 Determination of Shear Strength (Translational)

The behaviour of CS and clay masonry under translational shear was evaluated in accordance to the recommendations of EN 1052-3 (1998) and EN 1052-3/A1:2007. This test allowed the determination of initial shear strength of bed joints of masonry in terms of cohesion (f_{v0}) and friction coefficient (μ).

SPECIMENS

Direct shear tests were performed on CS and clay masonry triplets composed of three units and two bed joints. All the specimens corresponded to Type A / Type I specimens as per EN 1052-3:2002 and EN 1052-3/A1:2007 for performing this test. A schematic of the masonry triplets as well as how they looked in the laboratory can be observed in Figure 2:21.

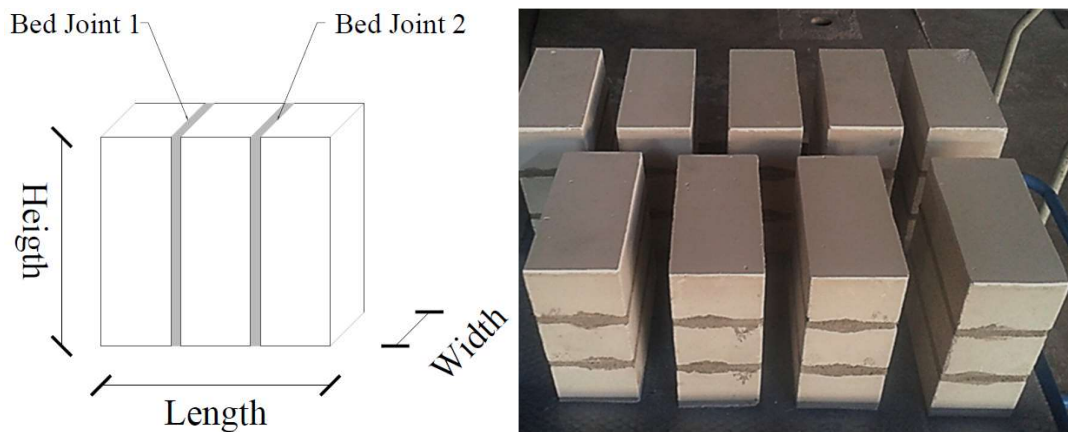


Figure 2:21: Schematic of masonry triplets tested under translational shear (left) and CS masonry specimens in the laboratory (right).

Thirteen triplets were constructed corresponding to both types of masonry, adhering to the requirements of EN 1052-3:2002 to test at least a minimum of at least nine triplets. However, results corresponding to only eleven CS masonry triplets and seven clay brick triplets could be used due to experimental anomalies.

TESTING PROCEDURE

All tests were performed in displacement control to ensure capturing of the post peak behaviour in addition to the strength to calculate the frictional coefficient. The test procedure followed in the laboratory can be summarised as:

- The specimen was rotated 90 degrees from the laying plane and then positioned in the test apparatus between two steel plates. A capping of gypsum layers was used to ensure uniform application of the pre-compression load. Two rollers were positioned below the specimen to support it. The position of these rollers corresponded to the schematic provided in Figure 2:23;
- The specimen was instrumented with one horizontal and two vertical LVDT's on both the front and back faces of the triplet. These were used for recording the evolution of the displacements in the specimens during the tests side with the purpose of analyzing the behavior of the block / mortar interface, thus registering the vertical displacement differential. A small plate fixed to the central brick, allowed the determination of the displacements in the extreme bricks relative to the central block (Figure 2:22);

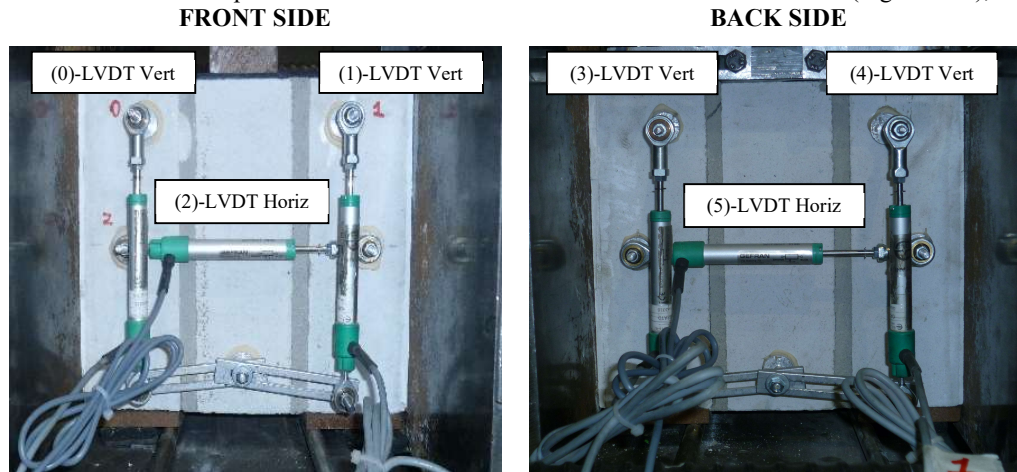


Figure 2:22: Instrumentation adopted for shear testing of triplets.

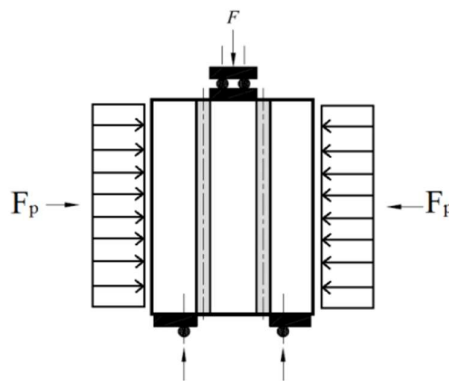


Figure 2:23: Applied loads during shear tests carried out on masonry triplets.

- A pre-compression load F_p was applied to the specimen with the help of a vertical actuator in series with a spring (Figure 2:24) . As per the recommendations of the EN 1052-3, units having a compressive resistance higher than 10 MPa (as in this case) must be subjected to three different values of F_p resulting in pre-compression stresses of 0.2 MPa, 0.6 MPa and 1.0 MPa respectively and this was maintained constant during various phases of the test. The spring in series with this actuator allowed the accommodation of dilatancy. This spring was measured to have a spring constant of 150 N/mm.



Figure 2:24: Part of test apparatus used to apply vertical pre-compression and accommodate dilatancy.

- The shear force F was applied by an actuator (functioning in displacement control) perpendicular to the central brick via two rollers placed on the inner brick and respecting the requirements of EN 1052-3 with respect to their distance from the two bed joints. This load was applied at a rate of 0.02 mm/sec respecting EN 1052-3 requirements limiting this rate to be between 0.1 MPa/min and 0.4 MPa/min and increased until failure;



Figure 2:25: Actuator used to apply shear load to the specimen.

- Post failure of the joint, the test was continued with required (if any) re-orientation of the specimen or the actuator and at different levels of pre-compression in order to estimate the frictional coefficient

The resulting test set-up adopted for evaluating the shear strength of masonry joints in the laboratory can be seen in Figure 2:26. Different failure modes observed in the lab for CS masonry triplets can be seen in Figure 2:27, which are compliant with the acceptable failure modes defined for this characterisation test by EN 1052-3 (Figure 2:28).



Figure 2:26: Test set-up in laboratory for evaluating the shear strength of masonry joints.



Figure 2:27: Failure modes observed for CS masonry triplets in the laboratory.

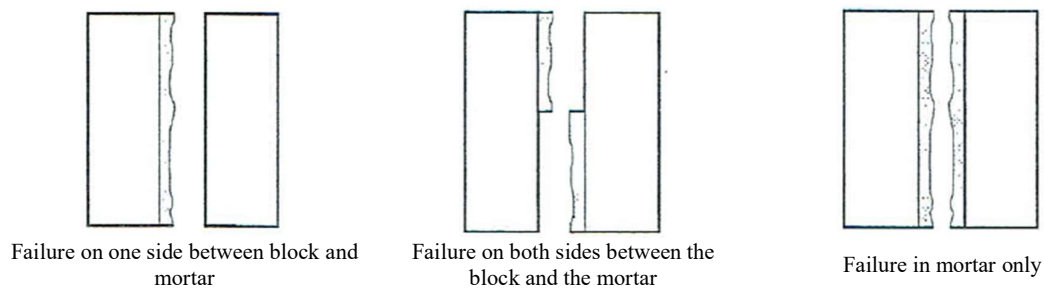


Figure 2:28: Acceptable failure modes while evaluating the initial shear strength of masonry.

RESULTS

For each specimen, the pre-compression stress and the shearing stress (at the instant of failure of the bed joint) were calculated according to the following formulas:

$$f_{pi} = \frac{F_{pi}}{A_{ei}}$$

$$f_{vi} = \frac{F_{i,max}}{2 \times A_{ei}}$$

where:

f_{pi} is the pre-compression stress ;

F_{pi} is the pre-compression force ;
 A_{ei} is the effective area of contact ;
 f_{vi} is the shear failure stress ;
 $F_{i,max}$ is the shear failure force .

Each specimen corresponds to a pair values (f_{pi} , f_{vi}). These values were plotted to obtain a Coulomb's law representation of the results (Figure 2:29). In such a representation, the shear strength of masonry triplets (f_v) depends on three parameters: cohesion, coefficient of friction and transversal compression. Cohesion contributes to the shear strength only if the bedding mortar is not cracked, while the frictional force also acts after cracking, as long as there is contact between the two materials. Thus, the shear strength (f_v) of masonry according to Coulomb's law, linearly depending on the pre-compression stress (f_p) can be mathematically represented as:

$$f_v = f_{v0} + \mu \times f_p$$

where:

f_{v0} is the cohesion ;
 μ is the friction coefficient.

For both the tested CS as well as clay masonry triplets, cohesion and internal friction angle were calculated from the results summarised in Table 2.9. It is to be noted that residual shear strengths of the bed joint calculated by continuing with the test post failure of the bed joint were used to verify the friction coefficient obtained from a Coulomb's law representation of these results (Figure 2:30).

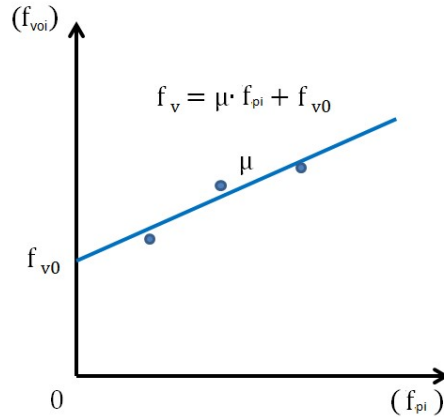


Figure 2:29 Graphical representation of Coulomb's friction law.

Table 2.9: Summary of results of direct shear testing of CS and clay masonry triplets.

No.	CS		Clay	
	f_{pi} [MPa]	f_{vi} [MPa]	f_{pi} [MPa]	f_{vi} [MPa]
1	0.199	0.848	0.200	0.364
2	0.594	0.989	0.208	0.293
3	0.950	1.248	0.209	0.235
4	0.199	0.891	0.612	0.702
5	0.597	1.118	0.595	0.562
6	0.970	1.366	0.583	0.525
7	0.196	0.922	0.926	0.751
8	0.596	1.089	-	-
9	0.972	1.367	-	-
10	0.956	1.066	-	-
11	0.188	0.982	-	-

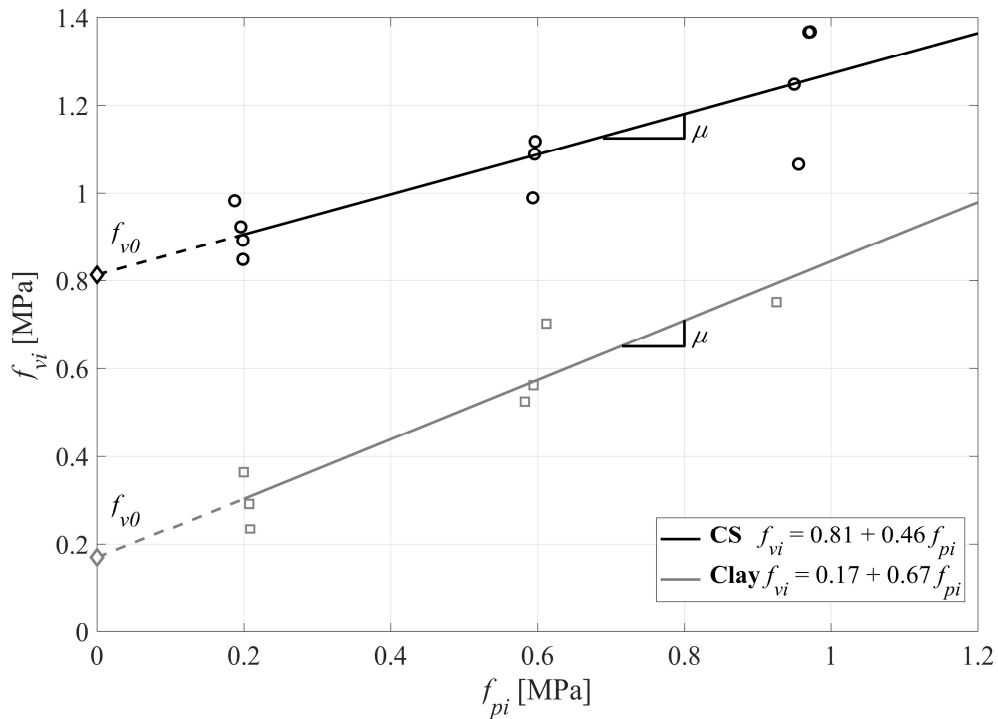


Figure 2:30: Coulomb's friction law representation of results of CS and clay triplets in direct shear.

2.1.3.3 Determination of Shear Strength (Torsional)

Unreinforced masonry when subjected to flexure about an axis normal to bed joints derives a considerable portion of its resistance from the torsional shear capacity of bed joints. While there exists a large amount of research on the behaviour of URM under the action of uniform shear stress at the brick mortar interface, very limited work is present on the response of bed joints in masonry under torsional shear where the distribution of shear stress is non-uniform. This test allowed the determination of initial shear strength of bed joints of masonry in terms of torsional cohesion ($f_{v0,tor}$) and torsional friction coefficient (μ_{tor}).

SPECIMENS

Torsional shear tests were performed on CS and clay masonry triplets composed of two units and a single bed joints. The area of this bed joint was also reduced in area to be representative of the amount of overlap over which torsional shear occurs in a real wall. A schematic of the masonry doublets as well as how they looked in the laboratory can be observed in Figure 2:31.

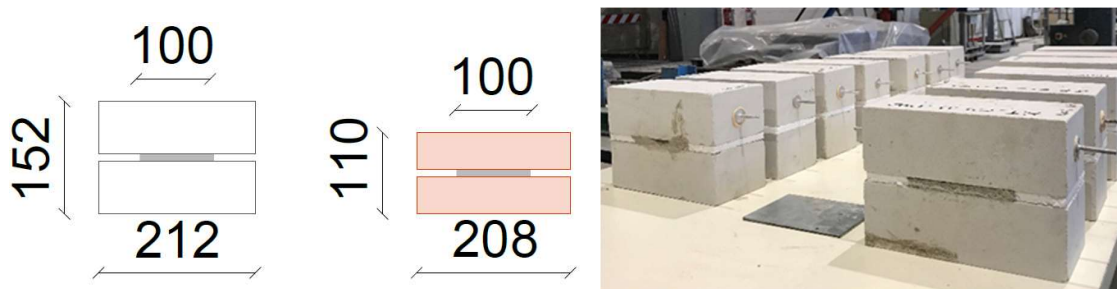


Figure 2:31: Schematic of masonry doublets tested under torsional shear (left) and CS masonry doublets in the laboratory (right).

TESTING PROCEDURE

The bottom unit was clamped and restrained from any possible movement with the help of steel profiles bolted to the test setup. A hydraulic jack was used to apply vertical pre-compression on the top of the upper brick through a thick steel plate to ensure a proper distribution of the applied stress. The level of pre-compression at which failure of the joint was envisaged was changed for each specimen in order to obtain a Coulomb's friction law representation of the results. A sheet of flexible elastomer was placed between the upper brick and this steel plate to allow dilatancy to occur while maintaining the vertical compression almost constant. Torsional shear stress in the bed joint was induced by two hydraulic jacks connected to the same circuit and hence applying the same pressure. This resulted in gradually increasing horizontal loads on steel triangular prisms attached to the bricks at a fixed distance from their ends forming a force couple. These horizontal forces were increased gradually up to failure of the bed joint was observed after which they were increased once again after changing the applied vertical pre-compression to obtain data on the post-peak residual behaviour. Horizontal displacements at both brick edges as well as vertical displacements were monitored using potentiometers. A schematic of how this test was performed and an image of the setup in the laboratory can be seen in Figure 2:32. Failure in CS masonry consisted of a crack through the mortar joint which then proceeded to the brick-mortar interface while for clay masonry, the failure always occurred only in the brick-mortar interface (Figure 2:33).

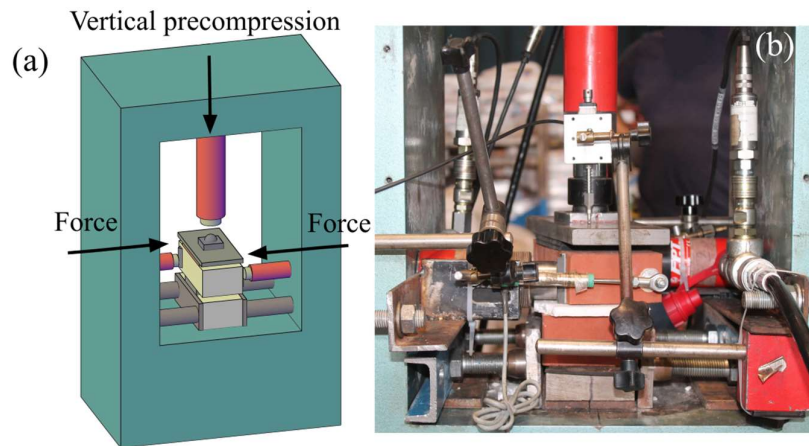


Figure 2:32: Schematic of torsional shear testing setup (left) and the testing setup in the laboratory (right).

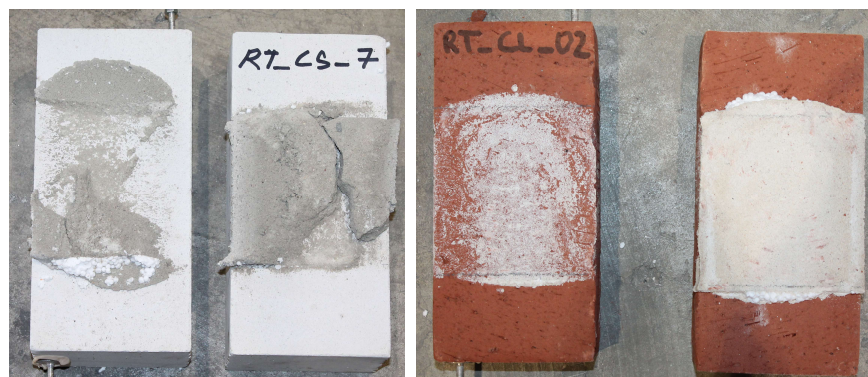


Figure 2:33: Failure modes observed for CS (left) and clay (right) masonry doublets in the laboratory.

RESULTS

For each specimen, the pre-compression stress and the torsional shearing stress (at the instant of failure of the bed joint) were calculated according to the following formulas:

$$f_{pi,tor} = \frac{F_{pi}}{A_{ei}}$$

$$f_{vi,tor} = \frac{T_{max}(3a+1.8b)}{a^2b^2}$$

where:

f_{pi} is the pre-compression stress ;

F_{pi} is the pre-compression force ;

A_{ei} is the effective area of contact ;

f_{vi} is the torsional shear failure stress ;

T_{max} is the shear failure torque;

a, b are dimensions of the mortar joint equal to 100 mm.

Each specimen corresponds to a pair of values ($f_{pi,tor}, f_{vi,tor}$). These values were plotted to obtain a Coulomb's law representation of the results, similar to what is done for direct shear testing of masonry triplets in section 2.1.3.2. For both the tested CS as well as clay masonry doublets, torsional cohesion and internal friction angle were calculated from the results summarised in Table 2.10. It is to be noted that also in this case, residual torsional shear strengths of the bed joint calculated by continuing with the test post failure of the bed joint were used to verify the torsional friction coefficient obtained from a Coulomb's law representation of these results

Table 2.10: Summary of results of torsional shear testing of CS and clay masonry doublets.

No.	CS		Clay	
	$f_{pi,tor}$ [MPa]	$f_{vi,tor}$ [MPa]	$f_{pi,tor}$ [MPa]	$f_{vi,tor}$ [MPa]
1	0.49	1.86	0.14	1.81
2	0.23	2.53	0.12	1.51
3	0.62	2.74	0.22	0.98
4	0.41	2.88	0.39	1.58
5	0.13	1.51	0.40	2.32
6	0.12	1.85	0.21	1.18
7	0.12	1.71	0.13	0.96
8	0.20	2.70	0.39	1.35
9	0.23	1.81	0.21	1.43
10	0.39	3.30	0.41	1.68
11	0.43	1.38	-	-
12	0.43	1.92	-	-
13	0.43	2.11	-	-

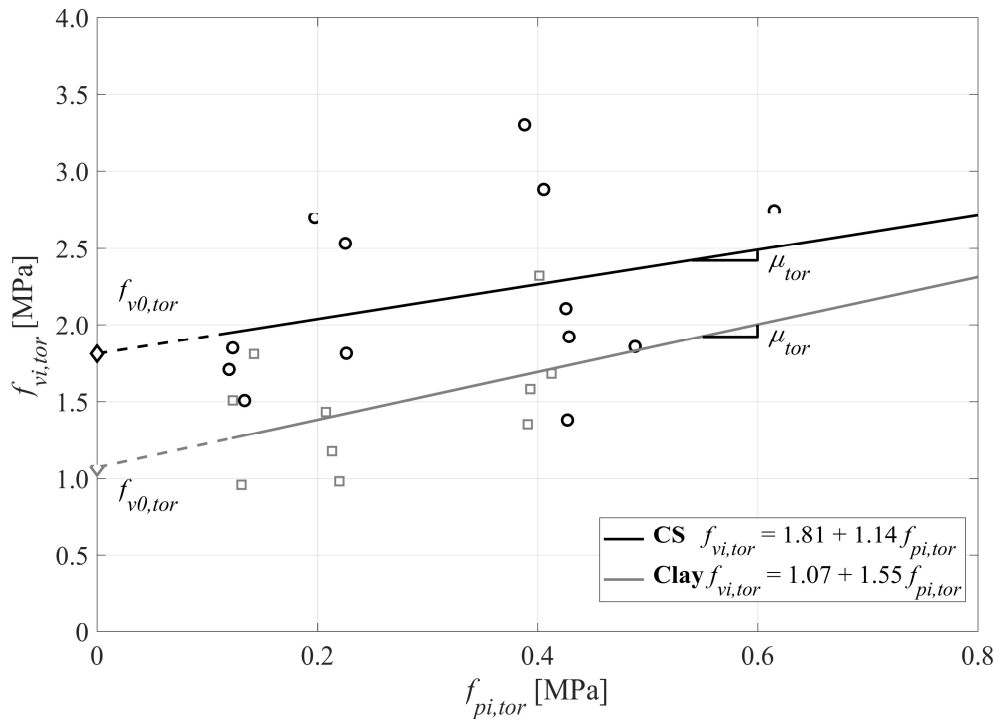


Figure 2:34: Coulomb's friction law representation of results of CS and clay doublets in torsional shear.

2.1.3.4 Determination of Bond Strength

Bond wrench tests were performed on both CS as well as clay brick masonry to evaluate the strength of the masonry joints. These tests were performed in accordance to the provisions of the European Norm EN 1052-5.

SPECIMENS

Masonry triplets i.e. three bricks bonded with two regular mortar bed-joints were used for performing the bond wrench tests. A schematic of the triplets corresponding to both types of masonry can be seen in Figure 2:35

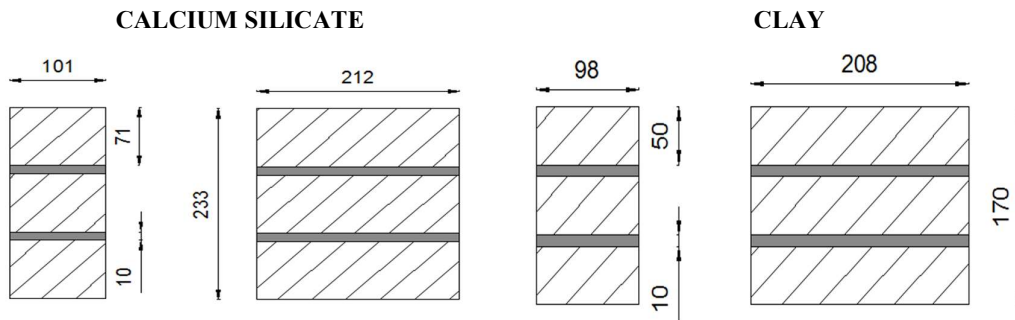


Figure 2:35: Schematic of CS (left) and clay (right) masonry triplets tested for bond strength.

TESTING PROCEDURE

A schematic of the test setup used for performing the test in the laboratory can be seen in Figure 2:36.

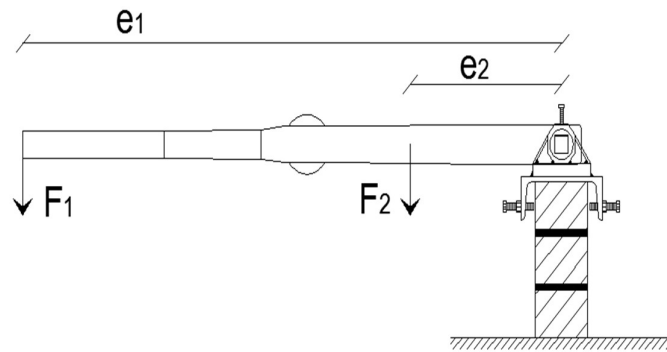


Figure 2:36: Schematic of the test setup adopted for the bond wrench test.

The triplets were first positioned on a perfectly horizontal plane and the lowermost brick was clamped between two steel profiles. This was done to ensure fixed condition of the bricks associated with the joint not being tested. This ensures that testing does not influence any bed joint other than the one being tested. A torque wrench was then connected to a steel profile (UPN UNI 5680-73) which was positioned on the top-brick and fixed to it with eight bolts. Using the instrumented torque wrench, a bending moment is applied to the clamp by a lever until the top unit is torn from the remaining part of the specimen. From the stresses achieved by the specimen, the bond strength of the masonry can be evaluated. Two different torque wrenches had to be used due to the variability of the bending moment needed to achieve failure of CS and clay masonry. The resulting test setups achieved in the laboratory can be seen in Figure 2:37.

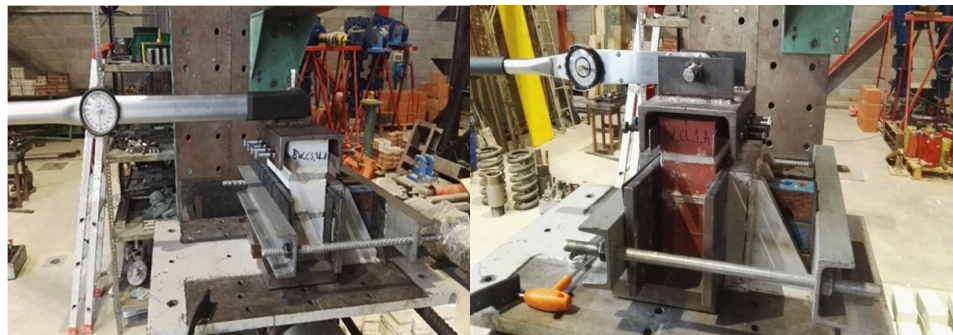


Figure 2:37: Setup for performing bond wrench tests on CS (left) and clay (right) brick masonry.

An illustration of acceptable modes of failure in accordance with EN 1052-5 can be seen in Figure 2:39. Examples of a few failure modes achieved in the laboratory can be seen in Figure 2:38. Only results conforming to failure modes acceptable as per the recommendations of EN 1052-5 (Figure 2:39).



Figure 2:38: Example of failure modes from bond wrench tests in the laboratory.

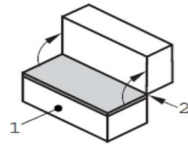


Figure A.1 — Failure at interface between mortar and upper unit

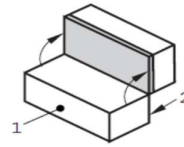


Figure A.2 — Failure at interface between mortar and lower unit

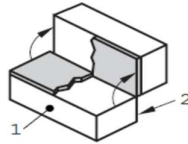


Figure A.3 — Failure at interface between mortar and both units

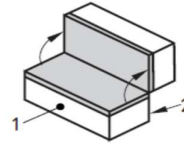


Figure A.4 — Tension failure within mortar bed

Figure 2:39: Acceptable modes of failure for measuring strength of a bond in accordance with EN 1052-5.

RESULTS

The bond wrench strength f_w associated with a bed joint was calculated with the formula:

$$f_w = \frac{F_1 \cdot e_1 + F_2 \cdot e_2 - \frac{2}{3} \cdot d \cdot (F_1 + F_2 + \frac{W}{4})}{Z}$$

where

F_1 is the failure load obtained with the torque wrench moment;

F_2 is the normal force as a result of the weight of the bond wrench apparatus;

e_1 is the distance from the applied load to the tension face of the specimen in mm;

e_2 is the distance from the centre of gravity of the lever and upper clamp from the tension face of the specimen in mm;

W is the weight of the masonry unit pulled of the specimen and any adherent mortar;

Z is the section modulus of the projected plan area of the failure surface;

d is the mean depth of the specimen.

A summary of the bond strengths measured for both CS and clay brick masonry along with the associated failure mode is provided in Table 2.11. Distribution of these strengths along with associated failure modes can be seen in Figure 2:40.

Table 2.11: Summary of results from bond wrench testing of CS and clay brick masonry.

No.	CS		Clay	
	f_w	Failure	f_w	Failure
	[MPa]	Mode	[MPa]	Mode
1	0.73	A2	0.33	A1
2	1.06	A2	0.47	A1
3	1.04	A2	0.14	A1
4	0.78	A3	0.26	A1
5	1.01	A1	0.31	A2
6	0.71	A1	0.21	A2
7	0.96	A2	0.47	A1
8	1.04	A1	0.22	A2
9	1.09	A2	0.52	A1
10	0.78	A2	0.65	A2
11	1.24	A2	0.90	A2
12	0.78	A2	-	-
13	1.14	A2	-	-
Mean	0.95		0.41	
St. Dev.	0.17		0.23	
C.o.V.	18.15%		55.25%	

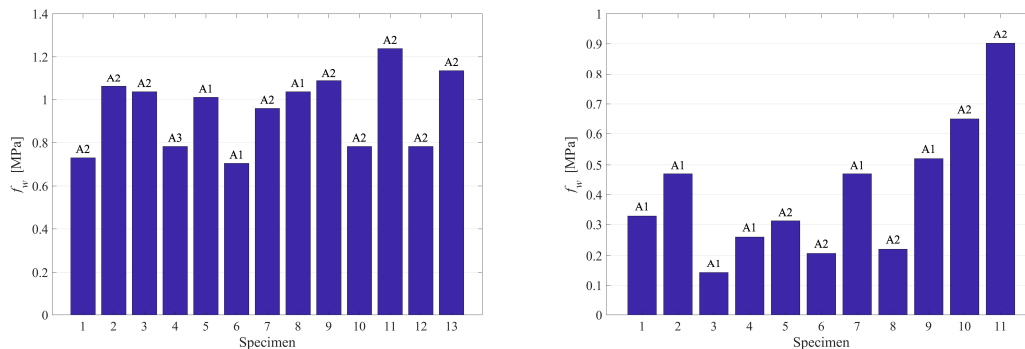


Figure 2:40: Distribution of bond strengths along with associated failure mode for CS (left) and clay (right) masonry.

2.1.3.5 Out-of-Plane Flexural Strength of Masonry

The out-of-plane flexural strength of CS and clay brick masonry in a plane perpendicular to bed-joints was evaluated in accordance with EN 1052-2. These tests allowed the determination of f_{xi} , the flexural strength of masonry.

SPECIMENS

EN 1052-2 requires a minimum of five specimens to be tested in a four point bending procedure for the evaluation of flexural strength of masonry. In accordance, six specimens of CS masonry were tested. Specimens of clay masonry were also tested but the tests were not successfully performed in a four point bending scheme and hence these results are not reported here.

Schematic diagrams of the specimens tested in laboratory along with the locations of load application can be observed in Figure 2:41. Pictures of the specimens in the laboratory can be seen in Figure 2:42.

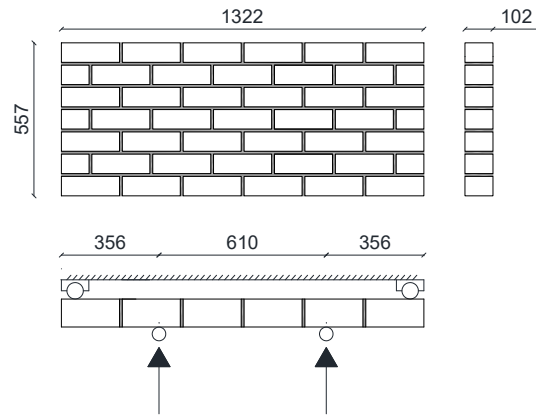


Figure 2:41: Schematic of specimens tested for evaluating flexural strength of CS masonry



Figure 2:42: CS masonry specimens tested for flexural strength in the laboratory.

TESTING PROCEDURE

The tests were performed in displacement control to allow the determination of the peak as well as to capture the post-peak behavior. In accordance to the recommendations of EN 1052-2, the tests were performed in four-point bending and failure of the specimen was reached due to a horizontal force applied by an hydraulic jack trough two rollers welded on a steel profile, as seen in Figure 2:43.

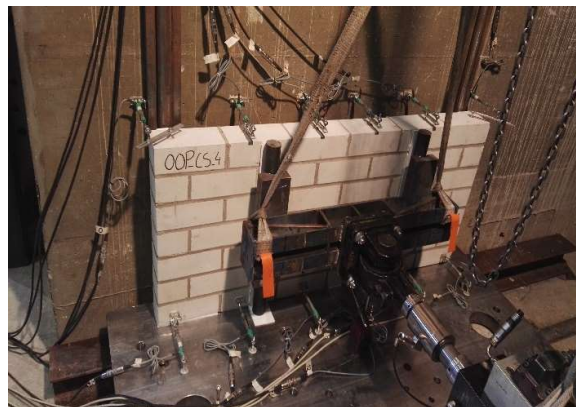


Figure 2:43: Load supports and instrumentation.

The testing procedure adopted can be summarized as:

- The specimen was positioned on a mobile steel platform and aligned with the supports. PTFE (Polytetrafluoroethylene) strips were inserted between the wall and the platform to reduce friction during the experiment. It is to be noted that the specimen was initially not in contact with the rollers bearings and this was done in order to measure and ultimately subtract the friction arising between the base of the wall and the surface on which the specimen was mounted from the failure load.
- In order to minimize imperfections and to achieve a uniform distribution of the load along the specimen, thin gypsum layers were applied on the wall in correspondence to the location of the roller bearings and the loading apparatus.
- Six horizontal potentiometers were positioned both on the top and bottom of the specimen. The specimen was also instrumented with a displacement feeler in order to control the deflection and curvature in the mid-span of the specimen. The instrumentation adopted for these tests can be observed in Figure 2:44.



Figure 2:44: Instrumentation used for each specimen.

- The load was applied monotonically in two phases. In the first phase, load was applied at a rate equal to 0.05 mm/s maintained constant until the wall and the roller bearings were in contact. This phase corresponded to the measurement of friction between the base of the specimen and the surface on which it was mounted. In the second phase, the loading velocity was reduced in order to obtain more detailed information. This was done in compliance with EN 1052-2 recommendations to apply load slower than a rate of 0.03-0.3 MPa/min. The load applied at any point during the experiment was recorded by the load cell attached to hydraulic jack. Loading was monotonically increased till failure of the specimens occurred in the region between the load application points/constant bending moment region (Figure 2:46). The complete test set-up used in the laboratory can be seen in Figure 2:45 .



Figure 2:45: Test setup adopted in the laboratory for determining the flexural strength of masonry.

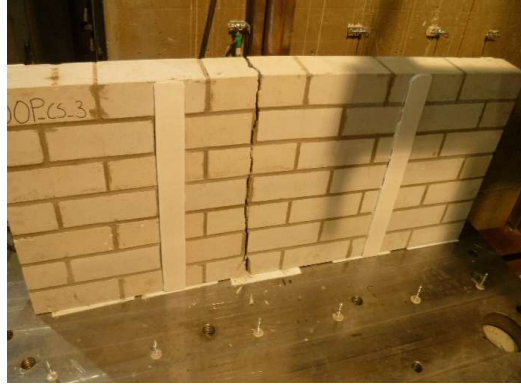


Figure 2:46: Line failure observed for CS masonry wallettes tested for flexural strength in the laboratory.

RESULTS

The flexural strength of the masonry wallettes was calculated using the expression:

$$f_{x2} = \frac{M_{max}}{W} = \frac{3 \cdot F_{i,max} \cdot (l_1 - l_2)}{2 \cdot b \cdot h_u^2}$$

$M_{i,max}$ is the maximum bending moment;

$F_{i,max}$ is the maximum total load at failure;

l_1 is the distance between the bearing supports distance;

l_2 is the distance between the rollers applying the load;

W is the section modulus of the wallette;

b is the height of the wallette;

h_u is the thickness of the Wallette.

Table 2.12 summarizes the maximum load, associated failure displacement and flexural strength of CS masonry. The applied force vs mid-span displacement for a CS and clay wallette has also been provided in Figure 2:47.

Table 2.12: Flexural strength of CS and clay masonry.

No.	CS		
	F_{max} [kN]	d_{fail} [mm]	f_{x2} [MPa]
1	9.06	0.66	1.38
2	7.36	0.51	1.13
3	7.97	0.55	1.23
4	8.28	0.58	1.3
5	8.97	0.63	1.38
Mean	8.33	0.58	1.29
St. Dev.	0.71	0.06	0.11
C.o.V.	8.52%	10.34%	8.52%

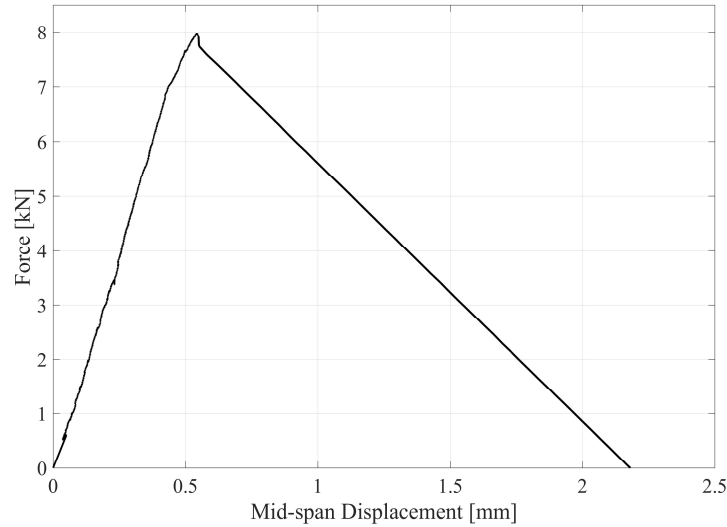


Figure 2:47: Force vs. mid-span displacement for CS masonry Wallethe.

2.2 CAMPAIGN B

As already mentioned in section 1, Campaign B involved testing of 4 new full scale specimens constructed in CS brick masonry with the same units as Campaign A but with a different and weaker mortar mix. Consequently, the same characterisation tests performed in Campaign A were performed again (wherever necessary) and adopting the same considerations reported earlier. Only results corresponding to these characterisation tests are provided here to forsake any repetition of the details related to specimens, testing procedure or processing of results. For such details, the reader is referred to section 2.1.

2.2.1 MORTAR CHARACTERISATION TESTS

SPECIMENS

It is important to note that the mortar mix used for CS masonry had higher sand content than the first campaign and corresponded to both weaker flexural and compressive strength. While the water content was kept the same, 50% (by volume) of the pre-mixed mortar was replaced by sand for the same mortar used for CS masonry in Campaign A (Table 2.3).

RESULTS

Mean flexural as well as compressive strengths of mortar used for CS brick masonry are summarised in Table 2.13.

Table 2.13: Mean compressive and flexural strengths of mortars used for CS brick masonry.

	CS	
	f_c	f_t
	[MPa]	[MPa]
Mean	1.39	0.31
St.dev.	0.44	0.16
C.o.V.	31.87%	50.30%

2.2.2 UNIT CHARACTERISATION TESTS

These tests were not performed again as the units used were the same CS units for whom compressive and flexural strengths along both axes have already been reported in section 2.1.2

2.2.3 MASONRY CHARACTERISATION TESTS

2.2.3.1 Determination of Compressive Strength

Three CS masonry wallettes were tested in compression in accordance to the recommendations of EN 1052-1:1998. The compressive strengths of these wallettes and their secant moduli are summarised in Table 2.14. The distribution of compressive strength and secant moduli can be seen in Figure 2:48 and Figure 2:49 respectively.

Table 2.14: Compressive strengths and elastic modulus of CS masonry wallettes.

No.	f_m	$E_1 (0-33\%f_m)$
	[MPa]	[MPa]
1	7.54	5363
2	6.58	5872
3	7.74	6594
Mean	7.29	5943
St.dev.	0.62	619
C.o.V.	11.75	9.61

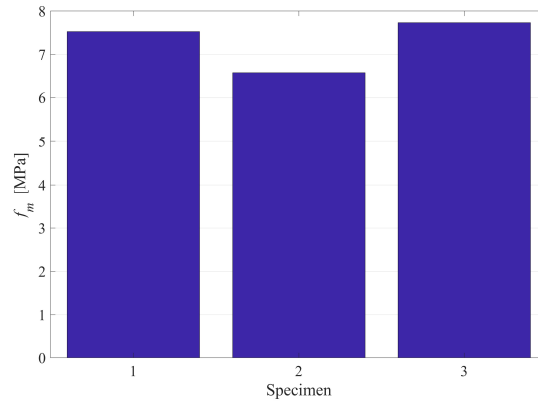


Figure 2:48: Distribution of compressive strength for CS masonry wallettes.

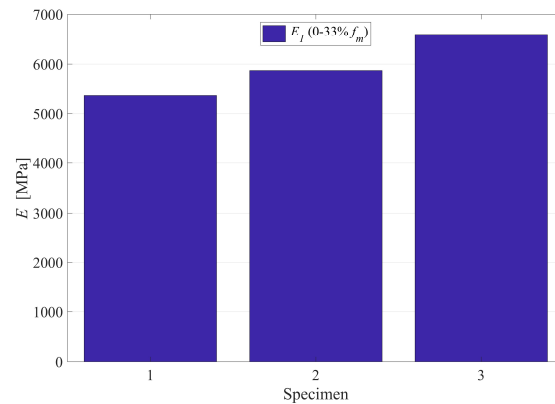


Figure 2:49: Distribution of secant elastic modulus for CS masonry wallettes.

2.2.3.2 Determination of Shear Strength (Translational)

The behaviour of CS masonry under translational shear was evaluated in accordance to the recommendations of EN 1052-3 (1998) and EN 1052-3/A1:2007. This test again allowed the determination of initial shear strength of

bed joints of masonry in terms of cohesion (f_{v0}) and friction coefficient (μ). A summary of the results tested in this part of the campaign along with a Coulomb's friction law representation of the same is provided in Table 2.15 and Figure 2:50.

Table 2.15: Summary of results of direct shear testing of CS masonry triplets.

No.	CS	
	f_{pi}	f_{vi}
	[MPa]	[MPa]
1	0.20	0.30
2	0.21	0.18
3	0.60	0.62
4	0.93	0.53
5	0.61	0.41
6	0.20	0.25
7	0.95	0.76
8	0.59	0.41

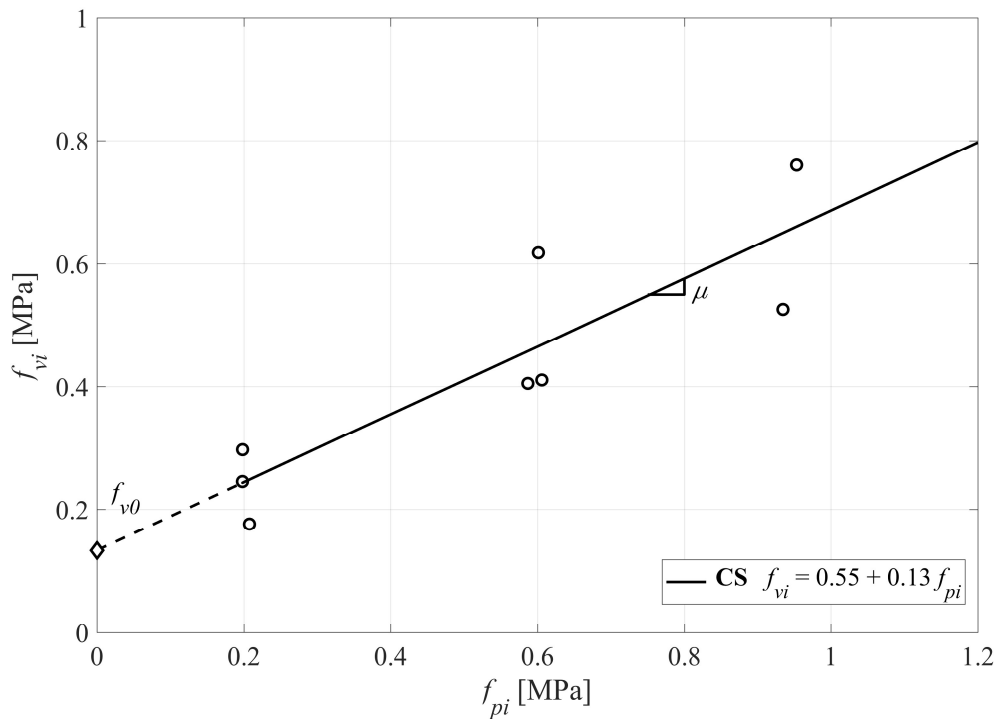


Figure 2:50: Coulomb's friction law representation of results of CS and clay triplets in direct shear.

2.2.3.3 Determination of Shear Strength (Torsional)

Torsional shear testing was performed for CS masonry doublets in this campaign as well. These results are summarized in Table 2.16 and their Coulomb's friction law representation is provided in Figure 2:51.

Table 2.16: Summary of results of torsional shear testing of CS masonry doublets.

No.	CS	
	$f_{pi,tor}$	$f_{vi,tor}$
	[MPa]	[MPa]
1	0.10	1.89
2	0.19	0.81
3	0.19	2.36
4	0.10	1.24
5	0.38	2.77
6	0.12	1.85
7	0.20	1.73
8	0.38	1.17
9	0.11	0.96
10	0.40	1.09
11	0.10	1.11
12	0.19	1.59

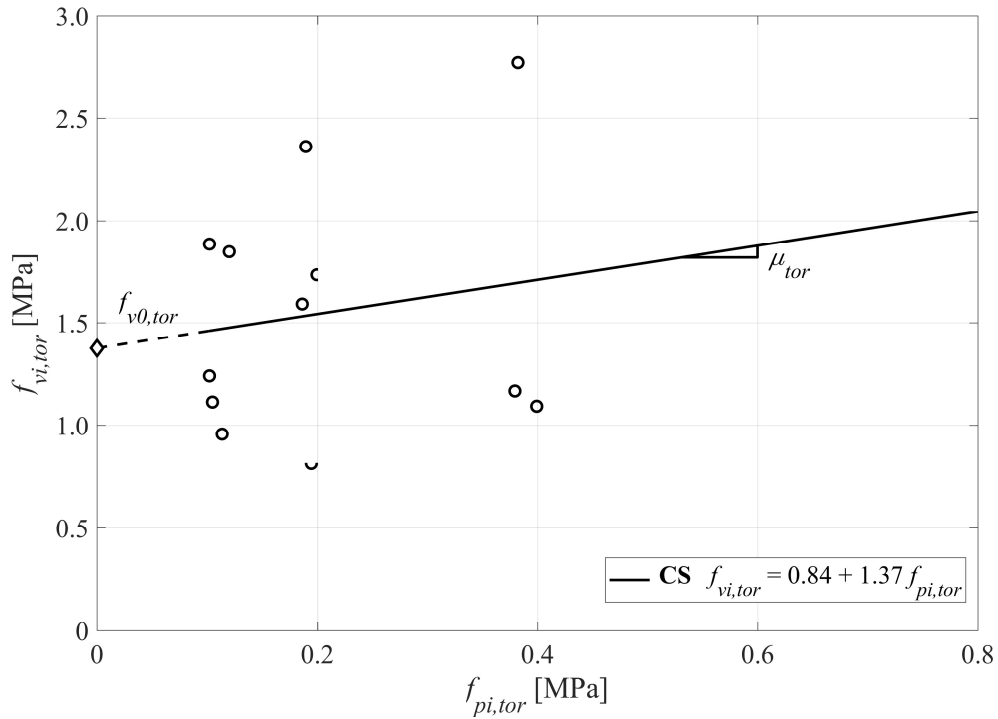


Figure 2.51: Coulomb's friction law representation of results of CS and clay doublets in torsional shear.

2.2.3.4 Determination of Bond Strength

Bond wrench tests were again performed on both CS masonry to evaluate the strength of the masonry joints. These tests were performed in accordance to the provisions of the European Norm EN 1052-5.

Table 2.17: Summary of results from bond wrench testing of CS brick masonry.

No.	<i>f_w</i>	<i>Failure</i>
	[MPa]	<i>Mode</i>
1	0.07	A1
2	0.31	A1
3	0.07	A1
4	0.39	A3
5	0.49	A4
6	0.22	A4
7	0.26	A2
8	0.14	A2
9	0.19	A4
10	0.31	A1
11	0.13	A1
12	0.24	A1
13	0.21	A1
14	0.14	A1
15	0.19	A1
Mean	0.22	
St. Dev.	0.11	
C.o.V.	51.05 %	

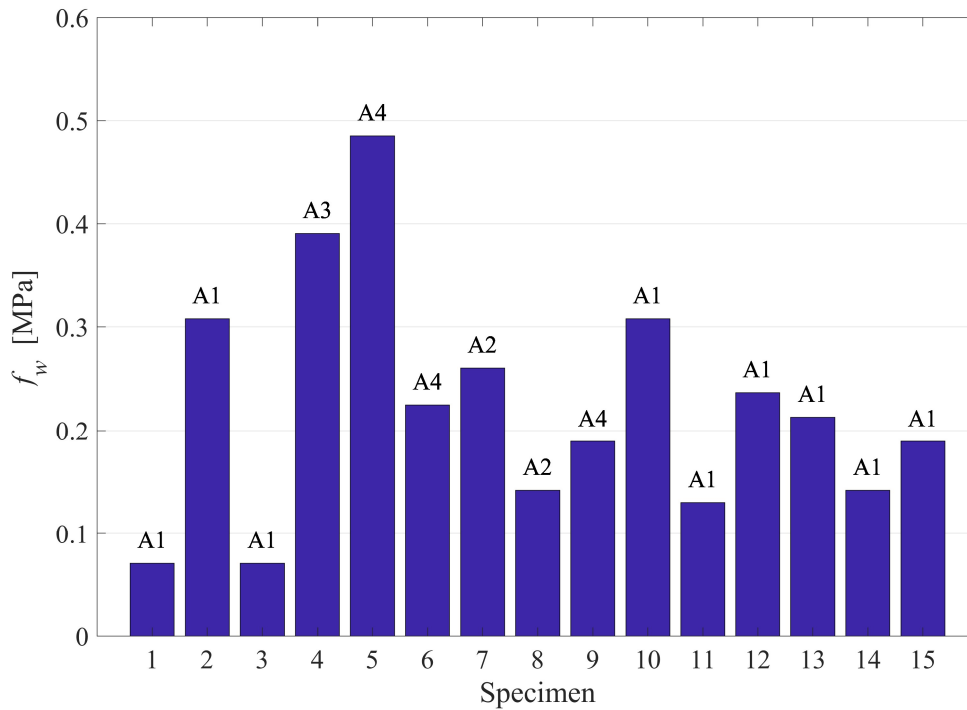


Figure 2:52: Distribution of bond strengths along with associated failure mode for CS masonry.

2.2.3.5 Out-of-Plane Flexural Strength of Masonry

The out-of-plane flexural strength of CS masonry in a plane perpendicular to bed-joints was evaluated in accordance with EN 1052-2. These tests allowed the determination of f_{xi} , the flexural strength of masonry. The dimensions of the specimen tested as well as the location of load application was changed in this part of the campaign and this can be observed in the schematic of the specimen provided in Figure 2:53

Table 2.18 summarizes the maximum load, associated failure displacement and flexural strength of CS masonry wallettes. The displacements reported here have been measured from the readings of the displacement feeler at the mid span of the wall. The applied force vs mid-span displacement for a CS wallete tested in this part of the campaign has also been provided in Figure 2:54.

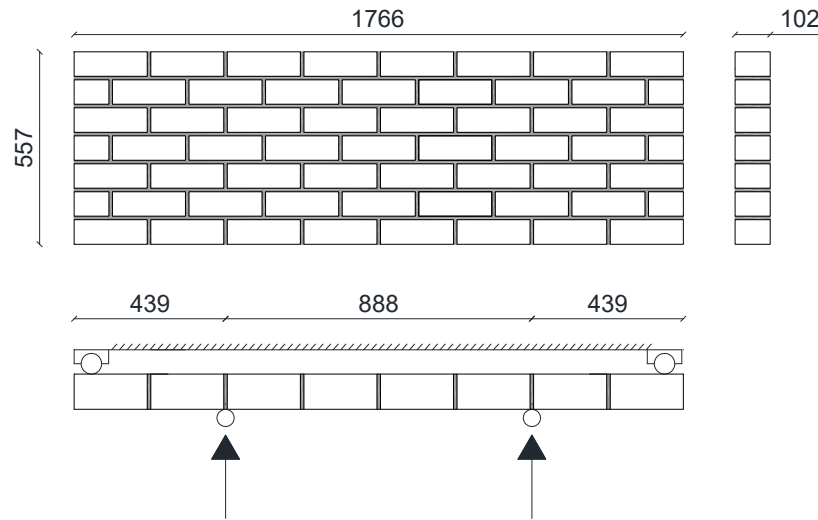


Figure 2:53: Schematic of CS masonry wallettes tested in Campaign B.

Table 2.18: Flexural strength of CS masonry.

No.	F_{max}	d_{fail}	f_{x2}
	[kN]	[mm]	[MPa]
1	6.46	0.02	0.75
2	4.52	0.01	0.64
3	5.24	0.02	0.74
4	4.95	0.03	0.70
5	5.54	0.02	0.78
6	5.87	0.02	0.83
Mean	5.43	0.02	0.74
St. Dev.	0.69	0.00	0.07
C.o.V.	12.64%	21.89%	8.93%

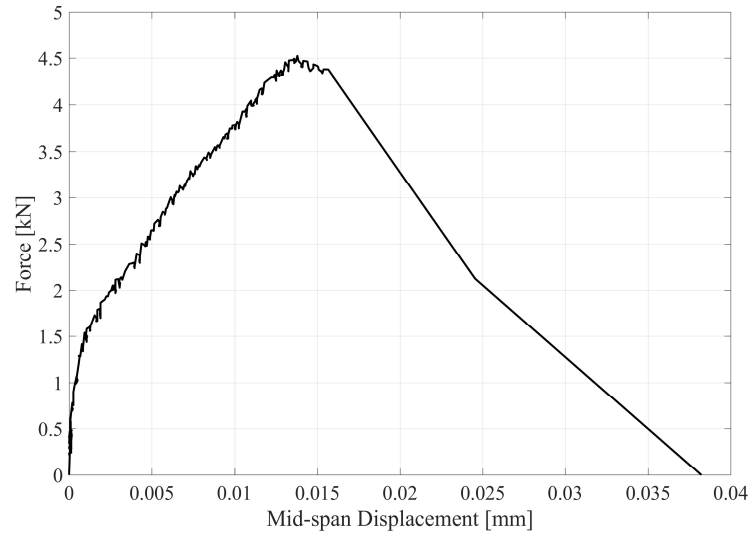


Figure 2:54: Force vs. mid-span displacement for a CS wallette.

3 SHAKE TABLE TESTING OF FULL SCALE SPECIMENS

3.1 CAMPAIGN A


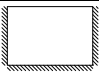
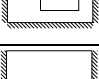
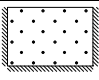
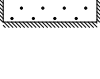


3.1.1 SPECIMENS GEOMETRY AND BOUNDARY CONDITIONS

Five full scale walls were tested dynamically in the OOP direction while being subjected to two-way bending condition in this phase of the campaign. Each tested specimen had a U-shaped plan, consisting of two 1-m-long return walls restraining a 4-m-long OOP panel on the two lateral vertical edges. Materials of the specimens were chosen to represent typical constructions of Groningen. The first three specimens corresponded to 100-mm-thick single leaf walls constructed with Calcium Silicate (CS) bricks measuring 212x102x71 mm while the fourth specimen was a single leaf wall constructed with clay bricks measuring 208x98x50 mm. Additionally, the third CS specimen had an opening which was located eccentrically. The CS walls were all constructed in 34 layers of bricks while the clay brick walls in 46 layers. Since all masonry joints were 10 mm thick, this corresponded to a total height of 2.75 m and 2.76 m for the CS and clay brick specimens. Detailed material characterisation for these specimens has already been reported in section 2.1 of this report.

The fifth specimen was a cavity wall with an outer leaf constructed with clay bricks and the inner leaf with CS bricks (having the same geometry as the first three specimens). Correspondingly, this specimen had four return walls, two per leaf. L-shaped metal connectors at a density of 2 ties/m² were used to connect the two masonry leaves. Table 3.1 specifies the specimens' name adopted throughout the rest of the article along with the OOP panel mass, boundary conditions and applied overburden pressure.

The OOP panel of the first specimen (*i.e.* tests CS-010-RR and CS-005-RR) was initially subjected to a vertical overburden stress value (σ_v) equal to 0.10 MPa. This was later decreased to 0.05 MPa to fully exploit the specimen's capacity. The resulting initial static scheme was double fixed in both, vertical and horizontal edges for both specimen configurations CS-010-RR and CS-005-RR. The OOP panel of all other specimens were unloaded with the top horizontal edge kept free. This led to a fixed-free restraint scheme in the vertical spanning direction. Such specimens can be considered representative of walls located at the top storey of a building and parallel to the spanning direction of the roof diaphragm and without any proper connection between the wall and the roof. It should be noted that a vertical overburden pressure, equal to 0.05 MPa, was applied on the top of the return walls regardless of the boundary conditions associated with the OOP panel.

Table 3.1: Test specimens: boundary conditions and applied overburden pressure.

Specimen	l_{oop} [m] h_{oop} [m]	m [kg]	σ_v OOP wall [MPa]	σ_v RET wall [MPa]	Horizontal restrain condition	Scheme
CS-010-RR	3.98	2056	0.10	0.10	Fixed (R) Fixed (R)	
	2.75					
CS-005-RR	3.98	2056	0.05	0.05	Fixed (R) Free (F)	
	2.75					
CS-000-RF	3.98	2056	0	0.05	Fixed (R) Free (F)	
	2.75					
CSW-000-RF	3.98	1530	0	0.05	Fixed (R) Free (F)	
	2.75					
CL-000-RF	4.02	2178	0	0.05	Fixed (R) Free (F)	
	2.76					
CAV-000-RF	CS	3.98	2056	0	Fixed (R) Free (F)	
		2.75				
	Clay	4.39	2375	0	Fixed (R) Free (F)	
		2.76				

3.1.2 TESTING SETUP AND INPUT MOTION SEQUENCES

3.1.2.1 Testing setup

All special considerations associated with test set-up installed and oriented to excite the specimens in OOP two-way bending condition on the uni-directional shake table of EUCENTRE are explained in this section. The specimens were anchored to the shake table through the reinforced concrete foundation by means of steel bolts. The bottom section of the specimens lay on a mortar bed-joint resting on the foundation, achieving the fixed boundary condition at the bottom. Two return walls ensured moment restraint at both the vertical edges of the OOP panel. A rigid steel frame was installed to transfer the input from the shaking table to the top of the wall. This frame was connected to a steel beam on top of the wall by four steel braces with mechanical hinges at one end (the extremity connected to the frame). Rigidly bolted connections at the other extremity prevented any relative rotations of this beam with respect to the bracing system. This system, shown in Figure 3:1 a-b, allowed any uplift of the wall while simultaneously transferring the horizontal dynamic input of the shake table to the top of the specimen with negligible amplification.

Vertical pre-compression was applied to the OOP panel in case of the first specimen (CS-010-RR) by pulling down the top beam by means of 4 steel hollow cantilevers bolted to the web of the top beam which were each connected to bars in series with a system of springs. The stiffness of the spring system was chosen to ensure that the increase in force at collapse (when the wall height is maximum assuming a rigid body uplift) is less than 5% of the initial static pre-compression. Springs having a stiffness of 53.5 N/mm were ultimately used to provide both 0.1 MPa and 0.05 MPa of vertical overburden.

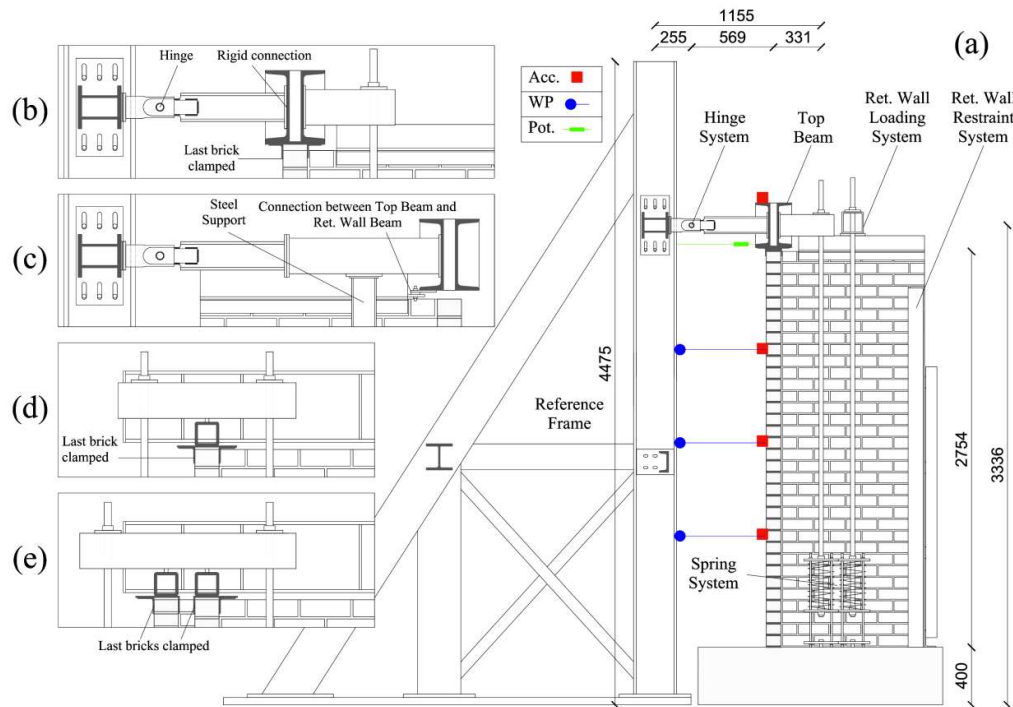


Figure 3:1: Overall geometry of the test set-up (a), connection between top beam and rigid frame in case of CS-010/005-RR (b) and all other specimens, (c); fixity of the return wall top for single leaf (d) and cavity (e) specimens.

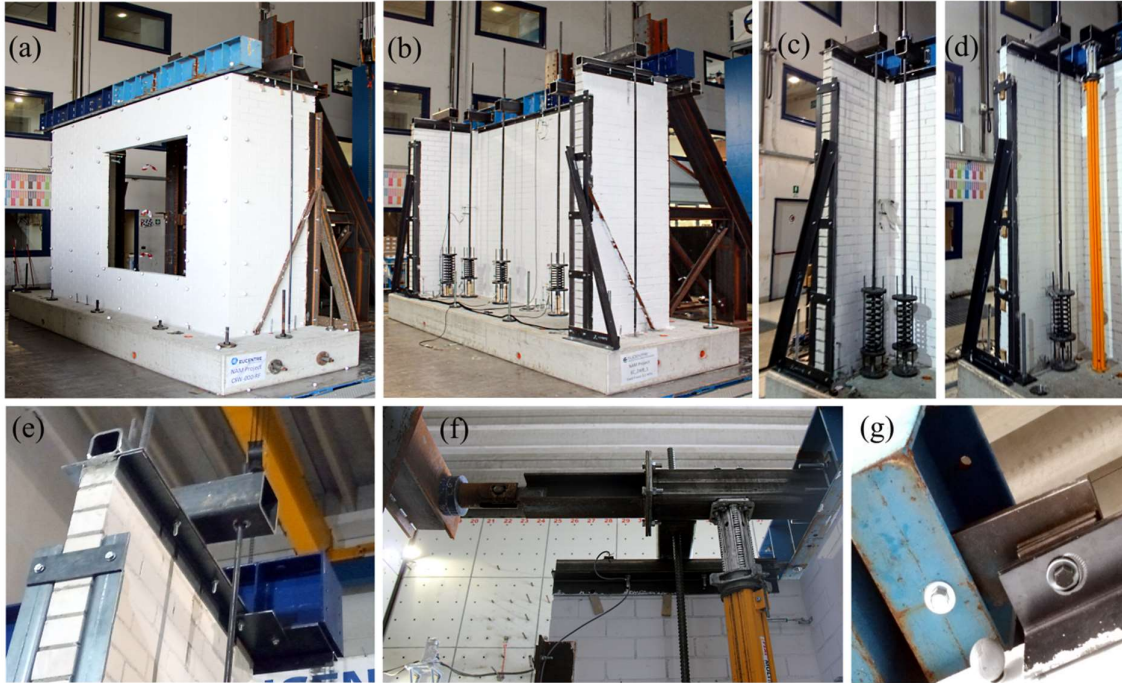


Figure 3:2: Testing layout: general view of CSW-000-RF (a) and CS-005-RR (b) testing setup, spring system for the application of the top overburden pressure (c), support for the uplift of the top beam in case of CS-000-RF (d); fixity of the top of return walls (e), elongation of connection between rigid frame and top beam (f), connection between the top beam and beam above the return walls (g).

A similar system was used to load the return walls in case of all other specimens (Figure 3:1d-e and Figure 3:2c-d-e). For the first specimen, the horizontal restraint (fixed) condition on the top of the OOP panel was guaranteed by L-shaped steel profiles bolted to the bottom of the top beam and clamping the top layer of bricks. Additionally, high strength mortar was used to fill the gap between the top row of bricks and the steel profiles (Figure 3:1b). For all other specimens, the OOP panel was unloaded and hence the top beam was lifted by steel supports in order to maintain a 30 mm air gap between the top row of bricks and the bottom edge of the top beam. Four steel plates (two per return wall) ensured the rigidity of the connection between the OOP panel top beam and the top beam for loading the return walls (Figure 3:1c and Figure 3:2g). This allowed for the transmission of the input acceleration also to the upper portion of the return walls, even in the case of OOP panels being free on top. Steel profiles were also used to clamp the free extremities of the return walls (Figure 3:2c-d) to prevent any possible OOP displacement transverse to the direction of input motion. Minor changes in terms of dimensions had to be made to the test setup in order to accommodate the cavity wall and when the entire setup was rotated to accommodate better recording of displacements using an optical acquisition system from the second specimen onwards (from Figure 3:2b to Figure 3:2a configuration and Figure 3:2f).

3.1.2.2 *Instrumentation and data acquisition*

The instrumentation adopted for each specimen in this phase of the campaign also consisted of accelerometers, potentiometers, wire potentiometers and a 3D optical acquisition system. The location of all the instrumentation adopted for each specimen was decided based on the boundary conditions envisaged and correspondingly expected deformed shapes. Accelerometers were installed on the OOP panel of the specimen in order to record acceleration-time histories. Additional accelerometers were also installed at the specimen foundation, top beam, rigid frame and the return walls. Potentiometers were used to measure relative displacements associated with various locations of the specimen. Wire potentiometers attached to the rigid frame in several locations were used to record horizontal displacements relative to the shake table. Some potentiometers were also adopted to record the relative displacements between the main panel and the return walls. Specific details of the instrumentation utilised for each wall is provided in Appendix A.

3.1.2.3 Input signals and testing sequence

Incremental dynamic tests, *i.e.* a series of table motions of increasing intensity, were performed on each specimen to fully exploit their horizontal load carrying capacity. The input sequence employed was the same as that performed by Graziotti *et al.* (Graziotti, Tomassetti, Kallioras, Penna, & Magenes, 2017). This was done to facilitate comparison between results observed for the wall specimens with that of a full-scale building prototype in which second and first-storey transverse walls were excited in the OOP direction. Primarily three input motions were used throughout the entire testing sequence: FHUIZ-DS0, FEQ2-DS3 and FEQ2-DS4. FHUIZ-DS0 was the second floor accelerogram obtained from a calibrated TREMURI (Lagomarsino, Penna, Galasco, & Cattari, 2013) model of the tested full-scale house (in an undamaged configuration) when subjected to the ground motion recorded at Huizinge, the Netherlands on 16th April 2012 (Kallioras, 2017). This represents the largest magnitude event which has occurred in Groningen field until now. FEQ2-DS3 and FEQ2-DS4 correspond to recorded second floor accelerograms of the full-scale house when subjected to ground motion EQ2 scaled up to 125% and 200%, respectively. The ground motion EQ2 was obtained from a 2015 hazard study of the Groningen region and can be deemed representative of the dynamic characteristics of the induced seismicity with an associated *PGA* of 0.16 g (Graziotti, et al., 2015). These two acceleration histories (FEQ2-DS3 and FEQ2-DS4) can be considered well representative of the progressive damage evolution between DS3/Moderate Damage and DS4/Extensive Damage which occurred in the house (Graziotti, Tomassetti, Kallioras, Penna, & Magenes, 2017).

A fourth artificial input signal, characterized by a wide spectral shape and long duration, was adopted only in order to induce a collapse of the first specimen while avoiding the unrealistic scaling of the experimental floor motions. This input signal consisted of a sequence of sine impulses with gradually increasing periods in order to excite a wide range of frequencies in the specimen. It should also be noted that the specimens were subjected to low amplitude random excitations (RN) in order to identify their dynamic properties in between test runs. Low intensity calibration runs were also performed in order to have a better control of the shaking table.

Table 3.6 specifies the adopted input floor motions and the ground motions they have been obtained from together with the associated *PGA* and *PTA*. Figure 3:13 illustrates their 100% scaled acceleration time histories along with associated acceleration and displacement (5% damped) spectra.

Table 3.2: Characteristics of employed input motions at scaling factor equal to 1.

Input	Description	GM input	GM <i>PGA</i> [g]	<i>PTA</i> [g]
FHUIZ-DS0	2 nd Floor Acc. (Numerical)	Huizinge	0.08	0.15
FEQ2-DS3	2 nd Floor Acc. (Experimental)	EQ2-125%	0.19	0.26
FEQ2-DS4	2 nd Floor Acc. (Experimental)	EQ2-200%	0.31	0.32
SSW	Artificial Record	-	-	0.5

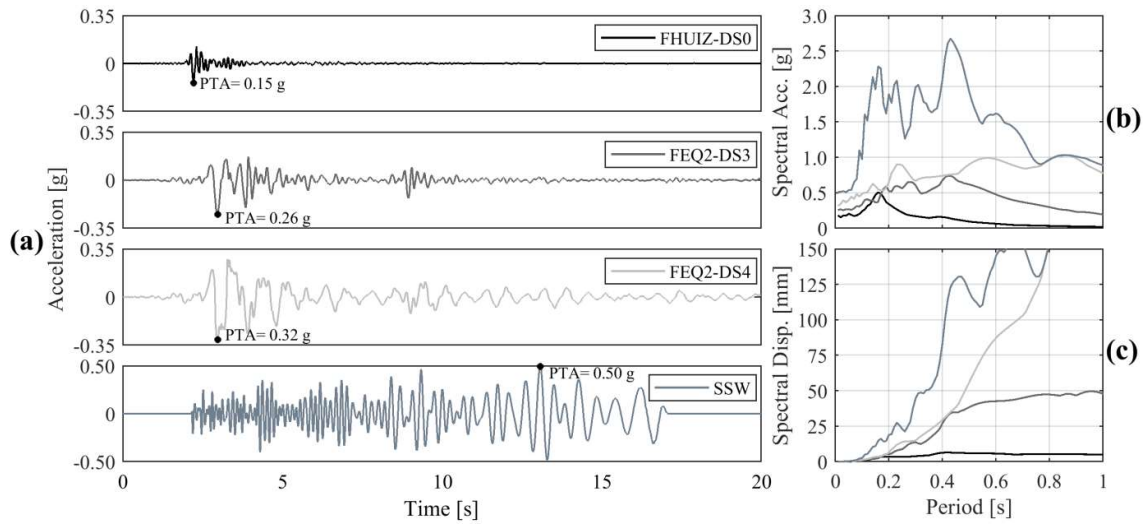


Figure 3.3. Acceleration time histories of the employed table motions (a) 5% damped acceleration (b) and displacement (c) response spectra.

The sequence of input motions each specimen was subjected to along with respective scaling factors (linear scaling with respect to *PTA*), measured *PTA* and maximum wall displacements are summarised in Table 3.3. For the first specimen (CS-010/005-RR), the reported displacement is measured at mid-height of the specimen (*MHD*-Mid height displacement) while for all other specimens this value is recorded at the top (*TD*-Top displacement). It should be noted that the part of the testing sequence when an overburden pressure of 0.10 MPa was maintained on the OOP panel has been highlighted in grey. The test marked in bold letters corresponds for each specimen the experiment after which first cracking was observed by visual inspection. No cracking prior to collapse was observed for the fifth specimen (CAV-000-RF). In general, after observations of damage which could potentially compromise the stability of the OOP panel, incremental testing was resumed again from a lower value of *PTA*.

3.1.3 TEST RESULTS

This section discusses the results of the tests: examining the wall dynamic properties and their evolution, the observed damage patterns and failure mechanisms, the specimens' capacity and hysteretic behaviour. Before discussing in detail the aforementioned aspects, it is worth noticing that the condition of each specimen at the end of each test was classified according to the definition of the following five damage states:

- DS1: no visible structural damage;
- DS2: slight structural damage;
- DS3: moderate damage with the full development of crack pattern corresponding to collapse mechanism;
- DS4: heavy damage with negligible residual capacity of resisting horizontal and vertical loads;
- DS5: very heavy damage with partial or global collapse of the panel.

Figure 3:4 shows qualitatively these different damage states. It is to be noted that the nature of dynamic testing did not allow a test-by-test stable transition between one damage state and the next one. Very often the specimens experienced more than one damage states during a single test (*e.g.* CAV-000-RF during just Test #21 transitioned from DS1 to DS5).

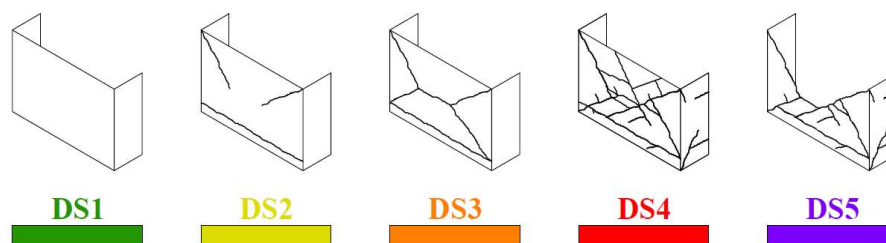


Figure 3:4. Example scheme of crack pattern associated with different damage states.

3.1.3.1 Dynamic Identification

As already mentioned in section 3.2.2.3, low amplitude random excitations (RN) were used in between test runs to identify the dynamic properties of the specimens. These tests were conducted in the testing sequence corresponding to transitions between FEQ2-DS3 and FEQ2-DS4 or when structural distress was observed. Particular interest was given especially to the frequency and time period associated with the first natural mode of vibration of the specimens. Frequency domain decomposition which is an output only system identification technique was implemented in order to identify these natural frequencies (Brincker, Zhang, & Andersen, 2000). The first natural mode of vibration of the specimens was observed to be dependent highly on the boundary conditions adopted. All specimens that had their top edge free: a wall with an opening, walls in CS and clay masonry and the cavity wall exhibited a first mode of vibration around 0.075 s (13.3 Hz) compared to 0.044 s (22.7 Hz) for the specimen with its top edge fixed in their undamaged configurations. These periods are in agreement with linear elastic eigenvalue analyses carried out for each of the walls using shell FE models constructed in SAP (Wilson, Bathe, Peterson, & Dovey, 1973). Distinct increases in the time period associated with the first natural mode of vibration could be observed in RN tests conducted after runs in which the specimen transitioned between the defined damage states (Table 3.4).

Table 3.4: Dynamic identification of the specimens.

CS-010/005-RR			CS-000-RF			CSW-000-RF			CL-000-RF			CAV-000-RF			
T#	DSi	Freq. [Hz]	T [s]	T#	DSi	Freq. [Hz]	T [s]	T#	DSi	Freq. [Hz]	T [s]	T#	DSi	Freq. [Hz]	T [s]
1	DS1	22.9	0.044	1	DS1	13.7	0.073	1	DS1	13.5	0.074	1	DS1	12.8	0.078
9	DS1	22.9	0.044	5	DS1	13.4	0.074	2	DS1	12.8	0.078	9	DS1	12.6	0.080
23	DS2	17.0	0.059	19	DS3	6.8	0.148	10	DS1	12.6	0.080	19	DS2	12.4	0.081
27	DS2	17.0	0.059	-	-	-	-	21	DS2	9.9	0.101	22	DS2	11.6	0.087

3.1.3.2 Damage Patterns and Failure Mechanisms

The progression of damage in each specimen was quite complex. Nature and location of damage often changed with increasing seismic input as the incremental dynamic test progressed. Nevertheless, detailed condition mapping was carried out after each run in the incremental dynamic test sequence and all observed cracks are reported in this section along with the test in which they were observed. In tests where the wall collapsed onto the shake table, the cracks responsible allowing for the development of the failure mechanism were reproduced from videos of the test.

To facilitate a better understanding of the failure modes of each wall, 3D deformed shapes were also constructed for critical tests. In each test, these shapes were produced at the instants in which the OOP panel had maximum displacement towards (positive) and away (negative) from the return walls. Such shapes (with a mesh of 50x50 elements along width and height of the panel) were constructed by performing linear interpolation for all points in the wall between locations where displacements were recorded and indicated by black spheres. The reported wall deflections were normalised with respect to the peak displacements occurring at that instant. Videos documenting the failure of each specimen can be viewed online (EUCENTRE. URM walls in out-of-plane two way bending (YouTube playlist). Pavia, Italy;, 2017).

CS-010-RR/CS-005-RR

The first specimen in the CS-010-RR configuration remained in the elastic range (correspondingly to DS1) over the duration of its entire testing sequence. This corresponded to a *PTA* of 0.90 g and an associated peak *MHD* of 0.6 mm. Such a stiff response indicated that the specimen in this configuration was likely to fail at table accelerations nonrealistic for low-rise URM building. Consequently, the vertical overburden on the OOP panel was reduced to 0.05 MPa. In this configuration, the specimen attained first cracking (DS2) during Test #22 (*PTA*=1.93 g, peak *MHD*=8.0 mm). First cracking consisted of a horizontal crack developed in the OOP panel and right return wall on the 2nd and 4th bed joints from the bottom. Additionally, two stepped diagonal cracks appeared from the upper right and left corners, which met around the center of the panel and continued down to the horizontal crack in the form of an almost completely straight-line crack (Figure 3:5a). The deformed shape in the negative direction was seen to be very similar to what is expected for a slab fixed in both horizontal and vertical directions. In Test #26 (*PTA*=1.39 g, peak *MHD*=9.0 mm), a line crack appeared in the connection with the right return wall extending from the horizontal crack which appeared in Test #22. Additionally, an elongation of the pre-existing horizontal crack was observed in the left return wall (Figure 3:5b). Despite the increase in observed structural distress, the specimen can be still considered to be in DS2 and this is also reflected by the fact that no change in dynamic properties of the specimen could be observed after this test (Table 3.9). The specimen collapsed (DS5) transitioning through DS3/DS4 during Test #31 (*PTA*=1.42 g). The cracks leading to the activation of the failure mechanism have been reproduced (in blue) from a careful examination of the video of the ultimate test (Figure 3:5c). It can be observed from all the deformed shapes that the part of the OOP panel below the horizontal crack occurring in Test #22 remained relatively immobilized.

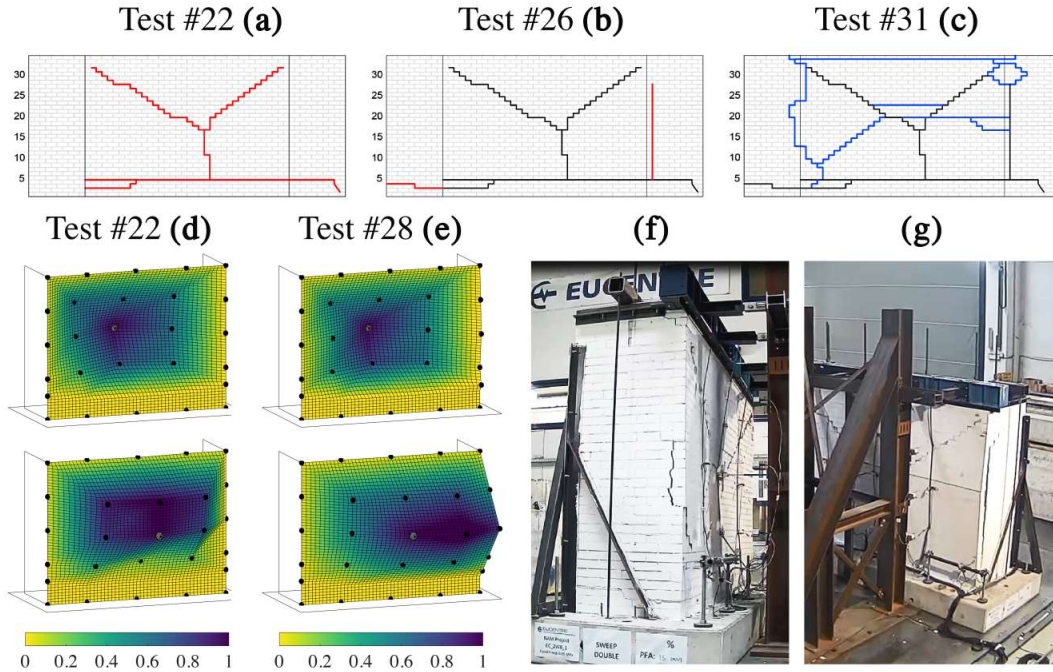


Figure 3:5: CS-005-RR: evolution of the crack pattern (a-c). 3D deformed shapes in positive (top) and negative (bottom) directions: first cracking (Test #22, $PTA=1.93$ g, Peak MHD= $+8.0$ mm/ -2.4 mm) (d) and failure mechanism (Test #28, $PTA=0.92$ g, Peak MHD= $+7.2$ mm/ -2.9 mm) (e); pictures of specimen collapse (f-g).

CS-000-RF

This wall reached first cracking condition associated with a complete development of a mechanism of the left portion of the OOP panel (DS3) during Test #18 ($PTA=1.28$ g, peak $TD=12.8$ mm). Two vertical line cracks appeared at the connection of the left return wall and at the center of the OOP panel. A smaller vertical line crack was also seen near the connection with the right return wall. Horizontal and stepped diagonal cracks could also be observed in the lower part of the OOP panel (Figure 3:6a). Deformed shapes during this test were very similar in both the positive and negative directions with highest displacements observed along the central line crack (Figure 3:6c).

The specimen reached collapse (DS5) during Test #22 ($PTA=0.62$ g). The cracks that led to the development of DS3 during this test have also been carefully reproduced from a video of the test. Full development of line cracks along the connections with both the return wall was observed (Figure 3:6b). This led to the collapse of the specimen by overturning of the part of the OOP panel above the horizontal crack together with rotation of the right and left panels about their connections with the return walls (Figure 3:6e-f). Since only limited instruments were acquiring data at this level of high seismic input, the deformed shape in Figure 3:6d does not correspond to recorded experimental data and was produced to give only a better visual representation of the failure mechanism.

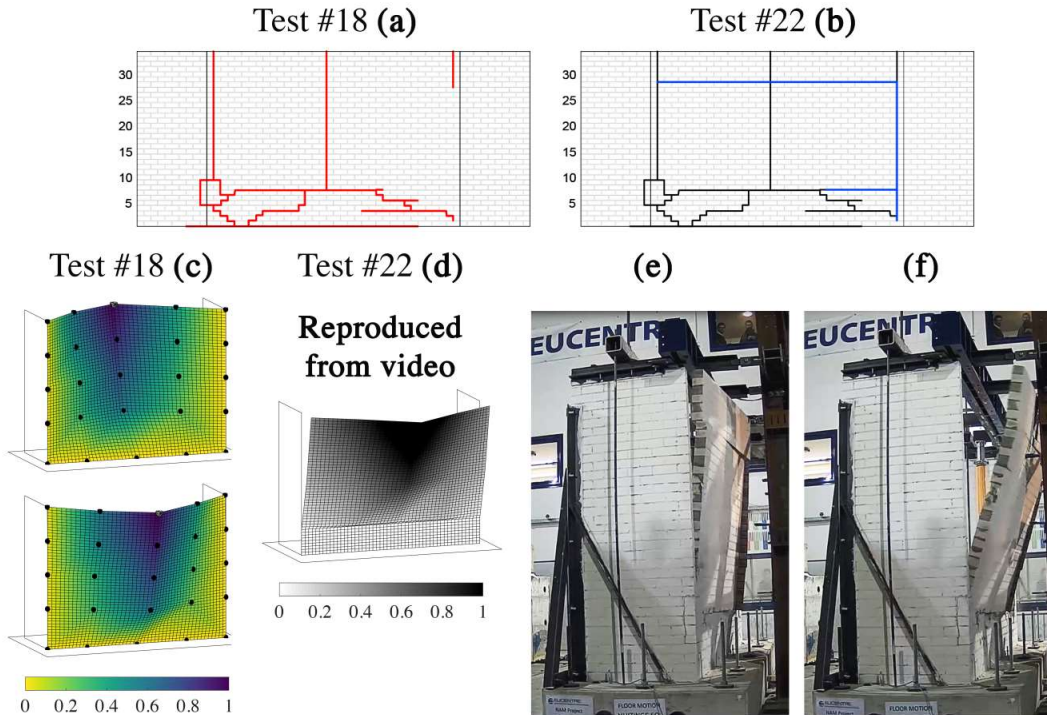


Figure 3:6. CS-000-RF: evolution of the crack pattern (a-b). 3D deformed shapes in positive (top) and negative (bottom) directions: first cracking (Test #18, $PTA=1.28$ g, Peak $TD=+12.8$ mm/ -8.4 mm) (c) and failure mechanism (reproduced from video); pictures of OOP panel overturning (e-f).

CSW-000-RF

For CSW-000-RF, DS2 was realised under significant seismic input occurred during Test #20 ($PTA=1.28$ g, peak $TD=8.9$ mm). Observed damage consisted of a vertical line crack at the connection with the left return wall and a stepped crack extending from the upper left corner of the window to the top of the specimen. The initiation of a horizontal crack along the bed joint from the lower left corner of the window was also observed (Figure 3:7a). Both deformed shapes in positive and negative directions show the rotation of the longer part of the OOP panel and the part on top of the window (Figure 3:7c). The part of the specimen below the opening showed relatively less deformation.

The specimen underwent very extensive damage (DS4) during Test #27 ($PTA=0.91$ g, peak $TD=68$ mm). Since DS5 was not attained, the crack pattern reported was produced by visual examination after the experiment was over (Figure 3:7b). Despite the extensive cracking surveyed at the end of the test, the mechanism was triggered by the horizontal crack around the mid-height of the panel on the left of the opening and the diagonal crack propagating towards the left return wall. The resulting deformed shapes (almost symmetric in both directions) are indicative of the failure mechanism showing a localisation of the deformation in the portion of the specimen above these cracks (Figure 3:7d). These shapes are well indicative of the complexity that was involved in the failure mechanism. Rotation of the multiple panels into which the wall was divided can be clearly observed from the residual deformation at the end of the test (Figure 3:7e).

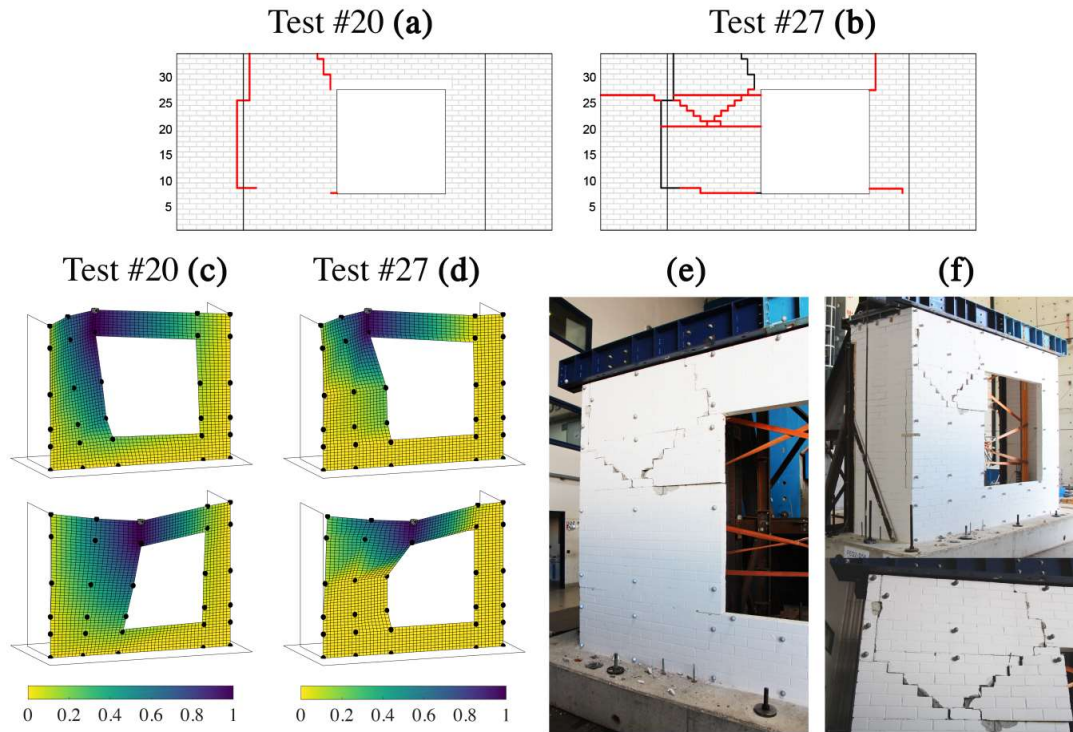


Figure 3.7. CSW-000-RF: evolution of the crack pattern (a-b). 3D deformed shapes in positive (top) and negative (bottom) directions: first cracking (Test #20, $PTA=1.28$ g, Peak $MHD=+8.9$ mm/ -7.3 mm) (c) and failure mechanism (Test #27, $PTA=0.91$ g, Peak $TD=+68.3$ mm/ -55.3 mm) (d); pictures of the residual deformation at the end of the test (e-f).

CL-000-RF

DS2 of the CL-000-RF specimen occurred during Test #18 ($PTA=1.11$ g, peak $TD=5.0$ mm). A horizontal crack in the 3rd bed joint from the bottom throughout the OOP panel could be observed. Additionally, initiation of some stepped diagonal cracks could be seen in the left return wall and corner of the OOP panel above this horizontal crack (Figure 3:8a). The collapse (DS5) of this specimen was reached during Test #23 ($PTA=1.71$ g). Although the ultimate test led to collapse and extensive cracking, careful examination of the video of the test revealed that the complete development of the failure mechanism (DS3) also occurred in the same test by the formation of two stepped diagonal cracks starting from the two lower corners of the OOP panel above the horizontal crack. These two diagonal cracks meet near the centre of the OOP panel and propagate to the top of the specimen in the form of another stepped crack (Figure 3:8b and Figure 3:8f). The analysis of the specimen deformation shows the evolution of the deflected shape from an almost fixed-fixed horizontally spanning beam (Test #21, Figure 3:8d) towards a concentration of displacement along the central crack (Test #23, Figure 3:8e). This latter deformed shape was constructed at a particular instant of the ultimate test before the specimen collapse when it was clearly representative of the failure mechanism. Figure 3:8c and Figure 3:8g represents the collapsed state of the specimen at the end of the testing sequence.

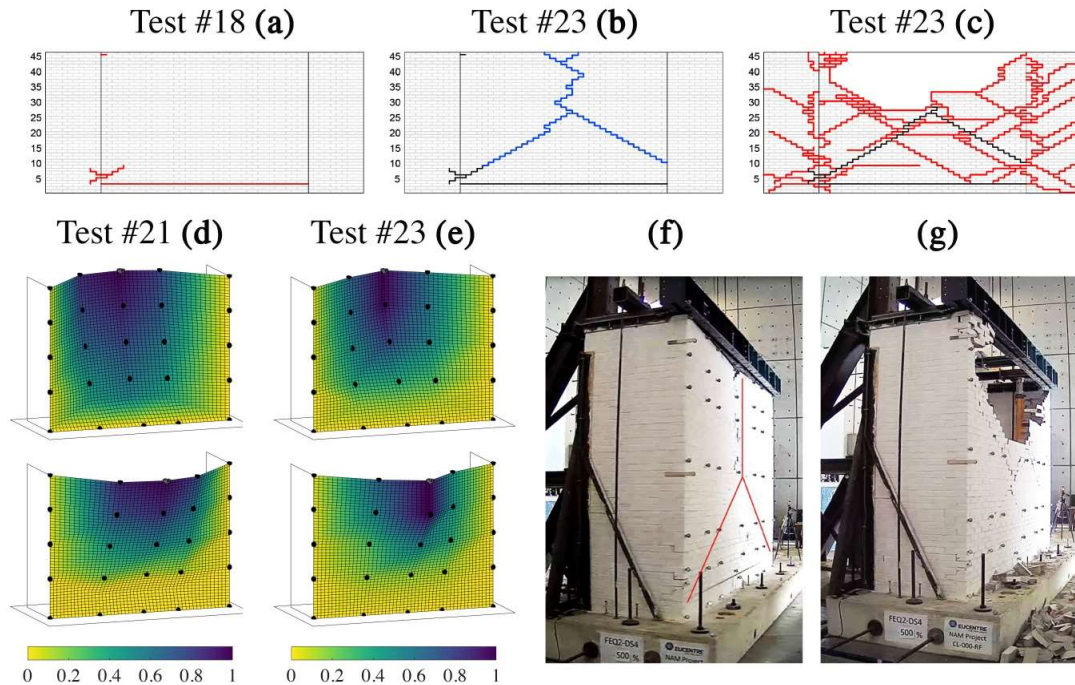


Figure 3.8. CL-000-RF: evolution of the crack pattern (a-b-c). 3D deformed shapes in positive (top) and negative (bottom) directions: first cracking (Test #21, $PTA=1.33$ g, Peak TD=+8.5 mm/-5.4 mm) (d) and failure mechanism (Test #23, $PTA=0.91$ g, Peak TD=+113.9 mm/-172.0 mm) (e); pictures of the residual deformation at the end of the test (f-g).

CAV-000-RF

Similar to previous experiments (Graziotti, Tomassetti, Penna, & Magenes, 2016), the adopted L-shaped ties despite having negligible flexural stiffness ensured a sufficient coupling of the horizontal displacement of the two leaves (*i.e.* limiting the differential displacement and maintaining the gap) up to collapse. This was due to the axial stiffness and bond of the ties as well as the slenderness of the two leaves. Damage pattern and failure mechanisms observed for the clay leaf of CAV-000-RF specimen were very similar to K1Y. Both clay and CS leaves exhibited failure mechanism consistent with the ones observed for CL-000-RF and CS-000-RF, respectively. Unlike all other specimens, no cracking was observed for any of the two leaves composing the cavity wall until the ultimate test. The specimen reached extensive damage condition (DS4) directly in Test #21 ($PTA=1.37$ g). Also in this case, DS5 was not attained and the crack patterns reported were produced by visual examination at the end of the test sequence. Cracks in the CS leaf included line cracks at the centre of the OOP panel and at the connection with the return walls (with significant residual displacement at the end of the test). A horizontal crack was detected at the first bed joint from the bottom. Another horizontal crack was observed at the mid-height of this leaf corresponding to the location of the ties (Figure 3:9a).

The deformed shape in the positive direction shows the rotation of the two panels individuated by the central line crack as well as sliding of the wall on the horizontal crack (Figure 3:9c). Since this sliding was not directly measured, it was reproduced from a critical assessment of the video. Because of this sliding, a residual displacement of approximately 40 mm (in the positive direction) could be observed in the inner CS leaf at the end of Test #21. The outer clay leaf showed extensive diagonal cracking at the end of the ultimate test (Figure 3:9b). The deformed shapes in both positive and negative directions however confirm the activation of the K1Y mechanism (Figure 3:9d). All deformed shapes were constructed at a particular instant of the ultimate test when they were clearly representative of the failure mechanism (DS3).

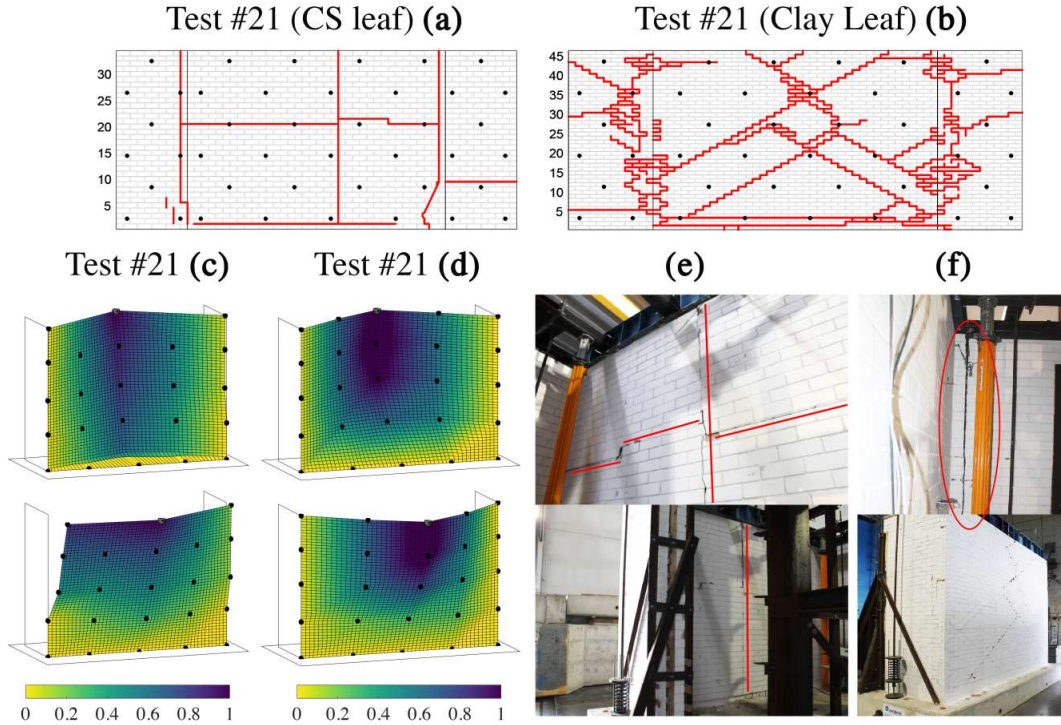


Figure 3:9. CAV-000-RF: crack pattern (a-b). 3D deformed shapes in positive (top) and negative (bottom) directions: CS inner leaf (Test #21, PTA=1.37 g, Peak TD=+40.4 mm/-25.0 mm) (c) and clay outer leaf (Peak TD=+35.8 mm/-25.4 mm) (d); pictures of residual deformation on CS inner leaf (e), failure of CS left return wall connection (f, top), clay leaf damage (f, bottom).

3.1.3.3 Hysteretic Behaviour

The evolution of hysteretic response of each specimen is illustrated in Figure 3:10. In order to facilitate the comparison between all the specimens, these responses have been computed in terms of shear coefficient (SC) vs. MHD (mid-height displacement) for CS-000-RR and SC vs. TD (top displacement) for all other specimens. The SC was calculated from the walls' inertial force (V_w) as follow:

$$SC = \frac{V_w}{m \cdot g}$$

where m is the mass of the OOP panel of each specimen (Table 3.1) and g is the acceleration due to gravity. Time-histories of inertial forces associated with the OOP panel were computed by multiplying the acceleration recorded by accelerometers with a tributary mass assigned to them. The mass of the OOP panel was assumed to be lumped at the accelerometer locations. Tributary mass assigned to each accelerometer were modified throughout the testing sequence based on the progression of damage and crack pattern. The evolution of the masses assigned to each accelerometer for every specimen can be viewed in Appendix A.

The hysteretic response of each specimen has been divided into three phases superimposed on each other with different colours: pre-cracking, first cracking and post cracking tests. The pre-cracking phase corresponds to tests in which the specimens remained in DS1. It is to be noted that peak strength in term of forces was often realised before the failure mechanism was fully activated *i.e.* attainment of DS3. As an example, for CS-000-RF and making reference to Table 3.3, Test #1-17 are included in the pre-cracking, Test #18 in the first cracking and Test #19-22 in the post-cracking phases respectively. The inertial force values associated with the peak SC and corresponding displacements, in both positive and negative cycles are provided in the legend of each hysteretic response. The peak response displacement and associated inertial force before the loss of equilibrium are also

reported. It is to be noted that the TD plotted in the hysteretic response of CAV-000-RF is measured on top of the CS leaf.

All specimens exhibited a rather brittle response. This holds particularly for the CS specimens where the cracking was controlled by line failure (*i.e.* the flexural tensile strength of units). Peak inertial force that was sustained by specimens CS-005-RR, CS-000-RF and CSW-000-RF corresponded to very low (less than 6 mm) values of MHD and TD respectively. Strength and stiffness degradation took place quite quickly over a few response cycles and very limited range of displacement. This is also reflected by the number of tests in the testing sequence between DS2 being reached and the ultimate test for these specimens (Table 3.3).

The MHD associated with peak inertial strength for CS-005-RR, attained during the Test #22 when first cracking was observed, was relatively lower compared to the other specimens (less than 3 mm). The wall was also able to sustain a large number of tests adopting a very demanding signal (SSW) post-cracking. This is due to the combined effect of the top horizontal restraint and the higher acting axial load. The failure mechanism completely developed only at MHD of 15 mm, with stiffness and strength degradation taking place within this range of displacement (3-15 mm). Beyond this limit, the wall lateral resistance relied only on the combination of rocking and friction (coming from the frictional torsional resistance of bed-joints). Although associated with higher energy dissipation, the shape of the resulting force-displacement loops is very similar to the ones observed in one-way bending behaviour of vertically spanning walls.

Regarding CL-000-RF, the peak inertial force was attained at higher level of TD (12.7 mm) compared to all other specimens. Post-peak response cycles (associated with stiffness degradation) showed the capability of resisting significant values of lateral load up to TD of 100 mm and also higher energy dissipation. This is in accordance with observed extensive stepped cracking where the energy dissipation is mainly controlled by the torsional friction response.

CS-000-RF exhibited a particularly brittle response. At the attainment of peak inertial force associated with a TD of 5.9 mm, the failure mechanism had almost completely developed. Given the predominant occurrence of line cracking, the very limited post peak capacity was primarily controlled by rocking.

CSW-000-RF was able to sustain peak inertial force up to TD of approximately 10 mm. At higher displacements, significant stiffness and strength reduction was observed with limited residual lateral capacity mainly coming from the torsional friction resistance of bed-joints.

The hysteretic response exhibited by the CAV-000-RF was very similar to CL-000-RF. Also in both specimens, significant cracking occurred only in the ultimate test. Peak inertial force was attained at a TD of 17.3 mm and quick strength and stiffness degradation were observed after attainment of peak strength. Due to the nature of the testing performed it was not possible to quantify an exact ultimate displacement associated with each specimen.

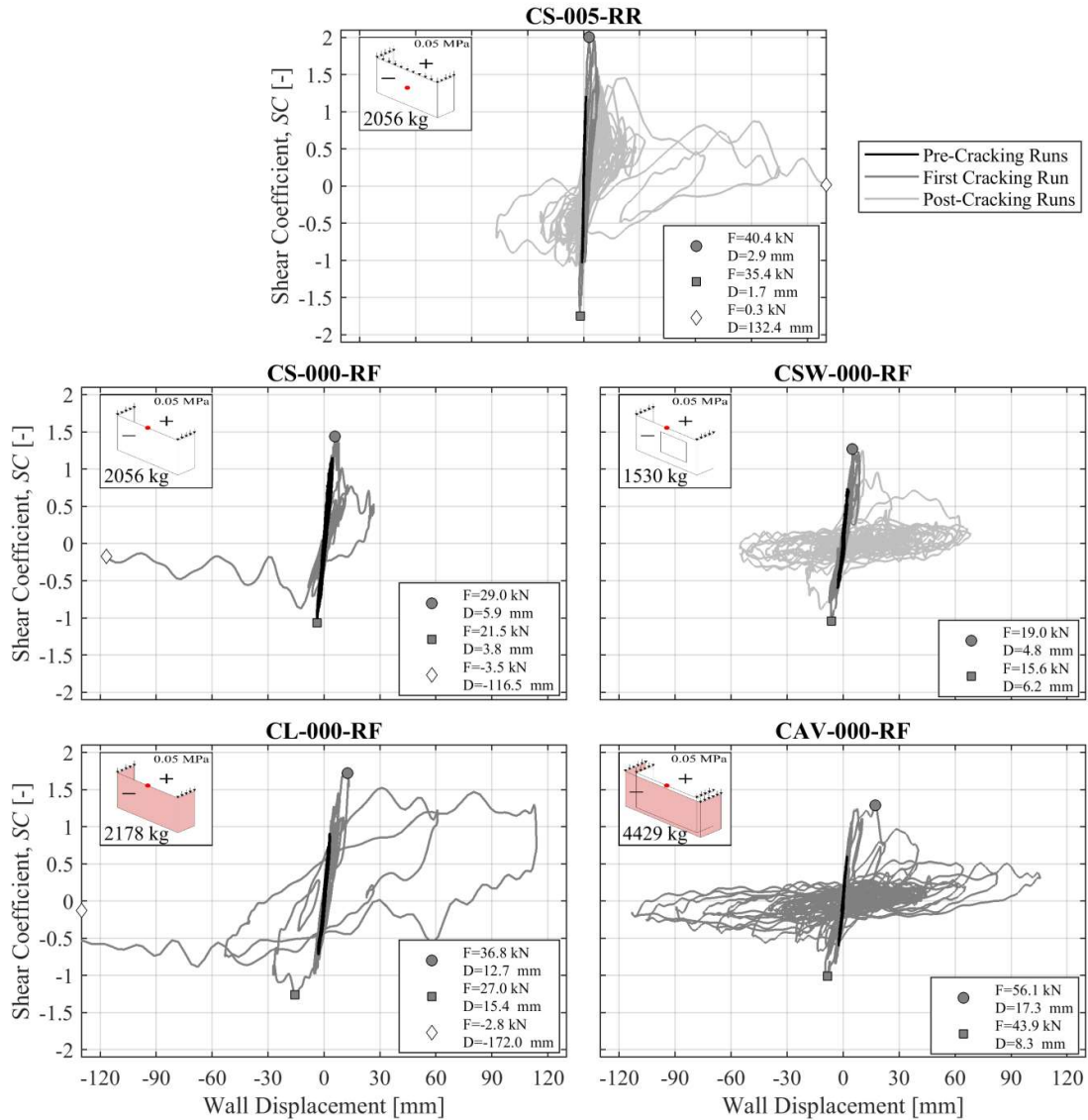


Figure 3:10: Hysteretic response of every specimen (Location of displacement indicated by red dot).

3.1.3.4 Specimen Strength Capacity

Specimen capacities were plotted in terms of *PTA* sustained by the walls vs. peak *MHD* or *TD* exhibited in the corresponding test (Figure 3:11). These values were plotted only for the tests in which the employed signal was FEQ2-DS4 and SSW. *PTA* values corresponding to the ultimate test are provided even if the associated displacement is not known for tests in which the specimen collapsed onto the shake table. In case of CSW-000-RF and CAV-000-RF, associated peak response displacement recorded before loss of equilibrium occurred are mentioned. The curves are not extended until that point in order to appreciate the initial and changes in stiffness associated with the specimens. The change in applied overburden pressure for the first specimen (from CS-010-RR to CS-005-RR configuration) did not affect the specimen initial stiffness too much. CS-010-RR/CS-005-RR was much stiffer compared to all other specimens which presented a very similar initial stiffness. This is in agreement with results of dynamic identification (Table 3.4).

In case of CS-005-RR, distinct changes in stiffness coincided with Test #18 and #26 which corresponded to tests in which first cracking and consequent damage at the connection with the right return wall respectively were observed. Similar behaviour is also noticed for CSW-000-RF. The low post cracking residual strength capacity associated with CS-000-RF resulted in it collapsing very soon after cracking. Cracking and collapse coincided for

CL-000-RF and CAV-000-RF but at a higher *PTA* with respect to the other specimens under same boundary conditions. It is to be noted that the use of dashed line in the ultimate parts of the capacity curve indicates that the stiffness or change in stiffness observed for a specimen during that part of the testing sequence is not quantitative as only the plotted *PTA* and not the displacement value was measured experimentally.

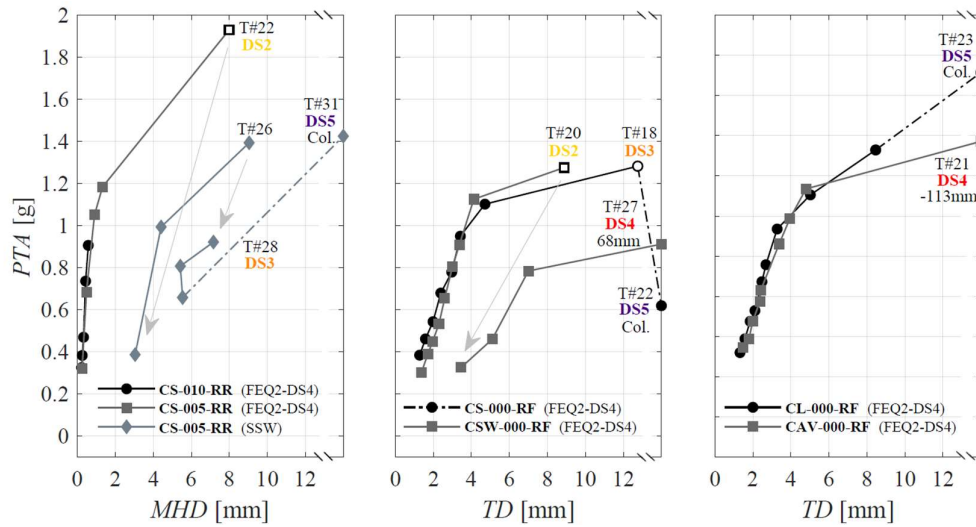


Figure 3:11. Specimen capacities in terms of *PTA* vs. Wall Displacement.

3.2 CAMPAIGN B


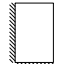
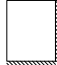

3.2.1 SPECIMENS GEOMETRY AND BOUNDARY CONDITIONS

Four full scale walls were tested dynamically in the OOP direction while being subjected to two-way bending condition in this phase of the campaign. All specimens again corresponded to 100-mm-thick single leaf walls constructed with Calcium Silicate (CS) bricks measuring 212x102x71 mm. All the walls were again constructed in 34 layers of bricks. Since all masonry joints were 10 mm thick, this corresponded to a total height of 2.75 m. Detailed material characterisation performed for all of the specimens has already been reported in the section 2.2 of this report. The specimens again differed from each other either in terms of geometry, boundary conditions or applied excitation.

Each specimen consisted of an OOP panel and one or two return walls (depending on the envisaged boundary conditions). Two return walls were present for the first two specimens: CS-000-RFV, CS-000-RF2 which were tested with both vertical edges and the bottom horizontal edges completely restrained (fixed). These two specimens differed only in terms of the fact that the adopted seismic excitation had a vertical component as well in case of the first specimen which is also reflected in the name adopted for it (“V” in CS-000-RFV). More details about the adopted input seismic excitation are provided in the following sections.

The latter two specimens possessed one return wall each as they were envisaged to be tested with one each of both their vertical and horizontal edge unrestrained (free). This resulted in a “L-shaped” boundary condition configuration which is also reflected in the naming adopted for them: CS-000-L1, CS-000-L2. These specimens differed only in terms of the length of their OOP panels and consequently in their aspect ratio. It is to be noted that both of these specimens were constructed on the same foundation and hence were tested simultaneously on the shaking table. No vertical overburden was applied on the OOP panel of any of the tested specimens. The return walls of each of the specimens however were loaded with a vertical overburden of 0.05 MPa. Details on how this was applied are provided in section 3.1.2.1. The dimensions of the various specimens along with their boundary conditions are summarised in Table 3.5.

Table 3.5: Test specimens: boundary conditions and applied overburden pressure.

Specimen	l_{OOP} [m] h_{OOP} [m]	m [kg]	σ_v OOP wall [MPa]	σ_v RET wall [MPa]	Horizontal restrain condition	Scheme
CS-000-RFV	3.98 2.75	2056	0	0.05	Fixed (R) Free (F)	
CS-000-L1&L2	L1 1.76 2.75	910	0	0.05	Fixed (R) Free (F)	
	L2 2.21 2.75	1140	0	0.05	Fixed (R) Free (F)	
CS-000-RF2	3.98 2.75	2056	0	0.05	Fixed (R) Free (F)	

3.2.2 TESTING SETUP AND INPUT MOTION SEQUENCES

3.2.2.1 Testing setup

All considerations associated with test set-up installed and used in Campaign A were also used in this part of the campaign. However, it is interesting to note that this campaign was performed on the new multi-axial shake table of EUCENTRE (Figure 3:12)



Figure 3:12: Testing layout: general view of the shaking table and the testing setup (a), general view of CS-000-RF2 (plaster applied to investigate non-structural damage, more details in section 3.2.3.2) (b) and CS-000-L1&L2 (c), return wall restrain system fixed with diagonal to the rigid frame (d), spring system for the application of the top overburden pressure and support for the uplift of the top beam (e).

3.2.2.2 Instrumentation and data acquisition

The instrumentation adopted for each specimen in this phase of the campaign also consisted of accelerometers, potentiometers, wire potentiometers and a 3D optical acquisition system. The location of all the instrumentation adopted for each specimen was decided based on the boundary conditions envisaged and correspondingly expected deformed shapes. Accelerometers were installed on the OOP panel of the specimen in order to record acceleration-time histories. Additional accelerometers were also installed at the specimen foundation, top beam, rigid frame and the return walls. Potentiometers were used to measure relative displacements associated with various locations of the specimen. Wire potentiometers attached to the rigid frame in several locations were used to record horizontal displacements relative to the shake table. Some potentiometers were also adopted to record the relative displacements between the main panel and the return walls. Specific details of the instrumentation utilised for each wall is provided in Appendix A.

3.2.2.3 Input signals and testing sequence

Incremental dynamic tests, i.e. a series of table motions of increasing intensity, were performed on each specimen to fully exploit their horizontal load carrying capacity. The input sequence employed was the same as that performed by Graziotti *et al.* (Graziotti, Tomassetti, Kallioras, Penna, & Magenes, 2017). This was done to facilitate comparison between results observed for the wall specimens with that of a full-scale building prototype in which second and first-storey transverse walls were excited in the OOP direction. Primarily three input motions were used throughout the entire testing sequence to excite the specimen in the OOP direction: FEQ1-DS0, FEQ2-DS3 and FEQ2-DS4. FEQ1-DS0 corresponds to recorded first floor accelerogram of the full-scale house when subjected to ground motion EQ1 scaled up to 100%. FEQ2-DS3 and FEQ2-DS4 correspond to recorded first floor accelerograms of the full-scale house when subjected to ground motion EQ2 scaled up to 125% and 200%, respectively. Ground motions EQ1 and EQ2 were obtained from a hazard study of the Groningen region and can be deemed representative of the dynamic characteristics of the induced seismicity (Graziotti, et al., 2015). These acceleration histories can be considered well representative of the progressive damage evolution between DS0/No Damage through DS3/Moderate Damage into DS4/Extensive Damage which occurred in the house (Graziotti,

Tomassetti, Kallioras, Penna, & Magenes, 2017). It is worthy to note here that the same ground motions used in Campaign A corresponded to second floor not first floor accelerograms.

The specimen CS-000-RFV was also additionally subjected to vertical excitation simultaneously with the horizontal out of-plane excitation. The applied vertical excitation were directly the EQ1 and EQ2 vertical ground motions scaled linearly at the considered level of intensity (see response spectra in Figure 3:14), assuming, hence, the ground floor of EUC-BUILD-1 as rigid in the vertical direction.

It should also be noted that the specimens were again subjected to low amplitude random excitations (RN) in order to identify their dynamic properties in between test runs. Low intensity calibration runs were also performed in order to have a better control of the shaking table. Table 3.6 specifies the adopted input floor motions and the ground motions they have been obtained from together with the associated *PGA* and *PTA*. Figure 3:13 and Figure 3:14 illustrates their 100% scaled acceleration time histories along with associated acceleration and displacement (5% damped) spectra.

Table 3.6: Characteristics of employed horizontal input motions at scaling factor equal to 1.

Input	Description	GM input	GM PGA [g]	PTA [g]
FEQ1-DS0	1 st Floor Acc. (Experimental)	EQ1-100%	0.10	0.13
FEQ2-DS3	1 st Floor Acc. (Experimental)	EQ2-125%	0.19	0.23
FEQ2-DS4	1 st Floor Acc. (Experimental)	EQ2-200%	0.31	0.33

Table 3.7: Characteristics of employed vertical input motions at scaling factor equal to 1

Input	Description	GM input	GM PGA [g]	PTA [g]
FEQ1-DS0	1 st Floor Acc. (Experimental)	EQ1-100%	0.10	0.07
FEQ2-DS3	1 st Floor Acc. (Experimental)	EQ2-125%	0.19	0.10
FEQ2-DS4	1 st Floor Acc. (Experimental)	EQ2-200%	0.31	0.16

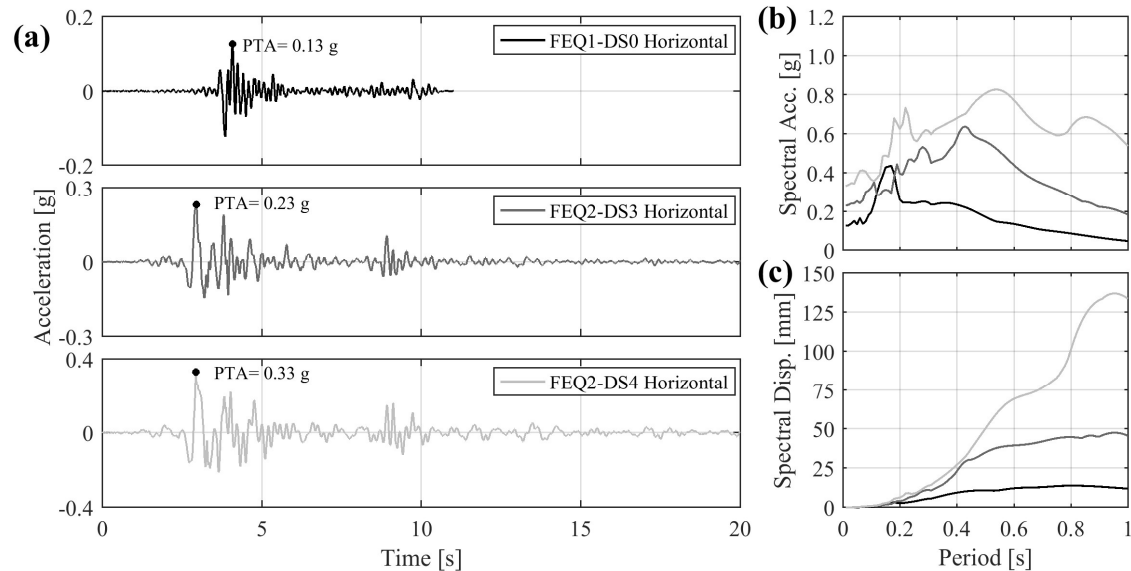


Figure 3.13. Acceleration time histories of the employed horizontal input motions (a) 5% damped acceleration (b) and displacement (c) response spectra.

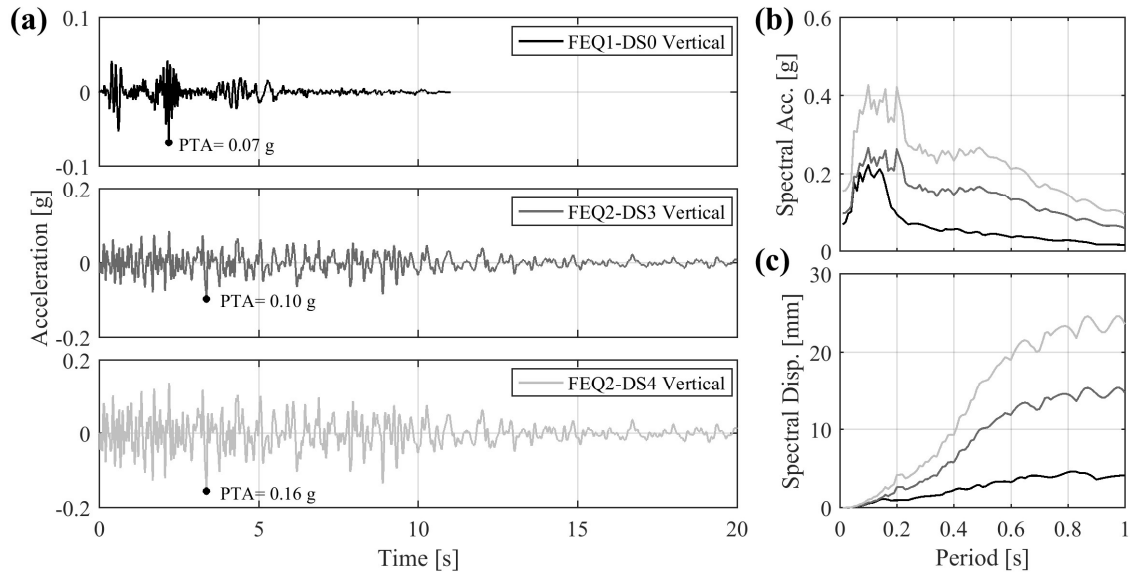


Figure 3:14. Acceleration time histories of the employed vertical input motions (a) 5% damped acceleration (b) and displacement (c) response spectra.

The sequence of input motions each specimen was subjected to along with respective scaling factors (linear scaling w.r.t. to PTA), measured PTA and maximum wall displacements are summarised in Table 3.8. For all specimens this value is recorded at the top (TD-Top displacement): mid-point of the unrestrained top edge for CS-000-RFV, CS-000-RF2 and on top of the unrestrained vertical edge for CS-000-L1, CS-000-L2. The test marked in bold letters for CS-000-RFV and CS-000-L2 is the experiment after which first cracking was observed by visual inspection. After observations of damage which could potentially compromise the stability of the OOP panel, incremental testing was resumed again from a lower value of PTA. No cracking prior to collapse was observed for CS-000-RF2.

3.2.3 TEST RESULTS

This section discusses the results of the tests: examining the wall dynamic properties and their evolution, the observed damage patterns and failure mechanisms, the specimens' capacity and hysteretic behaviour. The condition of each specimen at the end of each test was classified according to the definition of the following same damage states as used in Campaign A. More details about the damage states can be found in section 3.1.3

3.2.3.1 Dynamic Identification

As already mentioned in section 3.2.2.3, every specimen was subject to low amplitude random excitations (RN) in between test runs. These tests were conducted in regular intervals throughout the testing sequence to identify the dynamic properties of the specimens or any changes in them indicating damage which could not be visually observed. Particular interest was given especially to the frequency and time period associated with the first natural mode of vibration of the specimens. Frequency domain decomposition which is an output only system identification technique was implemented in order to identify these natural frequencies (Brincker, Zhang, & Andersen, 2000). The first natural mode of vibration of the specimens was observed to be dependent highly on the boundary conditions adopted.

Table 3.9: Dynamic identification of the specimens.

CS-000-RFV			CS-000-L1			CS-000-L2			CS-000-RF2		
T#	DSi	Freq. [Hz]	T [s]	T#	DSi	Freq. [Hz]	T [s]	T#	DSi	Freq. [Hz]	T [s]
1	DS1	12.4	0.080	1	DS1	12.5	0.080	1	DS1	10.1	0.099
19	DS1	11.3	0.088	9	DS1	12.3	0.081	9	DS1	9.8	0.103
21	DS2	9.9	0.101	16	DS1	11.5	0.087	16	DS1	9.4	0.107
25	DS2	8.2	0.122	18	DS1	11.5	0.087	18	DS2	9.0	0.111
27	DS3	7.6	0.132								

3.2.3.2 Damage pattern and failure mechanisms

The progression of damage in each specimen was quite complex. Nature and location of damage often changed with increasing seismic input as the incremental dynamic test progressed. Nevertheless, detailed condition mapping was carried out after each run in the incremental dynamic test sequence and all observed cracks are reported in this section along with the test in which they were observed.

To facilitate a better understanding of the failure modes of each wall, 3D deformed shapes were also constructed for critical tests. In each test, these shapes were produced at the instants in which the OOP panel had maximum displacement towards (positive) and away (negative) from the return walls. Such shapes (with a mesh of 50x50 elements along width and height of the panel) were constructed by performing linear interpolation for all points in the wall between locations where displacements were recorded and indicated by black spheres. The reported wall deflections were normalized with respect to the peak displacements occurring at that instant. Videos documenting the failure of each specimen can be viewed online (EUCENTRE. URM walls in out-of-plane two way bending (YouTube playlist). Pavia, Italy;, 2017).

CS-000-RFV

Specimen CS-000-RFV attained first cracking (DS2) during Test #20 (PTA X=1.07g, PTA Z=0.51g peak TD=6.6 mm). First cracking consisted of a vertical line crack at the connection of the OOP panel and right return wall developing from a height of approximately 1 m from the bottom up to the top edge of the wall. Additionally, cracks could also be seen in the upper left corner of the OOP panel as well as the left return wall (Figure 3:15a). Deformed shapes in both positive and negative directions were very similar. High displacements were observed along the entire free top edge with the lower part of the OOP panel remaining relatively immobilized (Figure 3:15d).

More distress was observed in Test #24 (PTA X=0.65g, PTA Z=0.50g peak TD=6.4 mm) with an additional vertical line crack appearing in the center of the OOP panel (Figure 3:15b). This crack also extended to the top edge of the wall from the same height as the crack at the connection with the right return wall. Despite the increase in observed structural distress as well as change in dynamic properties (Table 3.9) the specimen can be still considered to be in DS2 as DS3 (full development of crack pattern corresponding to collapse mechanism) was reached only in Test #26 (PTA X=0.76g, PTA Z=0.52g peak TD=10.7 mm). This test saw the development of a horizontal cracking from the base of the central line crack towards the left return wall. A diagonal crack also extended from the same crack towards the left return wall. Deformed shapes provided from Test #26 which can

be considered representative of the occurring failure mechanism (Figure 3:15e) show a shift of maximum displacements along the entire top edge to being localized along the central vertical section of the OOP panel corresponding to the formation of the central line crack. Relatively less displacement can also be observed for the part of the panel below the horizontal crack.

The specimen collapsed (DS5) during Test #28 (PTA X=0.92g, PTA Z=0.55g). Collapse of the specimen occurred by development of another line crack at the connection with the right return wall and the consequent overturning of the OOP panel about a horizontal crack passing through the base of all three vertical line cracks. Additional horizontal and diagonal cracking was observed at the portion of the wall below the panels which overturned. This cracking has been documented in Figure 3:15c/d. Figure 3:15g and Figure 3:15h show the development of the collapse mechanism of the specimen.

CS-000-L1 and L2

This specimen actually consisted of two separate specimens of the same height but different lengths (hence different aspect ratio) resting on the same foundation. The two specimens were separated by a gap of approximately 20 mm to avoid any interaction between them during the incremental dynamic test. Of the two specimens, CS-000-L1 which corresponded to a shorter OOP panel with respect to CS-000-L2 remained in DS1 throughout the entire testing sequence. CS-000-L2 reached DS2 in Test#17 (PTA=0.75 g, Peak TD=10.5 mm). Initiation of cracking was restricted to a vertical line crack in the vicinity of the connection of the OOP panel with its return wall (Figure 3:16a). In the same test, CS-000-L1 exhibited a much stiffer response (TD= 4.9mm) as expected and confirmed by the dynamic properties of both walls (Table 3.9).

CS-000-L2 reached DS5 in Test 19. Collapse of the specimen occurred via extension of the existing vertical line crack and consequent overturning of the OOP panel as well as a portion of the return wall about a horizontal crack approximately 1.1 m from the base of the wall. This progression of events is illustrated in Figure 3:16e and Figure 3:16f. Deformed shapes constructed throughout the testing sequence exhibited a concentration of high displacements above a diagonal connecting the free extremities of the fixed edges (Figure 3:16c and Figure 3:16d).

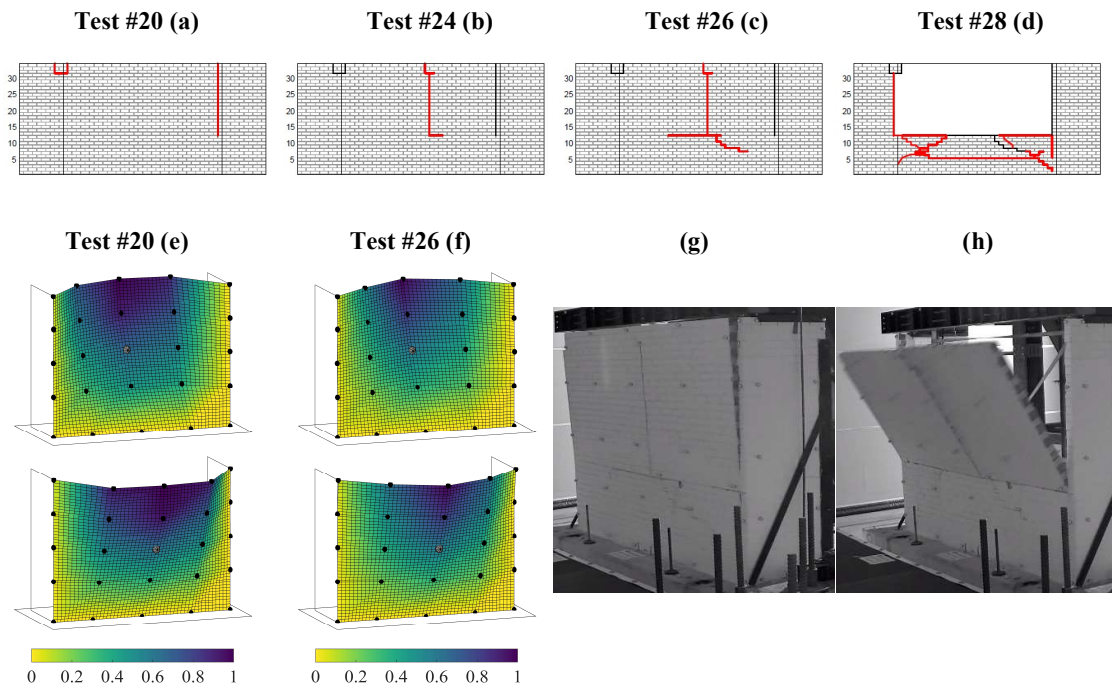


Figure 3:15. CS-000-RFV: crack pattern Test #20 (a), crack pattern Test #24 (b), crack pattern Test #26 (c), crack pattern Test #28 (d). 3D deformed shapes in positive (top) and negative (bottom) directions: (Test #20, PTA X=-1.07 g, PTA Z=0.51 g, Peak TD=+6.2 mm/-6.6 mm) (e), (Test #26, PTA X=0.76 g, PTA Z=-0.52 g, Peak TD=+6.2 mm/-10.7 mm) (f); pictures of specimen collapse (g-h).

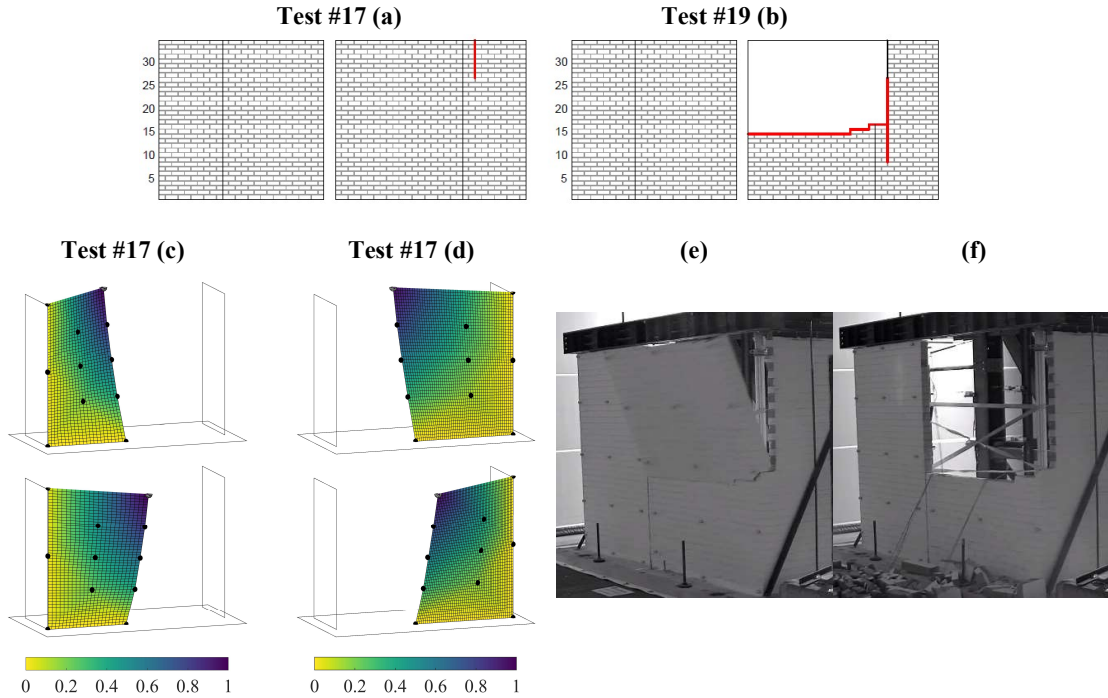


Figure 3:16. CS-000-L1&L2: crack pattern Test #17 (a), crack pattern Test #19 (b). 3D deformed shapes in positive (top) and negative (bottom) directions: L1 portion (Test #17, PTA=0.75 g, Peak TD=+2.1 mm/-4.9 mm) (c), L2 portion (Test #17, PTA=0.75 g, Peak TD=+4.9 mm/-10.5 mm) (d); pictures of specimen collapse (e-f).

CS-000-RF2

Strips of plaster were put on this specimen to investigate non-structural damage if any. However, CS-000-RF2 remained in DS1 until the ultimate test and interestingly the plaster also did not exhibit any damage till then. This non occurrence of damage is also confirmed by its dynamic properties remaining constant throughout the testing sequence and reported in Table 3.9. The specimen reached DS5 progressing through other damage states in Test#19. The state of the specimen at the end of the ultimate test is illustrated in Figure 3:17a. The progression of various damage states within this test can be observed in Figure 3:17c, Figure 3:17d and Figure 3:17e. Damage initiated in the wall in the form of vertical line cracks appearing at the connections with the return walls and at the centre of the OOP panel. This was followed by the initiation of a horizontal crack at a height of 0.6 m from the base of the wall. Collapse of the specimen ultimately occurred in the form of overturning of the OOP panel about another horizontal crack at a height of 1.5 m from the base of the panel. The formation of this second horizontal crack was very likely to be caused by the wire potentiometers which had not been removed (the wire potentiometers can be observed very clearly in Figure 3:17e) even at this intensity of testing since no damage had been seen prior to the ultimate test. Thus, though Figure 3:17a indicates the condition of the specimen at the end of testing, it would be prudent to consider the horizontal crack at a height of 0.6m from the base as the part of DS3 (as indicated by the transparent box in Figure 3:17a) and the horizontal crack at 1.5 m to be caused by the wire potentiometers. Deformed shapes reported in Figure 3:17b from Test#18 confirm that the collapse mechanism was very similar to walls CS-000-RF, CL-000-RF and CS-000-RFV.

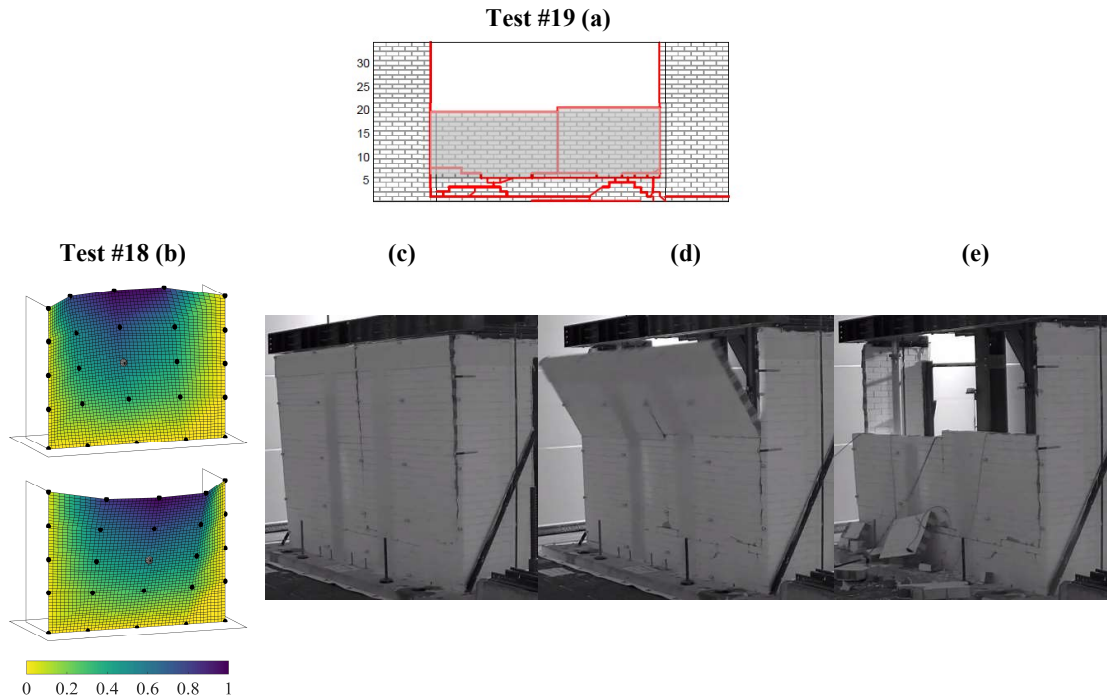


Figure 3:17. CS-000-RF2: crack pattern Test #19 (a). 3D deformed shapes in positive (top) and negative (bottom) directions: (Test #18, PTA=0.90 g, Peak TD=+2.8 mm/-8.2 mm) (b); pictures of specimen collapse (c-e).

3.2.3.3 Hysteretic Behaviour

The evolution of hysteretic response of each specimen is illustrated in Figure 3:18. In order to facilitate the comparison between all the specimens having different masses, these responses have been computed in terms of shear coefficient (SC) was calculated from the walls' inertial force (V_w) as :

$$SC = \frac{V_w}{m \cdot g}$$

where m is the mass of the OOP panel of each specimen (Table 3.5) and g is the acceleration due to gravity. Time-histories of inertial forces associated with the OOP panel were computed by multiplying the acceleration recorded by accelerometers with a tributary mass assigned to them. The mass of the OOP panel was assumed to be lumped at the accelerometer locations. Tributary masses assigned to each accelerometer were modified throughout the testing sequence based on the progression of damage and crack pattern. The evolution of the masses assigned to each accelerometer for every specimen can be observed in Appendix A. For all specimens, displacements provided here are recorded at the top (TD-Top displacement): mid-point of the unrestrained top edge for CS-000-RFV, CS-000-RF2 and on top of the unrestrained vertical edge for CS-000-L1, CS-000-L2.

The hysteretic response of each specimen has been divided into three phases superimposed on each other with different colours: pre-cracking, first cracking and post cracking tests. The pre-cracking phase corresponds to tests in which the specimens remained in DS1. All specimens exhibited a rather brittle response similar to the first four CS specimens tested in campaign A, failure being controlled by line failure i.e. tensile splitting of units. In fact, the progression from DS3 to DS5 for specimens CS-000L2 and CS-000-RF2 occurred in the same run. The same for specimen CS-000-RSV occurred in consecutive runs (separated by RN test performed to evaluate the change in dynamic properties). This is indicative of the very quick stiffness and strength degradation that took place for all the specimens and can be noticed clearly in their hysteretic behaviour.

Peak inertial force for both CS-000-RFV and CS-000-RF2 was sustained only up to displacements of around 6 mm. For CS-000-L2, this value was considerably higher (around 14 mm) but this is a result of its boundary conditions i.e. having an additional vertical edge free. It is brought to the attention of the reader once again, that

CS-000-L1 remained in DS1 i.e. linear elastic throughout the entire testing sequence and the same is reflected in its hysteretic behaviour. Due to the nature of the testing performed it was not possible to quantify an exact ultimate displacement associated with each specimen.

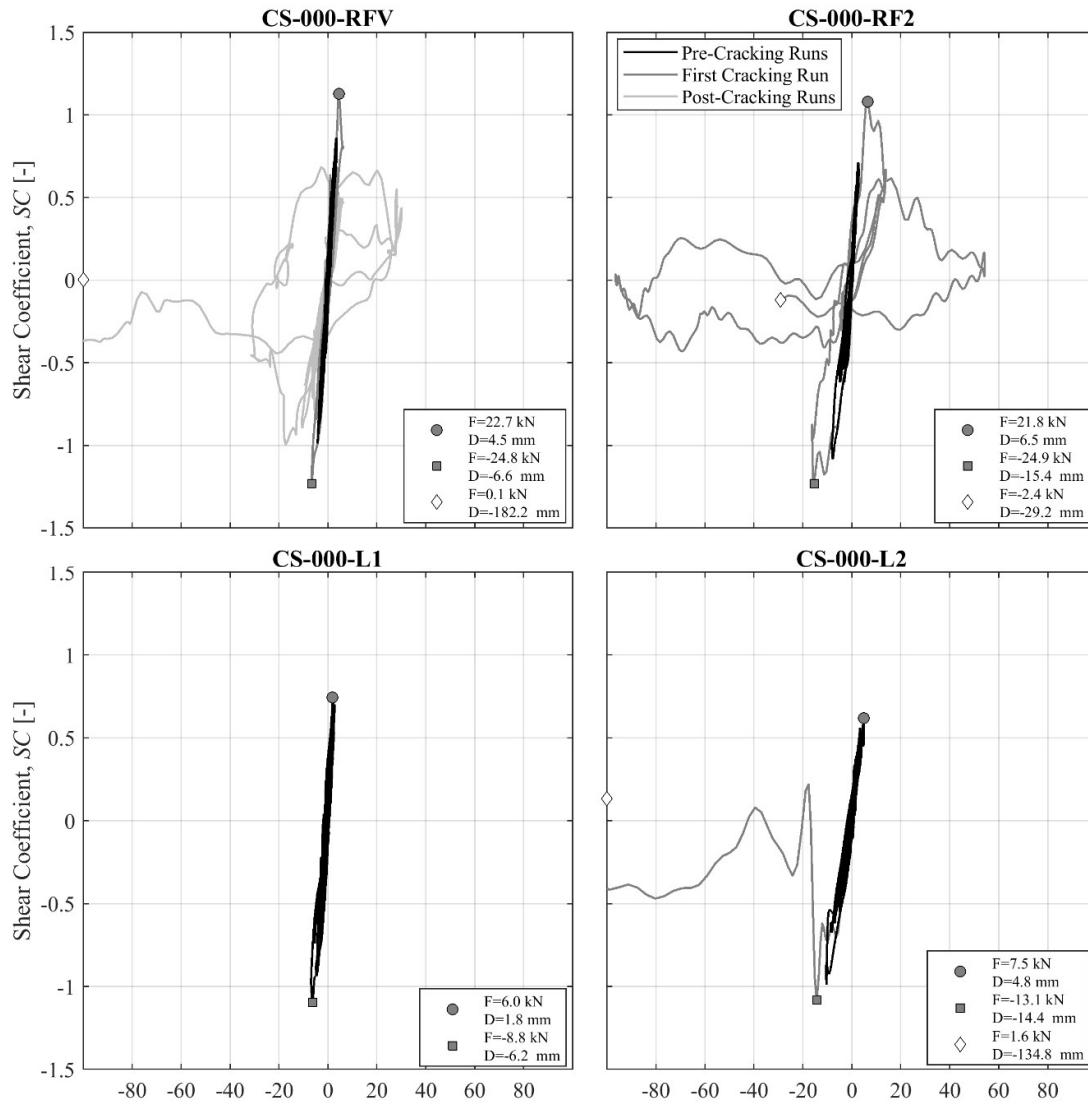


Figure 3:18: Hysteretic response of every specimen.

3.2.3.4 Specimen Strength Capacity

Specimen capacities were plotted in terms of PTA sustained by the walls vs. peak TD exhibited in the corresponding test (Figure 16). These values were plotted only for the tests in which the employed signal was FEQ2-DS4. PTA values corresponding to the ultimate test are provided even if the associated displacement is not known for tests in which the specimen collapsed onto the shake table.

In case of CS-000-RFV, distinct changes in stiffness coincided with Test #20 and Test#26 in which DS2 and DS3 were attained. Similar behavior is not observed for CS-000-L2 on the attainment of DS2 in Test#17 but this is a result of distress being limited to a small crack at the connection with the right return wall. Concurrent with experimental observations, no change in stiffness was observed for CS-000-RF2 until the ultimate test. Use of dashed line in the ultimate part of the capacity curve indicates the stiffness or change in stiffness observed for each of the walls is qualitative and not quantitative as only the plotted PTA was measured experimentally.

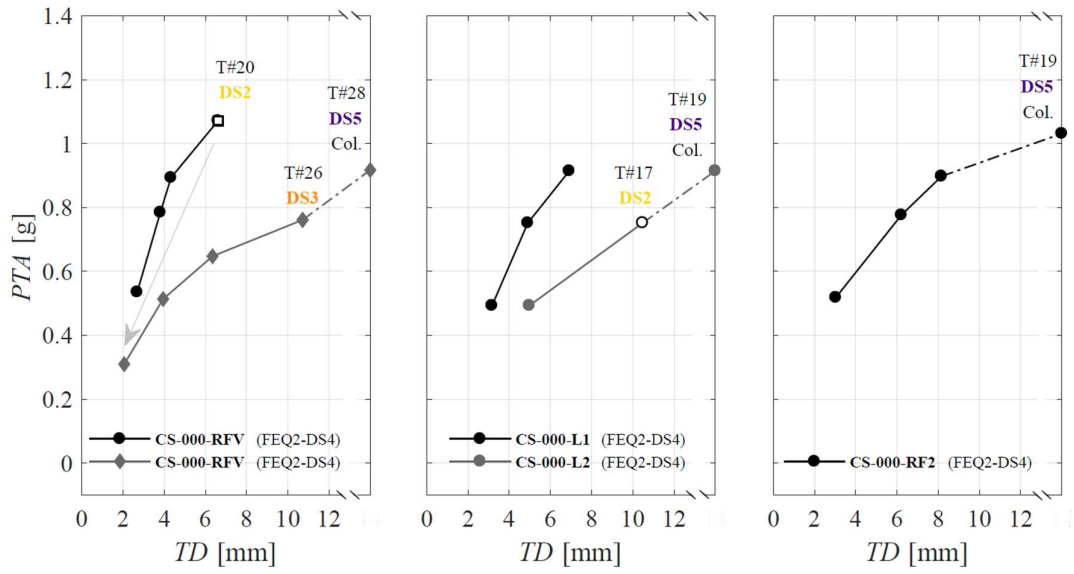


Figure 3:19. Specimen capacities in terms of PTA vs. Wall Top Displacement (TD).

REFERENCES

- Graziotti F, Tomassetti U, Kallioras S, Penna A, Magenes G. Shaking table test on a full scale URM cavity wall building. *Bull Earthq Eng.* 2017;15(12). doi:10.1007/s10518-017-0185-8
- Kallioras S. Numerical Simulation of Shaking Table Tests on a URM Cavity-Wall Building. *J Int Mason Soc.* 2017;30(2):39.
- EN 1015-11. Methods of test for mortar for masonry – Part 11: Determination of flexural and compressive strength of hardened mortar. Brussels, Belgium: European Standards, CEN/TC; 1999.
- EN 772-1. Methods of test for masonry units – Part 1: Determination of compressive strength. Brussels, Belgium: European Standards, CEN/TC; 2011.
- NEN-6790. Technische grondslagen voor bouwconstructies - TGB 1990 - Steenconstructies - Basiseisen en bepalingmethoden Zie. The Netherlands: Dutch Standards, Nederlands Normalisatie Instituut; 2005.
- EN 1052-1. Methods of test for masonry – Part 1: Determination of compressive strength. Brussels, Belgium: European Standards, CEN/TC; 1998.
- EN 1052-3. Methods of test for masonry – Part 3: Determination of initial shear strength. Brussels, Belgium: European Standards, CEN/TC; 2002.
- EN 1052-5. Methods of test for masonry – Part 5: Determination of bond strength by the bond wrench method. Brussels, Belgium: European Standards, CEN/TC; 2005.
- EN 1052-2. Methods of test for masonry - Part 2: Determination of flexural strength. Brussels, Belgium: European Standards, CEN/TC; 1999.
- EUCENTRE. URM walls in out-of-plane two way bending (YouTube playlist). www.youtube.com/watch?v=WvYS91br9HQ&list=PLRDMVFxhFvQnMRn7SDXreqbcg044logeB. Published 2017.
- Graziotti F, Tomassetti U, Sharma S, Grotoli L, Magenes G. Experimental response of URM single leaf and cavity walls in out-of-plane two-way bending generated by seismic excitation. *Construction and Building Materials.* 2018; In Review

APPENDIX A

This appendix provides information related to the sensor measurements obtained from eight different unreinforced masonry (URM) walls subjected to incremental dynamic shake-table tests at the EUCENTRE testing facility in Pavia, Italy. This information has been made available to assist in the development and calibration of analytical and numerical models intended to simulate the out-of-plane response of unreinforced masonry.

All data acquired was filtered from frequencies higher than 50 Hz. All displacements are expressed in [mm] and accelerations are expressed in [g]. For each specimen, a folder is created named as the specimen e.g. the folder containing data from all the tests corresponding to the second specimen is named as “CS-000-RF”. This folder contains a txt file for each test named as “TestT# - Test Input S.F.” where “T#”, “Test Input” and “S.F.” refer to the same provided as in the testing sequences (Table 3.3 and Table 3.8 of the report). It is to be noted that S.F. has been provided as 100% for each RN test as all of them were performed at the same intensity though no SF for them are provided in the testing sequences. Within each txt file, each column corresponds again to the readings of each instrument or time. The order of this also provided in the tables provided below. For walls CS-000-L1 and CS-000-L2, which were tested simultaneously on the shake table, the results of each test are provided in a single txt file named in the form “TestT# - Test Input S.F.1- S.F.2” where “S.F.1” and “S.F.2” refer to the S.F. for CS-000-L1 and CS-000-L2 respectively provided in Table 3.8. For e.g. Column 3 of the file “Test6 - FEQ2-DS3-C 50%.txt” in the folder “CS-000-RF” corresponds to recordings of the ‘Foundation Acc.’ when specimen CS-000-RF was subjected to FEQ2-DS3 scaled at 50% i.e. T#6 in Table 3.3.

In all tables and figures provided in the following parts of this appendix, Acc. Refers to accelerometer, WP refers to wire potentiometer and Pot. refers to potentiometer.

Table 1: CS-010/005-RR instrumentation, data acquisition and assigned lumped masses.

Col.	Instr.	Description	Offline	Location		Lumped Mass		
				X [mm]	Y [mm]	1 st [kg]	2 nd [kg]	3 rd [kg]
1	-	'Time [s]'	-	-	-	-	-	-
2	Acc.	'Shake Table Acc. [g]'	-	-	-	-	-	-
3	Acc.	'Foundation Acc. [g]'	-	-	-	449	449	284
4	Acc.	'Frame Acc. [g]'	-	-	-	-	-	-
5	Acc.	'Side A Beam Acc. [g]'	-	-	-	-	-	-
6	Acc.	'Centre Beam Acc. [g]'	-	-	-	412	412	260
7	Acc.	'Side C Beam Acc. [g]'	-	-	-	-	-	-
8	Acc.	'1/4 B Wall Acc. [g]'	-	1995	775	294	206	206
9	Acc.	'1/2 A Wall Acc. [g]'	-	885	1425	229	228	402
10	Acc.	'1/2 B Wall Acc. [g]'	-	1995	1425	163	137	136
11	Acc.	'1/2 C Wall Acc. [g]'	-	3105	1425	229	357	531
12	Acc.	'3/4 B Wall Acc. [g]'	-	1995	2070	281	268	267
13	Pot.	'Shake Table Disp. [mm]'	-	-	-	-	-	-
14	WP	'1/4 A Wall Disp. [mm]'	1, 9, 23, 27	885	775	-	-	-
15	WP	'1/4 B Wall Disp. [mm]'	1, 9, 23, 27	1995	775	-	-	-
16	WP	'1/4 C Wall Disp. [mm]'	1, 9, 23, 27	3105	775	-	-	-
17	WP	'1/2 A Wall Disp. [mm]'	1, 9, 23, 27	885	1425	-	-	-
18	WP	'1/2 B Wall Disp. [mm]'	1, 9, 23, 27	1995	1425	-	-	-
19	WP	'1/2 C Wall Disp. [mm]'	1, 9, 23, 27	3105	1425	-	-	-
20	WP	'3/4 A Wall Disp. [mm]'	1, 9, 23, 27	885	2070	-	-	-
21	WP	'3/4 B Wall Disp. [mm]'	1, 9, 23, 27	1995	2070	-	-	-
22	WP	'3/4 C Wall Disp. [mm]'	1, 9, 23, 27	3105	2070	-	-	-
23	Pot.	'4/4 A Wall Disp. [mm]'	All Tests	-	-	-	-	-
24	Pot.	'Top Beam Disp. [mm]'	-	-	-	-	-	-
25	Pot.	'4/4 C Wall Disp. [mm]'	All Tests	-	-	-	-	-
26	Pot.	'1/2 Side A OOP Detachment [mm]'	-	220	1425	-	-	-
27	Pot.	'Side A Ret. Wall Sliding [mm]'	1-27	50	450	-	-	-
28	Pot.	'1/2 Side C OOP Detachment [mm]'	-	3770	1425	-	-	-
29	Pot.	'Side C Ret. Wall Sliding [mm]'	1-27	3935	450	-	-	-
30	-	'Inertial Force [kN]'	1, 9, 23, 27	-	-	-	-	-

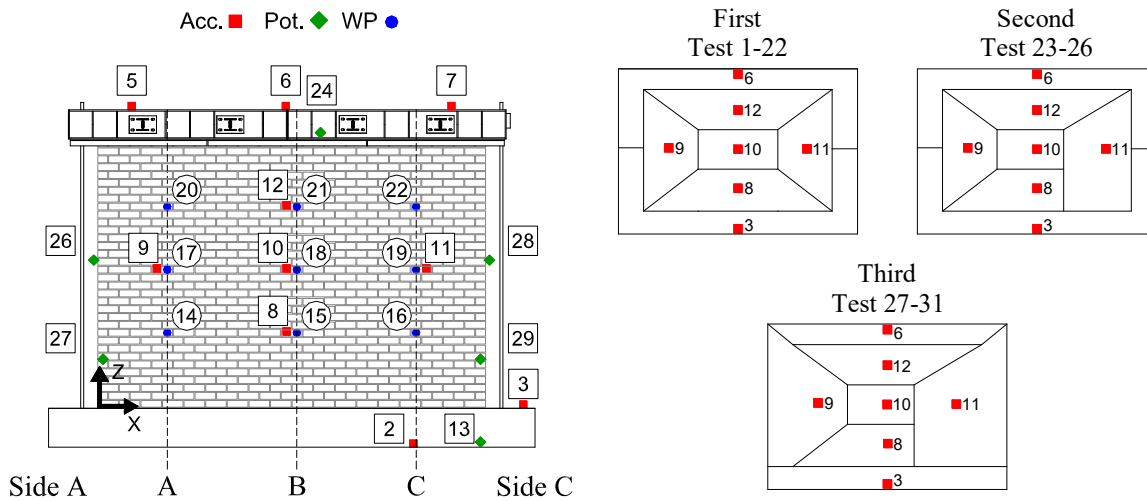


Figure 1. Instrumentation of CS-010/005-RR and adopted lumped mass distribution.

Table 2. CS-000-RF instrumentation, data acquisition and assigned lumped masses.

Col.	Instr.	Description	Offline	Location		Lumped Mass	
				X [mm]	Z [mm]	1 st [kg]	2 nd [kg]
1	-	'Time [s]'	-	-	-	-	-
2	Acc.	'Shake Table Acc. [g]'	-	-	-	-	-
3	Acc.	'Foundation Acc. [g]'	-	-	-	452	432
4	Acc.	'Frame Acc. [g]'	-	-	-	-	-
5	Acc.	'Side A Ret. Wall Acc. [g]'	-	-	-	103	-
6	Acc.	'Top Beam Acc. [g]'	All Tests	-	-	-	-
7	Acc.	'Side C Ret. Wall Acc. [g]'	-	-	-	103	-
8	Acc.	'1/4 B Wall Acc. [g]'	20-22	1995	615	294	-
9	Acc.	'1/2 A Wall Acc. [g]'	20-22	885	1425	287	-
10	Acc.	'1/2 B Wall Acc. [g]'	20-22	1995	1425	249	1625
11	Acc.	'1/2 C Wall Acc. [g]'	20-22	3105	1425	287	-
12	Acc.	'4/4 B Wall Acc. [g]'	-	1995	2070	281	-
13	Pot.	'Shake Table Disp. [mm]'	-	-	-	-	-
14	Opt.	'1/4 A Wall Disp. [mm]'	1, 5, 19-22	885	775	-	-
15	Opt.	'1/4 B Wall Disp. [mm]'	1, 5, 19-22	1995	775	-	-
16	Opt.	'1/4 C Wall Disp. [mm]'	1, 5, 19-22	3105	775	-	-
17	Opt.	'1/2 A Wall Disp. [mm]'	1, 5, 19-22	885	1425	-	-
18	Pot./Opt.	'1/2 B Wall Disp. [mm]'	1, 5, 18-22	1995	1425	-	-
19	Opt.	'1/2 C Wall Disp. [mm]'	1, 5, 19-22	3105	1425	-	-
20	Opt.	'3/4 A Wall Disp. [mm]'	1, 5, 19-22	885	2070	-	-
21	Opt.	'3/4 B Wall Disp. [mm]'	1, 5, 19-22	1995	2070	-	-
22	Opt.	'3/4 C Wall Disp. [mm]'	1, 5, 19-22	3105	2070	-	-
23	Opt.	'4/4 A Wall Disp. [mm]'	19-22	885	2720	-	-
24	Pot.	'4/4 B Wall Disp. [mm]'	1, 5, 19	1995	2720	-	-
25	Opt.	'4/4 C Wall Disp. [mm]'	19-22	3105	2720	-	-
26	Pot./Opt.	'1/2 Side A OOP Detachment [mm]'	19-22	105	1340	-	-
27	Pot./Opt.	'4/4 Side A OOP Detachment [mm]'	19-22	105	2640	-	-
28	Pot./Opt.	'1/2 Side C OOP Detachment [mm]'	19-22	3880	1340	-	-
29	Pot./Opt.	'4/4 Side C OOP Detachment [mm]'	19-22	3880	2640	-	-
30	-	'Inertial Force [kN]'	1, 5, 19	-	-	-	-

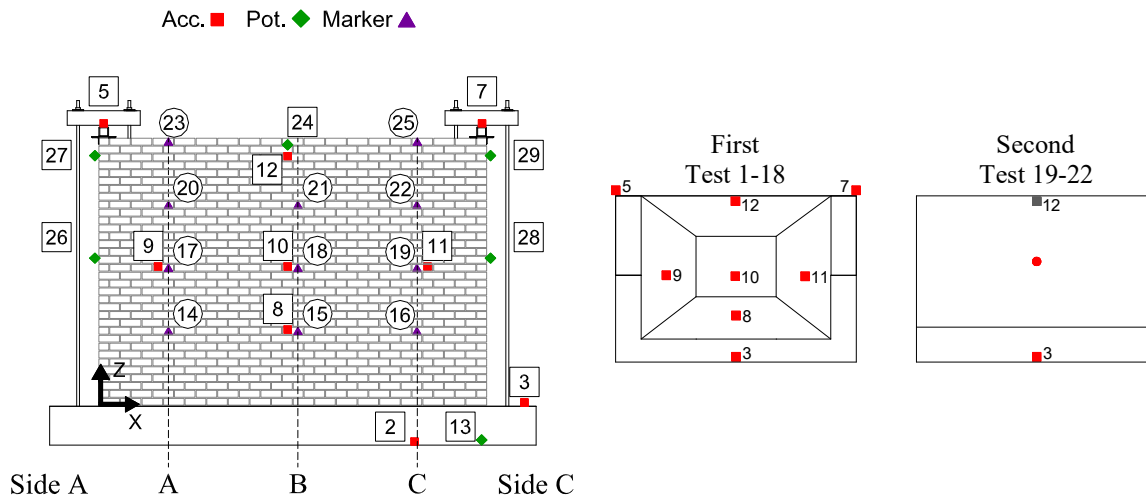


Figure 2. Instrumentation of CS-000-RF and adopted lumped mass distribution.

Table 3. CSW-000-RF instrumentation, data acquisition and assigned lumped masses.

Col.	Instr.	Description	Offline	Location		Lumped Mass	
				X [mm]	Z [mm]	1 st [kg]	2 nd [kg]
1	-	'Time [s]'	-	-	-	-	-
2	Acc.	'Shake Table Acc. [g]'	-	-	-	-	-
3	Acc.	'Foundation Acc. [g]'	-	-	-	369	417
4	Acc.	'Frame Acc. [g]'	21-27	-	-	-	-
5	Acc.	'Side A Ret. Wall Acc. [g]'	-	-	-	103	-
6	Acc.	'Top Beam Acc. [g]'	All Tests	-	-	-	-
7	Acc.	'Side C Ret. Wall Acc. [g]'	-	-	-	84	-
8	Acc.	'1/4 B Wall Acc. [g]'	21-27	2325	615	72	-
9	Acc.	'1/2 A Wall Acc. [g]'	-	885	1425	98	331
10	Acc.	'1/2 B Wall Acc. [g]'	21-27	1330	1425	99	-
11	Acc.	'1/2 C Wall Acc. [g]'	-	3380	1425	47	235
12	Acc.	'4/4 B Wall Acc. [g]'	-	1975	2560	237	548
13	Pot.	'Shake Table Disp. [mm]'	-	-	-	-	-
14	Opt.	'1/4 A Wall Disp. [mm]'	1-2, 10, 21	665	775	-	-
15	WP/Opt.	'1/4 B Wall Disp. [mm]'	1-2, 10, 21	1495	775	-	-
16	Opt.	'1/4 C Wall Disp. [mm]'	1-2, 10, 21	3380	775	-	-
17	Opt.	'1/2 A Wall Disp. [mm]'	1-2, 10, 21	665	1425	-	-
18	WP/Opt.	'1/2 B Wall Disp. [mm]'	1-2, 10, 21	1495	1425	-	-
19	Opt.	'1/2 C Wall Disp. [mm]'	1-2, 10, 21	3380	1425	-	-
20	Opt.	'3/4 A Wall Disp. [mm]'	1-2, 10, 21	665	2315	-	-
21	WP/Opt.	'3/4 B Wall Disp. [mm]'	1-2, 10, 21	1495	2315	-	-
22	Opt.	'3/4 C Wall Disp. [mm]'	1-2, 10, 21	3380	2315	-	-
23	Opt.	'4/4 A Wall Disp. [mm]'	1-2, 10, 21	665	2720	-	-
24	Opt.	'4/4 B Wall Disp. [mm]'	1-2, 10, 21	1495	2720	-	-
25	Opt.	'4/4 C Wall Disp. [mm]'	1-2, 10, 21	3380	2720	-	-
26	Pot./Opt.	'1/2 Side A OOP Detachment [mm]'	1-2, 10, 21	220	1425	-	-
27	Pot./Opt.	'4/4 Side A OOP Detachment [mm]'	1-2, 10, 21	220	2560	-	-
28	Pot./Opt.	'1/2 Side C OOP Detachment [mm]'	1-2, 10, 21	3770	1425	-	-
29	Pot./Opt.	'4/4 Side C OOP Detachment [mm]'	1-2, 10, 21	3770	2560	-	-
30	-	'Inertial Force [kN]'	1-2, 10, 22	-	-	-	-
31	Acc.	'1/4 A Wall Acc. [g]'	21-27	885	615	138	-
32	Acc.	'1/4 C Wall Acc. [g]'	21-27	3380	615	69	-
33	Acc.	'3/4 A Wall Acc. [g]'	21-27	885	2150	176	-
34	Acc.	'3/4 C Wall Acc. [g]'	21-27	3380	2150	42	-
35	Opt.	'1/8 A Wall Disp. [mm]'	1-2, 10, 21	665	450	-	-
36	Opt.	'1/8 B Wall Disp. [mm]'	1-2, 10, 21	1495	450	-	-
37	Opt.	'1/8 C Wall Disp. [mm]'	1-2, 10, 21	3380	450	-	-
38	Opt.	'Side A Window Corner Disp. [mm]'	1-2, 10, 21	1660	530	-	-
39	Opt.	'Side C Window Corner Disp. [mm]'	1-2, 10, 21	3125	530	-	-

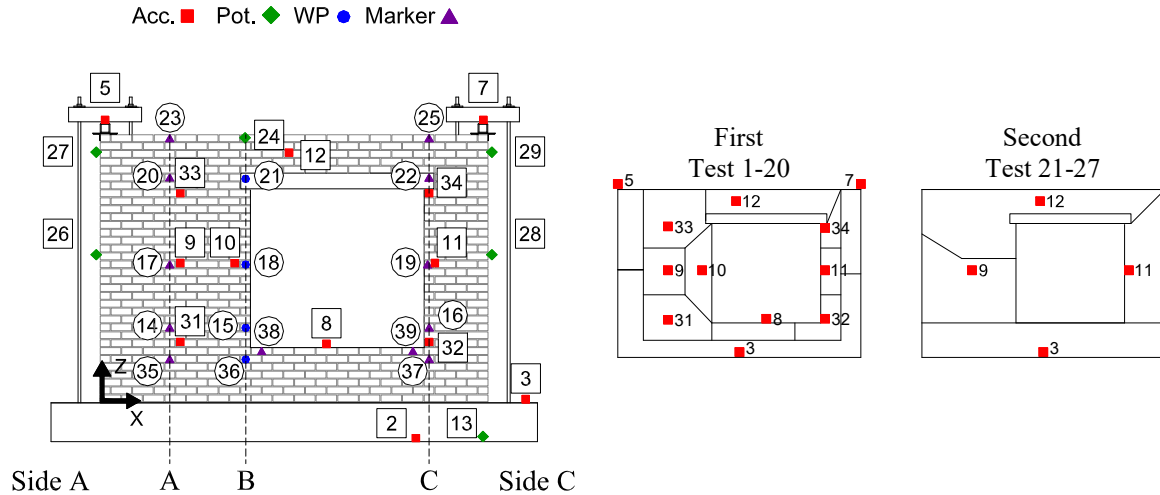


Figure 3. Instrumentation of CSW-000-RF and adopted lumped mass distribution.

Table 4. CL-000-RF instrumentation, data acquisition and assigned lumped masses.

Col.	Instr.	Description	Offline	Location		Lumped Mass	
				X [mm]	Z [mm]	1 st [kg]	2 nd [kg]
1	-	'Time [s]'	-	-	-	-	-
2	Acc.	'Shake Table Acc. [g]'	-	-	-	-	-
3	Acc.	'Foundation Acc. [g]'	-	-	-	445	141
4	Acc.	'Frame Acc. [g]'	23	-	-	-	-
5	Acc.	'Side A Ret. Wall Acc. [g]'	-	-	-	108	98
6	Acc.	'Top Beam Acc. [g]'	All Tests	-	-	-	-
7	Acc.	'Side C Ret. Wall Acc. [g]'	-	-	-	108	98
8	Acc.	'1/4 B Wall Acc. [g]'	-	2065	755	319	455
9	Acc.	'1/2 A Wall Acc. [g]'	-	650	1415	241	333
10	Acc.	'1/2 B Wall Acc. [g]'	-	2065	1415	176	177
11	Acc.	'1/2 C Wall Acc. [g]'	-	3265	1415	241	333
12	Acc.	'4/4 B Wall Acc. [g]'	-	2065	2555	284	284
13	Pot.	'Shake Table Disp. [mm]'	-	-	-	-	-
14	Opt.	'1/4 A Wall Disp. [mm]'	1, 9, 19, 22	1195	755	-	-
15	WP/Opt.	'1/4 B Wall Disp. [mm]'	1, 9, 19, 22	2065	755	-	-
16	Opt.	'1/4 C Wall Disp. [mm]'	1, 9, 19, 22	2940	755	-	-
17	Opt.	'1/2 A Wall Disp. [mm]'	1, 9, 19, 22	1195	1415	-	-
18	WP/Opt.	'1/2 B Wall Disp. [mm]'	1, 9, 19, 22	2065	1415	-	-
19	Opt.	'1/2 C Wall Disp. [mm]'	1, 9, 19, 22	2940	1415	-	-
20	Opt.	'3/4 A Wall Disp. [mm]'	1, 9, 19, 22	1195	2075	-	-
21	WP/Opt.	'3/4 B Wall Disp. [mm]'	1, 9, 19, 22	2065	2075	-	-
22	Opt.	'3/4 C Wall Disp. [mm]'	1, 9, 19, 22	2940	2075	-	-
23	Opt.	'4/4 A Wall Disp. [mm]'	1, 9, 19, 22	1195	2735	-	-
24	Pot.	'4/4 B Wall Disp. [mm]'	1, 9, 19, 22	2065	2735	-	-
25	Opt.	'4/4 C Wall Disp. [mm]'	1, 9, 19, 22	2940	2735	-	-
26	Pot./Opt.	'1/2 Side A OOP Detachment [mm]'	1, 9, 19, 22	155	1535	-	-
27	Pot./Opt.	'4/4 Side A OOP Detachment [mm]'	1, 9, 19, 22	3865	2555	-	-
28	Pot./Opt.	'1/2 Side C OOP Detachment [mm]'	1, 9, 19, 22	155	1535	-	-
29	Pot./Opt.	'4/4 Side C OOP Detachment [mm]'	1, 9, 19, 22	3865	2555	-	-
30	-	'Inertial Force [kN]'	1, 9, 19, 22	-	-	-	-
31	Acc.	-	All Tests	-	-	-	-
32	Acc.	-	All Tests	-	-	-	-
33	Acc.	'3/4 B Wall Acc. [g]'	-	2065	2075	257	257
34	Acc.	-	All Tests	-	-	-	-
35	Opt.	'1/8 A Wall Disp. [mm]'	1, 9, 19, 22	1195	395	-	-
36	Opt.	'1/8 B Wall Disp. [mm]'	1, 9, 19, 22	2065	395	-	-
37	Opt.	'1/8 C Wall Disp. [mm]'	1, 9, 19, 22	2940	395	-	-
38	Opt.	-	All Tests	-	-	-	-
39	Opt.	-	All Tests	-	-	-	-

Acc. ■ Pot. ◆ Marker ▲

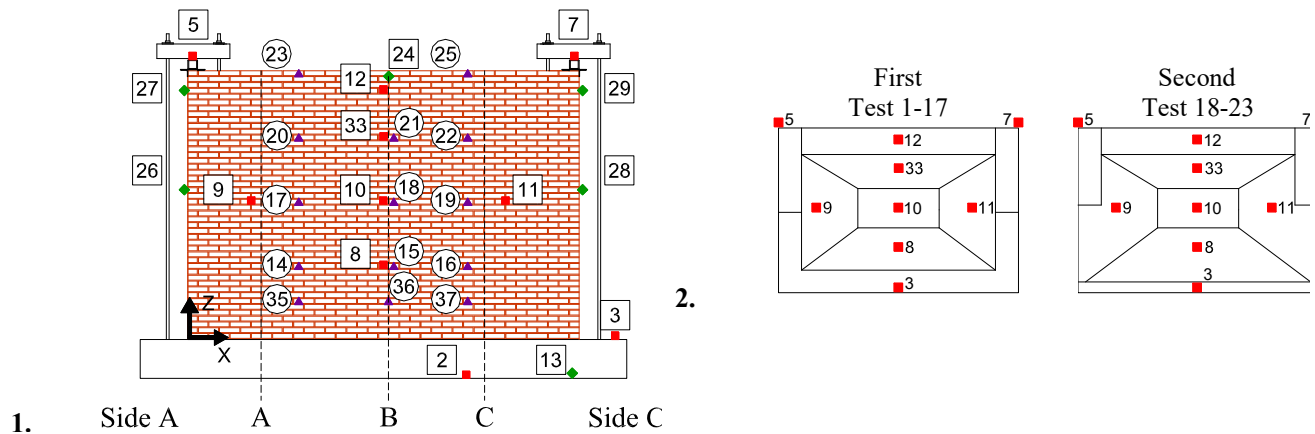


Figure 4. Instrumentation of CL-000-RF and adopted lumped mass distribution..

Table 5. CAV-000-RF instrumentation, data acquisition and assigned lumped masses.

Col.	Instr.	Description	Offline	Location		Lumped Mass
				X [mm]	Z [mm]	1 st [kg]
1	-	'Time [s]'	-	-	-	-
2	Acc.	'Shake Table Acc. [g]'	-	-	-	-
3	Acc.	'Foundation Acc. [g]'	-	-	-	460+530
4	Acc.	'Frame Acc. [g]'	-	-	-	-
5	Acc.	'Side A CS Ret. Wall Acc. [g]'	-	-	-	128
6	Acc.	'Top Beam Acc. [g]'	All Tests	-	-	-
7	Acc.	'Side C CS Ret. Wall Acc. [g]'	-	-	-	128
8	Acc.	'1/4 B CS Wall Acc. [g]'	-	2990	695	251
9	Acc.	'1/2 A CS Wall Acc. [g]'	-	995	1340	255
10	Acc.	'1/2 B CS Wall Acc. [g]'	-	2105	1340	126
11	Acc.	'1/2 C CS Wall Acc. [g]'	-	2990	1340	242
12	Acc.	'4/4 B CS Wall Acc. [g]'	-	2105	2640	223
13	Acc.	'Shake Table Disp. [mm]'	-	-	-	-
14	WP	'1/4 A CS Wall Disp. [mm]'	1, 9, 16	995	695	-
15	WP	'1/4 B CS Wall Disp. [mm]'	1, 9, 16	2105	695	-
16	WP	'1/4 C CS Wall Disp. [mm]'	1, 9, 16	2990	695	-
17	WP	'1/2 A CS Wall Disp. [mm]'	1, 9, 16	995	1340	-
18	WP	'1/2 B CS Wall Disp. [mm]'	1, 9, 16	2105	1340	-
19	WP	'1/2 C CS Wall Disp. [mm]'	1, 9, 16	2990	1340	-
20	WP	'3/4 A CS Wall Disp. [mm]'	1, 9, 16	995	2070	-
21	WP	'3/4 B CS Wall Disp. [mm]'	1, 9, 16	2105	2070	-
22	WP	'3/4 C CS Wall Disp. [mm]'	1, 9, 16	2990	2070	-
23	Pot.	'4/4 A CS Wall Disp. [mm]'	All Tests	-	-	-
24	Pot.	'4/4 B CS Wall Disp. [mm]'	1, 9, 16	1990	2720	-
25	Pot.	'4/4 C CS Wall Disp. [mm]'	All Tests	-	-	-
26	Pot.	'1/2 Side A OOP Detachment [mm]'	1, 9, 16	220	1425	-
27	Pot.	'4/4 Side A OOP Detachment [mm]'	1, 9, 16	220	2640	-
28	Pot.	'1/2 Side C OOP Detachment [mm]'	1, 9, 16	3770	1425	-
29	Pot.	'4/4 Side C OOP Detachment [mm]'	1, 9, 16	3770	2640	-
30	-	'Inertial Force [kN]'	1, 9, 16	-	-	-
31	Acc.	'3/4 B CS Wall Acc. [g]'	1, 9, 16	2105	2070	242
32	Acc.	'Side A CL Ret. Wall Acc. [g]'	1, 9, 16	-	-	137
33	Acc.	'Side C CL Ret. Wall Acc. [g]'	1, 9, 16	-	-	154
34	Acc.	'1/4 B CL Wall Acc. [g]'	-	2175	695	307
35	Acc.	'1/2 A CL Wall Acc. [g]'	-	1085	1415	286
36	Acc.	'1/2 B CL Wall Acc. [g]'	-	2175	1415	149
37	Acc.	'1/2 C CL Wall Acc. [g]'	-	3265	1415	300
38	Acc.	'3/4 B CL Wall Acc. [g]'	-	2175	2075	271
39	Acc.	'4/4 B CL Wall Acc. [g]'	-	2175	2735	240
40	Opt.	'1/4 A CL Wall Disp. [mm]'	1, 9, 16	1085	695	-
41	Opt.	'1/4 B CL Wall Disp. [mm]'	1, 9, 16	2175	695	-
42	Opt.	'1/4 C CL Wall Disp. [mm]'	1, 9, 16	3265	695	-
43	Opt.	'1/2 A CL Wall Disp. [mm]'	1, 9, 16	1085	1415	-
44	Opt.	'1/2 B CL Wall Disp. [mm]'	1, 9, 16	2175	1415	-
45	Opt.	'1/2 C CL Wall Disp. [mm]'	1, 9, 16	3265	1415	-
46	Opt.	'3/4 A CL Wall Disp. [mm]'	1, 9, 16	1085	2075	-
47	Opt.	'3/4 B CL Wall Disp. [mm]'	1, 9, 16	2175	2075	-
48	Opt.	'3/4 C CL Wall Disp. [mm]'	1, 9, 16	3265	2075	-
49	Opt.	'4/4 A CL Wall Disp. [mm]'	1, 9, 16	1085	2735	-
50	Opt.	'4/4 B CL Wall Disp. [mm]'	1, 9, 16	2175	2735	-
51	Opt.	'4/4 C CL Wall Disp. [mm]'	1, 9, 16	3265	2735	-
52	Pot.	'4/4 B CL Wall Disp. [mm]'	1, 9, 16	1960	2735	-

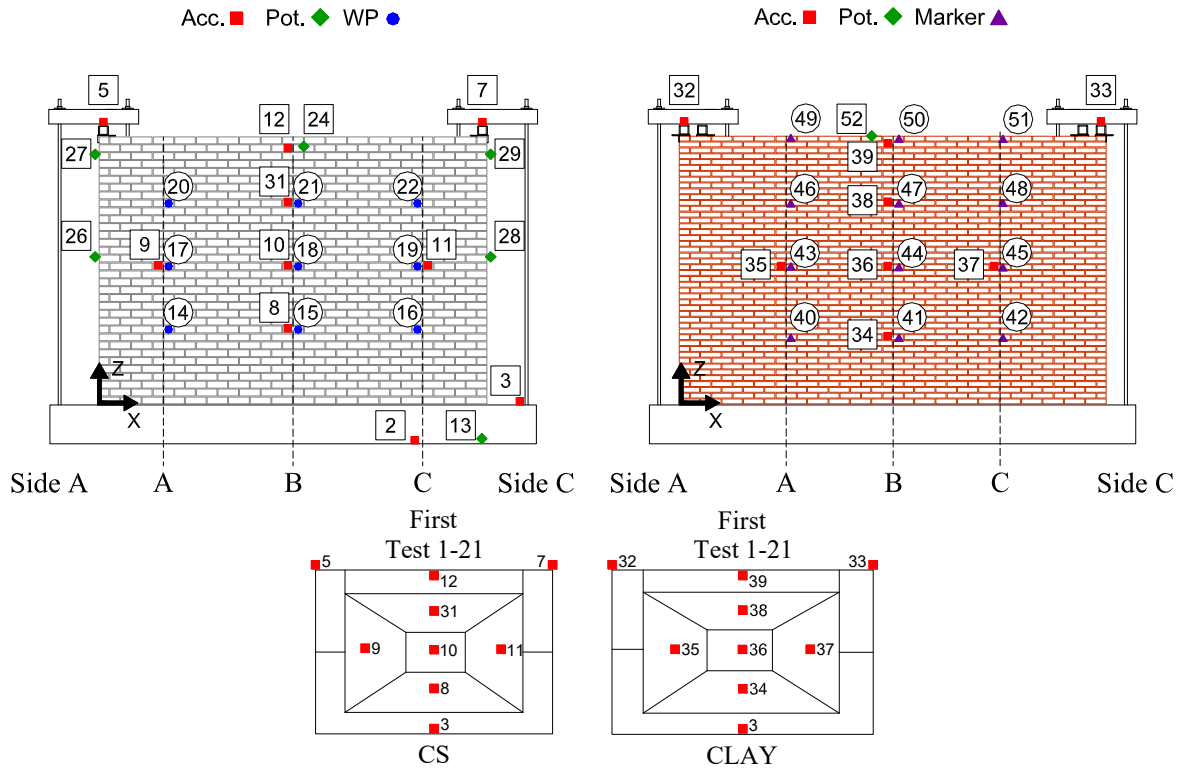


Figure 5. Instrumentation of CL-000-RF and adopted lumped mass distribution.

Table 6. CS-000-RFV instrumentation, data acquisition and assigned lumped masses.

Col.	Instr.	Description	Offline	Location		Lumped Mass		
				X [mm]	Z [mm]	1st [kg]	2nd [kg]	3rd [kg]
1	-	'Time [s]'	-	-	-	-	-	-
2	Acc.	'Shake Table X Acc. [g]'	-	-	-	-	-	-
3	Acc.	'Shake Table Z Acc. [g]'	-	-	-	-	-	-
4	Acc.	'Foundation X Acc. [g]'	-	-	-	460	428	725
5	Acc.	'Foundation Z Acc. [g]'	-	-	-	-	-	-
6	Acc.	'Frame X Acc. [g]'	-	-	-	-	-	-
7	Acc.	'Frame Z Acc. [g]'	-	-	-	-	-	-
8	Acc.	'Side A Ret. Wall X Acc. [g]'	-	-	-	128	128	166
9	Acc.	'Side A Ret. Wall Z Acc. [g]'	-	-	-	-	-	-
10	Acc.	'Side C Ret. Wall X Acc. [g]'	-	-	-	128	33	34
11	Acc.	'Side C Ret. Wall Z Acc. [g]'	-	-	-	-	-	-
12	Acc.	'1/4 B Wall X Acc. [g]'	28	1995	775	251	312	-
13	Acc.	'1/2 A Wall X Acc. [g]'	-	885	1425	255	255	195
14	Acc.	'1/2 B Wall X Acc. [g]'	-	1995	1505	126	126	131
15	Acc.	'1/2 B Wall Z Acc. [g]'	-	1995	1505	-	-	-
16	Acc.	'1/2 C Wall X Acc. [g]'	-	3105	1425	242	306	558
17	Acc.	'3/4 B Wall X Acc. [g]'	28	1995	2070	242	234	-
18	Acc.	'4/4 B Wall X Acc. [g]'	-	1995	2640	223	233	245
19	Acc.	'4/4 B Wall Z Acc. [g]'	1-16	1995	2640	-	-	-
20	Pot.	'Shake Table X Disp. [mm]'	-	-	-	-	-	-
21	Pot.	'Shake Table Z Disp. [mm]'	-	-	-	-	-	-
22	WP/Opt.	'1/4 A Wall Disp. [mm]'	21-28	885	775	-	-	-
23	WP/Opt.	'1/4 B Wall Disp. [mm]'	21-28	1995	775	-	-	-
24	WP/Opt.	'1/4 C Wall Disp. [mm]'	21-28	3105	775	-	-	-
25	WP/Opt.	'1/2 A Wall Disp. [mm]'	21-28	885	1425	-	-	-
26	WP/Opt.	'1/2 B Wall Disp. [mm]'	21-28	1995	1505	-	-	-
27	WP/Opt.	'1/2 C Wall Disp. [mm]'	21-28	3105	1425	-	-	-
28	WP/Opt.	'3/4 A Wall Disp. [mm]'	21-28	885	2070	-	-	-
29	WP/Opt.	'3/4 B Wall Disp. [mm]'	21-28	1995	2070	-	-	-
30	WP/Opt.	'3/4 C Wall Disp. [mm]'	21-28	3105	2070	-	-	-
31	Opt.	'4/4 A Wall Disp. [mm]'	-	885	2720	-	-	-
32	Pot./Opt.	'4/4 B Wall Disp. [mm]'	-	1995	2720	-	-	-
33	Opt.	'4/4 C Wall Disp. [mm]'	-	3105	2720	-	-	-
34	Pot./Opt.	'1/2 Side A OOP Detachment [mm]'	-	220	1425	-	-	-
35	Pot./Opt.	'4/4 Side A OOP Detachment [mm]'	-	220	2640	-	-	-
36	Pot./Opt.	'1/2 Side C OOP Detachment [mm]'	-	3770	1425	-	-	-
37	Pot./Opt.	'4/4 Side C OOP Detachment [mm]'	-	3770	2640	-	-	-
38	-	'Inertial Force [kN]'	-	-	-	-	-	-

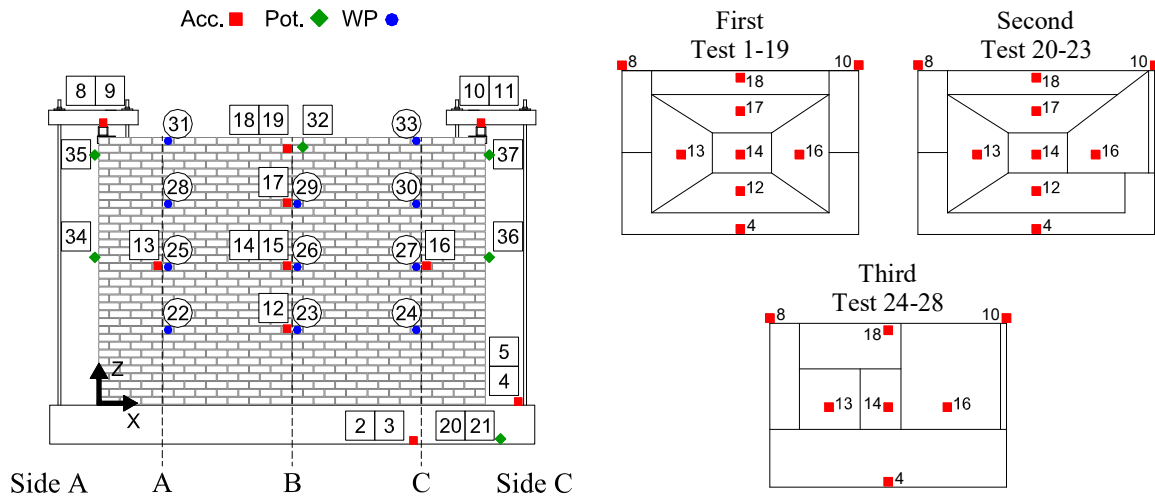


Figure 6. Instrumentation of CS-000-RFV and adopted lumped mass distribution..

Table 7. CS-000-L1&CS-000-L2 instrumentation, data acquisition and assigned lumped masses.

Col.	Instr.	Description	Offline	Location		Lumped Mass		
				X [mm]	Z [mm]	1 st [kg]	2 nd [kg]	3 rd [kg]
1	-	'Time [s]'	-	-	-	-	-	-
2	Acc.	'Shake Table Acc. [g]'	-	-	-	-	-	-
3	Acc.	'Foundation Acc. [g]'	-	-	-	460	481	412
4	Acc.	'Frame Acc. [g]'	-	-	-	-	-	-
5	Acc.	'Side A Ret. Wall Acc. [g]'	-	-	-	95	95	95
6	Acc.	'Side C Ret. Wall Acc. [g]'	-	-	-	122	-	-
7	Acc.	'1/4 A L1 Acc. [g]'	-	775	695	127	127	127
8	Acc.	'1/4 B L1 Acc. [g]'	-	1660	695	56	56	56
9	Acc.	'1/2 A L1 Acc. [g]'	-	775	1425	120	120	120
10	Acc.	'1/2 B L1 Acc. [g]'	-	1660	1425	52	52	52
11	Acc.	'3/4 A L1 Acc. [g]'	-	775	2070	176	176	176
12	Acc.	'3/4 B L1 Acc. [g]'	-	1660	2070	51	51	51
13	Acc.	'4/4 B L1 Acc. [g]'	-	1660	2640	28	28	28
14	Acc.	'1/4 B L2 Acc. [g]'	-	1885	695	80	80	80
15	Acc.	'1/4 C L2 Acc. [g]'	-	2880	695	150	150	150
16	Acc.	'1/2 B L2 Acc. [g]'	-	1885	1425	75	75	75
17	Acc.	'1/2 C L2 Acc. [g]'	-	2880	1425	140	140	210
18	Acc.	'3/4 B L2 Acc. [g]'	-	1885	2070	71	71	71
19	Acc.	'3/4 C L2 Acc. [g]'	-	2880	2070	206	307	307
20	Acc.	'4/4 B L2 Acc. [g]'	-	1885	2640	39	39	39
21	Pot.	'Shake Table Disp. [mm]'	-	-	-	-	-	-
22	WP	'1/4 A L1 Disp. [mm]'	-	775	695	-	-	-
23	WP	'1/4 B L1 Disp. [mm]'	-	1660	695	-	-	-
24	WP	'1/2 A L1 Disp. [mm]'	-	775	1425	-	-	-
25	WP	'1/2 B L1 Disp. [mm]'	-	1660	1425	-	-	-
26	WP	'3/4 A L1 Disp. [mm]'	-	775	2070	-	-	-
27	WP	'3/4 B L1 Disp. [mm]'	-	1660	2070	-	-	-
28	Pot.	'4/4 B L1 Disp. [mm]'	-	1660	2640	-	-	-
29	WP	'1/4 B L2 Disp. [mm]'	-	1885	695	-	-	-
30	Opt.	'1/4 C L2 Disp. [mm]'	-	2880	695	-	-	-
31	WP	'1/2 B L2 Disp. [mm]'	-	1885	1425	-	-	-
32	Opt.	'1/2 C L2 Disp. [mm]'	-	2880	1425	-	-	-
33	WP	'3/4 B L2 Disp. [mm]'	-	1885	2070	-	-	-
34	Opt.	'3/4 C L2 Disp. [mm]'	-	2880	2070	-	-	-
35	Pot.	'4/4 B L2 Disp. [mm]'	-	1885	2640	-	-	-
36	Pot.	'1/2 Side A L1 OOP Detachment [mm]'	-	220	1425	-	-	-
37	Pot.	'4/4 Side A L1 OOP Detachment [mm]'	-	220	2640	-	-	-
38	Pot.	'1/2 Side C L2 OOP Detachment [mm]'	-	3770	1425	-	-	-
39	Pot.	'4/4 Side C L2 OOP Detachment [mm]'	-	3770	2640	-	-	-
40	-	'Inertial Force L1 [kN]'	-	-	-	-	-	-
41	-	'Inertial Force L2 [kN]'	-	-	-	-	-	-
42	WP	'1/4 L2 Disp. [mm]'	-	3325	695	-	-	-
43	WP	'1/2 L2 Disp. [mm]'	-	3325	1425	-	-	-
44	WP	'3/4 L2 Disp. [mm]'	-	3325	2070	-	-	-

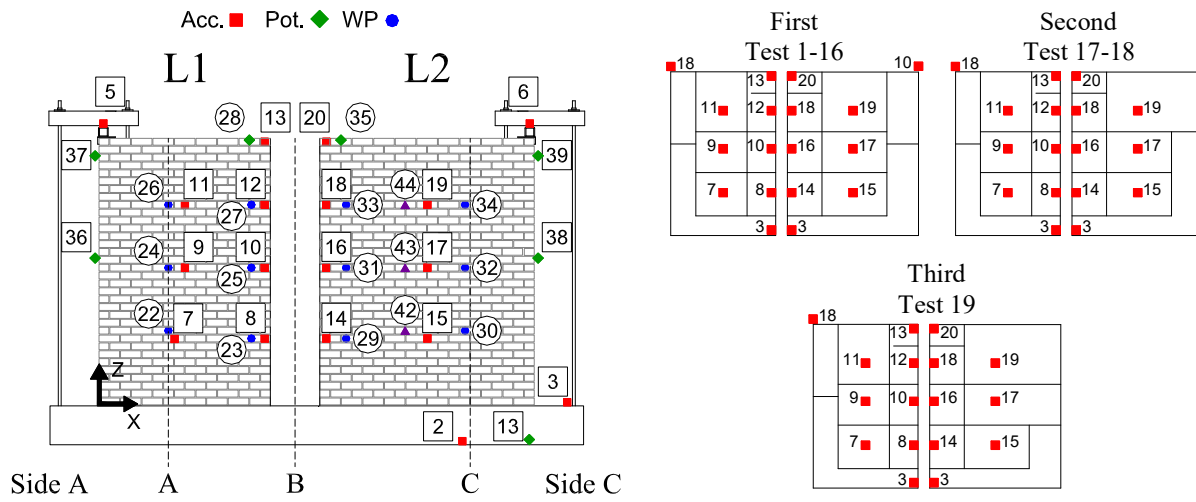


Figure 7. Instrumentation of CS-000-L1&L2 and adopted lumped mass distribution.

Table 8. CS-000-RF2 instrumentation, data acquisition and assigned lumped masses.

Col.	Instr.	Description	Offline	Location		Lumped Mass
				X [mm]	Z [mm]	1 st [kg]
1	-	'Time [s]'	-	-	-	-
2	Acc.	'Shake Table Acc. [g]'	-	-	-	-
3	Acc.	'Foundation Acc. [g]'	-	-	-	473
4	Acc.	'Frame Acc. [g]'	-	-	-	-
5	Acc.	'Side A Ret. Wall Acc. [g]'	-	-	-	108
6	Acc.	'Side C Ret. Wall Acc. [g]'	-	-	-	108
7	Acc.	'1/4 B Wall Acc. [g]'	-	1995	695	260
8	Acc.	'1/2 A Wall Acc. [g]'	-	885	1340	199
9	Acc.	'1/2 B Wall Acc. [g]'	-	1995	1340	126
10	Acc.	'1/2 C Wall Acc. [g]'	-	3105	1340	188
11	Acc.	'3/4 A Wall Acc. [g]'	-	885	2070	165
12	Acc.	'3/4 B Wall Acc. [g]'	-	1995	2070	121
13	Acc.	'3/4 C Wall Acc. [g]'	-	3105	2070	157
14	Acc.	'4/4 C Wall Acc. [g]'	-	1995	2640	150
15	Pot.	'Shake Table Disp. [mm]'	-	-	-	-
16	Pot.	'1/4 A Wall Disp. [mm]'	-	885	855	-
17	Pot.	'1/4 B Wall Disp. [mm]'	-	1995	855	-
18	Pot.	'1/4 C Wall Disp. [mm]'	-	3105	855	-
19	Pot.	'1/2 A Wall Disp. [mm]'	-	885	1425	-
20	Pot.	'1/2 B Wall Disp. [mm]'	-	1995	1425	-
21	Pot.	'1/2 C Wall Disp. [mm]'	-	3105	1425	-
22	Pot.	'3/4 A Wall Disp. [mm]'	-	885	2070	-
23	Pot.	'3/4 B Wall Disp. [mm]'	-	1995	2070	-
24	Pot.	'3/4 C Wall Disp. [mm]'	-	3105	2070	-
25	Pot.	'4/4 B Wall Disp. [mm]'	-	1995	2720	-
26	Pot.	'1/2 Side A OOP Detachment [mm]'	-	220	1425	-
27	Pot.	'4/4 Side A OOP Detachment [mm]'	-	220	2640	-
28	Pot.	'1/2 Side C OOP Detachment [mm]'	-	3770	1425	-
29	Pot.	'4/4 Side C OOP Detachment [mm]'	-	3770	2640	-
30	-	'Inertial Force [kN]'	-	-	-	-
31	Opt.	'4/4 A Wall Disp. [mm]'	-	885	2720	-
32	Opt.	'4/4 C Wall Disp. [mm]'	-	3105	2720	-

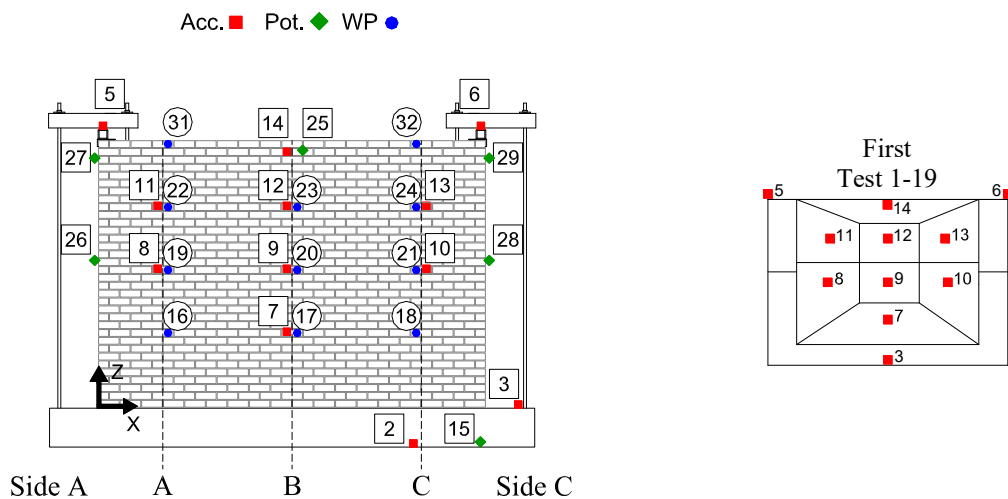


Figure 8. Instrumentation of CS-000-RF2 and adopted lumped mass distribution.